AD NUMBER
ADC009459
CLASSIFICATION CHANGES
TO: unclassified
FROM: confidential
LIMITATION CHANGES
TO: Approved for public release, distribution unlimited
FROM: Distribution limited to U.S. Gov't. agencies only; Test and Evaluation; Nov 76. Other requests for this document must be referred to Director, Naval Research Lab., Washington, D. C. 20375.
AUTHORITY
NRL ltr, 3 Mar 2004; NRL ltr, 3 Mar 2004

F6

CONFIDENTIAL

NRL Memorandum Report 3290

A Statistical Analysis of the Performance of a Towed Array System

[Unclassified Title]

RICHARD M. HEITMEYER, STEPHEN C. WALES, AND DAVID T. DEIHL

Large Aperture Acoustics Branch
Acoustics Division

November 1976

"NATIONAL SECURITY INFORMATION"

"Unauthorized Disclosure Subject to Criminal Sanctions"

NAVAL RESEARCH LABORATORY
Washington, D.C.

CONFIDENTIAL

NATIONAL SECURITY INFORMATION

Unauthorized Disclosure Subject to Criminal Sanctions.

CONFIDENTIAL

SECURITY CLASSIFICATION OF THIS PAGE (When Data Entered)

REPORT DOCUMENTATION PAGE

READ INSTRUCTIONS BEFORE COMPLETING FORM

1. REPORT NUMBER: Memorandum Report 3290	2. GOVT ACCESSION NO.
3. RECIPIENT'S CATALOG NUMBER	
4. TITLE (and Subtitle): A STATISTICAL ANALYSIS OF THE PERFORMANCE OF A TOWED ARRAY SYSTEM [redacted] (U)	5. TYPE OF REPORT & PERIOD COVERED: Interim report on a continuing NRL problem.
6. PERFORMING ORG. REPORT NUMBER	
7. AUTHOR(s): Richard M. Heitmeyer, Stephen C. Wales, and David T. Deihl	8. CONTRACT OR GRANT NUMBER(s): ARPA Order 2976
9. PERFORMING ORGANIZATION NAME AND ADDRESS: Naval Research Laboratory, Washington, D.C. 20375 (12) 112p.	10. PROGRAM ELEMENT, PROJECT, TASK AREA & WORK UNIT NUMBERS: NRL Problem S01-87 (14) NRL-MR-3290
11. CONTROLLING OFFICE NAME AND ADDRESS: Defense Advanced Research Project Agency, 1400 Wilson Boulevard, Arlington, Virginia 22209	12. REPORT DATE: November 1976 13. NUMBER OF PAGES: 114
14. MONITORING AGENCY NAME & ADDRESS (if different from Controlling Office): (15) ARPA Order-2976	15. SECURITY CLASS. (of this report): CONFIDENTIAL 15a. DECLASSIFICATION/DOWNGRADING SCHEDULE: XGDS-3-2006

16. DISTRIBUTION STATEMENT (of this Report)

Distribution limited to Government Agencies only; test and evaluation; November 1976. Other requests for this document must be referred to the Commanding Officer, Naval Research Laboratory, Washington, D.C. 20375.

17. DISTRIBUTION STATEMENT (of the abstract entered in Block 20, if different from Report)

18. SUPPLEMENTARY NOTES

19. KEY WORDS (Continue on reverse side if necessary and identify by block number)

Spatial and temporal statistics
Towed array system

20. ABSTRACT (Continue on reverse side if necessary and identify by block number)

(C) Spatial and temporal statistics have been computed for a three-section towed array system operating in the Mediterranean Sea. The statistics for each section of the system are computed at a different frequency as a function of aperture length. The results show that the two shorter array sections suffer only modest degradations in a signal gain Furthermore, the temporal statistics, and hence the effect on performance of system bandwidth and system averaging time, are independent of aperture. In contrast, the signal gain for the longest array section shows a significant degradation as

(Continues)

DD FORM 1 JAN 73 1473 EDITION OF 1 NOV 65 IS OBSOLETE S/N 0102-014-6601

CONFIDENTIAL

SECURITY CLASSIFICATION OF THIS PAGE (When Data Entered)

251 750

4/B

Abstra

20. Abstract (Continued)

the aperture length is doubled from half to full. Furthermore, the noise gain increases by more than 3 dB so that the combined effect is to reduce the array gain at the full aperture over that at the half aperture. The temporal statistics for the longest array section, however, show only a modest dependence on aperture length, even though the signal gain indicates a significant reduction in the spatial coherence. Thus, for all three array sections, the observed temporal statistics indicate that the effect on performance of system temporal processing parameters is essentially independent of aperture length.

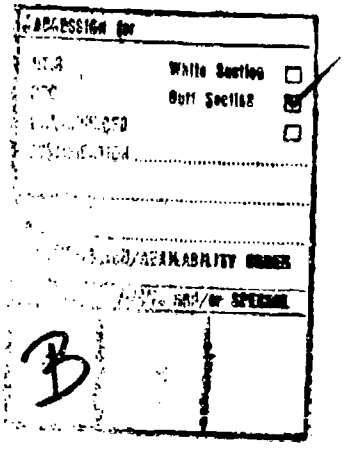

CONTENTS

CONTENTS (Con'd)

List of Illustrations

List of Illustrations (con'd)

List of Tables

A STATISTICAL ANALYSIS OF THE PERFORMANCE OF A TOWED ARRAY SYSTEM
[Unclassified Title]

I. INTRODUCTION

(U) In November 1974, a set of experiments were conducted in the Mediterranean using a three section towed array. Data were both analyzed on-line and recorded for later analysis. The results of the on-line analysis are reported in reference [1], along with a detailed description of the operating areas, the arrays and the associated on-line processing and recording hardware. This report presents the results of a detailed off-line analysis for the SEAGUARD Project of a portion of the data recorded during a radial source tow in the Ionian Basin.

(U) The objectives of the analysis are to measure the performance of the three arrays and to determine the relationship between the system performance and the three basic system parameters: array length, analysis bandwidth, and averaging time. These objectives provide a firm basis for SEAGUARD design and experiment. The approach is as follows: The system performance is characterized in terms of the mean values of the signal gain, the noise gain and the array gain. The gains are computed for three aperture lengths, quarter, half and full on each array to determine their dependence on array length. Histograms for these quantities show their general character. Standard deviations provide a simple measure of the fluctuations about the

Note: Manuscript submitted November 10, 1976.

means. The means and standard deviations of the constituents of the system gains are also computed as a function of aperture. These quantities are of interest in their own right. Furthermore, the standard deviations, together with the cross-correlation coefficients, determine the standard deviations of the system gains.

(U) The constituents of the sytem gains themselves are computed using a fixed analysis bandwidth (0.4Hz) and a fixed averaging time (12 min.). To determine the dependence of the results on these parameters, the temporal behavior of the instantaneous (unaveraged) constituents is characterized in terms of fluctuations spectra and covariance functions. The correlation times determine the extent to which the 12-minute averaging time reduces the fluctuations. The fluctuations bandwidths are used to infer the intrinsic frequency spread in the signal field and thus determine the extent to which the signal-to-noise ratio can be enhanced by narrowband processing. Histograms of the instantaneous constituents are used to evaluate the hypothesis that the signal field and/or the noise field is Gaussian and stantionary.

(U) The relevance of the analysis to the SEAGUARD Project is that it provides an experimental basis for both the design of the SEAGUARD/OMAT array system and for future experiments to be conducted under the SEAGUARD program. To the extent that the towed system results are degraded by the array dynamics, considerable improvement can be expected from the OMAT system. The majority of the results are, however, highly promising and consequently allow even greater Project expectations, as well as providing quantitative basis of support.

1.1 Experiment Description (U)

(C) The general source-receiver configuration is shown in Figure 1.1 The source tow ship, (R. V. AMERICAN DELTA II), towed a Vibrosis source at a depth of 91 m along the track shown beginning near the Straits of Messina at a nominal speed of 5.5 knots. The array tow ship, (R. V. PACIFIC APOLLO), towed the array system along tracks approximately perpendicular to the source tow tracks at a nominal speed of 3 knots.

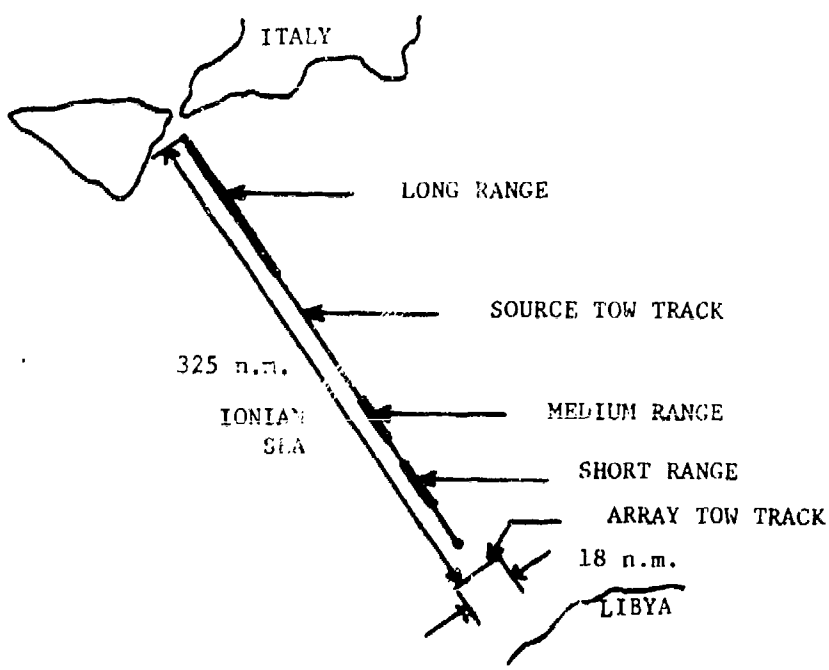

(U) Figure 1.1 Source-Receiver Configuration

(C) The transmission frequency of the Vibrosis source was switched between 20 Hz, 40 Hz and 210 Hz in 15 minute intervals at source levels of 190, 190 and 180 dB//μPa, respectively. Simultaneously, the three arrays were switched. The resulting array/frequency switching schedule is illustrated in Figure 1.2. It is noted that over any given 15-minute interval only one array is active and only one frequency is transmitted. Furthermore, the onset times for a particular array/frequency combination are separated by 45 minutes.

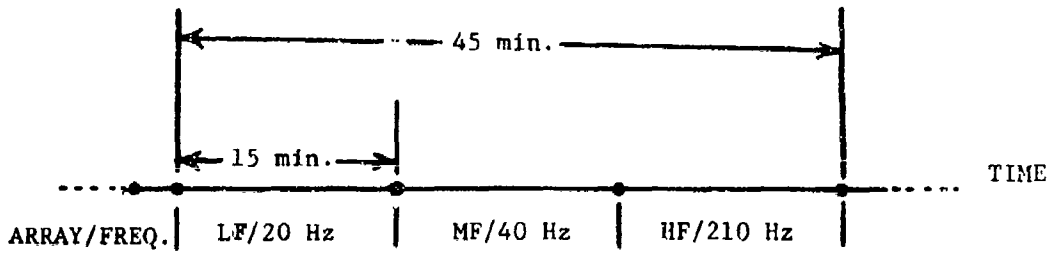

(C) Figure 1.2 Array/Frequency Switching Schedule

(U) Three segments of data from the tow were analyzed: a long range segment (LR), a medium range segment (MR), and a short range segment (SR). The ranges, range rates and the total durations for these data segments (shown as thick lines in Figure 1.1) are summarized in Table 1.1. During the data acquisition periods, it was necessary to reverse the array tow track direction and to allow a period of 1-2 hours for the arrays to stabilize. Data acquired during these periods was not analyzed. In addition, other short periods were excluded because of an occasional source failure, on-board calibrations and adjustments etc. The durations

of the resulting data bases are summarized in the right hand column of Table 1.

	Range (n.m.)	Range Rate (kts.)	Duration (hrs.)	Processed Data (hrs.)
LONG RANGE (LR)	327-238	5.4	16.6	11.0
MED. RANGE (MR)	138-102	5.5	6.5	4.8
SHORT RANGE (SR)	80-51	2.6 - 4.5	8.0	7.0

(U) Table 1.1 Data Set Descriptions

(C) The configuration of the three, equally-spaced, hydrophone element arrays is illustrated in Figure 1.3a. The HF and the LF arrays are physically distinct whereas the MF array is embedded in the front 1/3rd of the LF array. The acoustic parameters for the three array/frequency combinations are summarized in Table 1.2. Note that both the MF and HF arrays have nearly the same acoustical length and both were operated at approximately 2/3 of the $\lambda/2$ frequency, whereas the LF/20 Hz array is half again as long and was operated at the $\lambda/2$ frequency value.

(C) The aperture configuration is illustrated in Figuration 1.3b. The three apertures within each array were obtained from the first 16, 32 and 62 hydrophones respectively as measured from the array tow point. It is emphasized, that the designations, quarter, half and full refer to the number of hydrophones and not the acoustical length of the aperture.

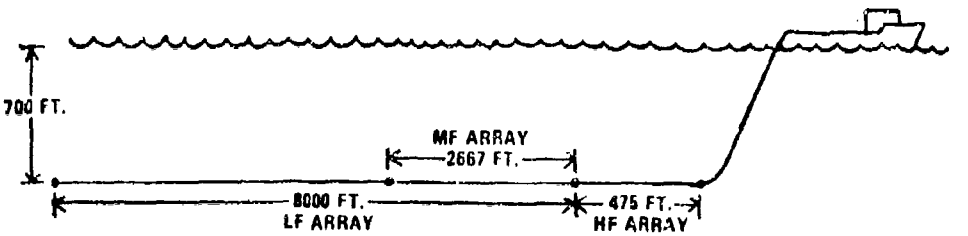

(C) Figure 1.3a Array Configuration

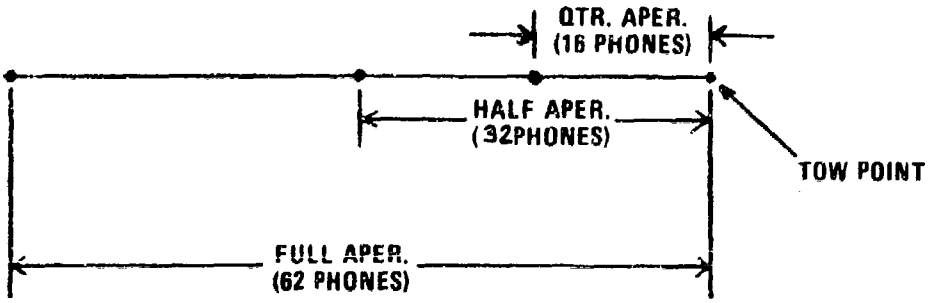

(C) Figure 1.3b Aperture Configuration

	LENGTH / λ	PHONE SEP. / λ	BEAMWIDTH
LF ARRAY – 20Hz	32.0	.5	2.8^0
MF ARRAY – 40Hz	21.3	.33	3.9^0
HF ARRAY – 210Hz	20.0	.31	4.1^0

(C) Table 1.2 Array Acoustic Parameters

1.2 Definitions and Terminology (U)

(U) The results presented in this report are derived from two basic sets of time series. The beamformer output time series, representing both beam signal power and beam noise power, are defined along tracks in the domain of the frequency-azimuth power spectrum as computed at the beamformer output. The hydrophone intensity times series, also representing both signal and noise power, are computed as power averages across all hydrophones in each of the three apertures at the same frequencies as the beam time series. In the interest of brievity, the hydrophone intensity time series will be referred to here as the omni time series, even though there is a small directivity index associated with each element of the array. The letters "B" and "O" will be used to denote a beam and an omni time series or statistic respectively, and the subscripts "S" and "N" refer to signal and noise. Allnoise statistics are referenced to a 1 Hz band.

(C) Both the beam and the omni time series are computed in frequency cells .4 Hz wide with time samples occurring every 20.2 seconds. The resulting time series are averaged over 36 values, corresponding to a time interval of 12.1 minutes, to produce a single value for each of the three apertures on the particular array/frequency combination that is active during the appropriate 15-minute switching interval. The unaveraged time series are referred to as instantaneous time series.

The time series of values at the output of the averager

for a given array occur at 45-minute intervals as determined by the array/frequency switching schedule. When the values of the averaged time series are expressed in a linear power scale (Chapter 4), the subscripts "i" and "a" will be used to distinguish between instantaneous and averaged time series statistics respectively.

(U) The beamformer is implemented using a two-dimensional FFT algorithm which generates the frequency-azimuth power spectrum at 64 beams equally spaced in the sine of the azimuth variable. Hanning shading is employed in both the time-to-frequency transform and the space-to-wavenumber transform with a slight modification in the latter to include all hydrophones in the aperture. An example of a typical instantaneous frequency-azimuth spectrum for the full aperture on the LF/20 Hz array is illustrated in Figure 1.4. The azimuth variable, Θ, is defined so that +90° represents the forward endfire direction, 0° represents broadside and -90° represents aft endfire. In this spectrum, the signal power is split between the frequency lines at 19.9 and 20.3 Hz and is concentrated in the beam at approximately +5° forward of broadside. The rough surface texture typical of an unaveraged spectrum is evident.

(C) The frequency-azimuth tracks used to define the instantaneous beam signal are obtained using a peak detection procedure on running two-minute averages of the instantaneous spectra to identify the frequency-azimuth resolution cells. The two-minute averaged spectra, used to obtain the value of the frequency-azimuth track for the spectrum in Figure 1.4, is shown in Figure 1.5. The averaging time was chosen to

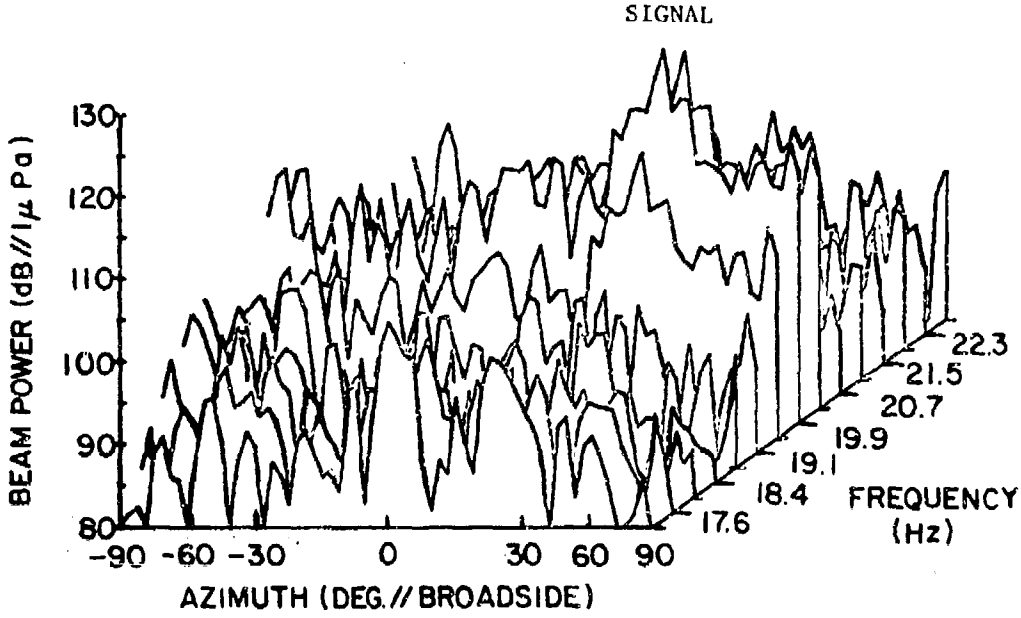

(C) Figure 1.4 Frequency-Azimuth Power Distribution, LF Array/20 Hz, Full Aperture Unaveraged Medium Range

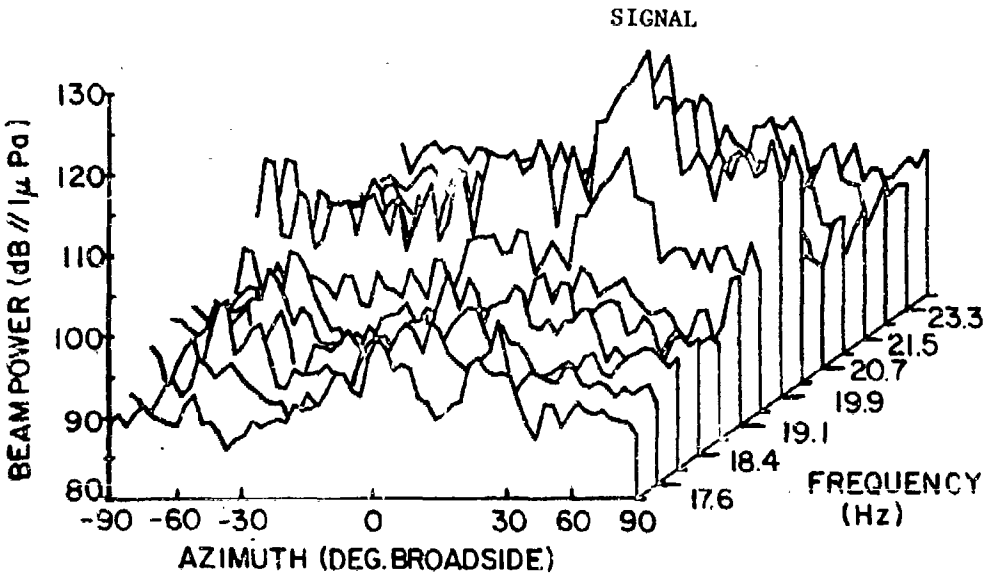

(C) Figure 1.5 Frequency-Azimuth Power Distribution, LF Array/20 Hz, Full Aperture 2 Minute Average Medium Range

be sufficiently long to remove variations in the track that would result had a peak detection algorithm been employed on the instantaneous spectrum. (Compare the surface texture of the spectra in Figures 1.4 and 1.5). At the same time, the averaging time was considered short enough to allow the track to follow relatively short-term variations in the frequency-azimuth track. Each of the three apertures for each array is tracked separately since differences in the tracks for the different apertures was observed. This phenomenon was discussed in reference [1] and attributed to array flexure. The present results support that view with 1° to a maximum of 8° differences in track bearing observed.

(C) For each beam signal time series, two beam noise time series are defined, each at the azimuth determined by the beam signal track. One is defined in a single resolution cell at a frequency 1.6 Hz (4 frequency lines) below the transmitted signal frequency. This time series will be referred to as the instantaneous beam noise since it is only used in the analysis of the instantaneous signal and noise properties in Chapter 4. The second is obtained as the average of the instantaneous beam noise and a time series defined in the resolution cell located 1.6 Hz above the transmitted signal frequency. The resulting beam noise is used in the computations of the system gains. Omni noise time series for each of the beam noises are defined in a similar manner. An illustration of the instantaneous beam signals and beam noise for all apertures and all arrays appears in Figure A.1 in the appendix. Plots of typical frequency-azimuth spectra for different apertures on the three arrays are found in Figures A.2 through A.6.

II. THE SYSTEM GAIN STATISTICS (U)

(U) In this chapter, and the following two chapters, the results of the analysis are described. In Chapter 5, these results are summarized and interpreted. The conclusions and the implications for the SEAGUARD/OMAT Project are presented in Chapter 6.

(U) The statistics for the signal gain, G_S, noise gain, G_N, and array gain, G_A, have been computed from the averaged beam and omni time series, according to the relationships

$$(2.1a) \quad G_S = B_S - O_S$$

$$(2.1b) \quad G_N = B_N - O_N$$

$$(2.1c) \quad G_A = G_S - G_N$$

where each element in the time series of the constituents is expressed in a decibel scale.

2.1 Signal Gain Statistics (U)

(C) The signal gain histograms for the full aperture on each of the three arrays are illustrated in Figure 2.1. The mean and standard deviation for each histogram is indicated at the side of each plot.[1] The ideal signal gain[2] that results from planewave incidence on an undeformed array

---

[1] Throughout this report, the symbol "($\bar{\ }$)" denotes the sample mean, σ, the standard deviation and, v, the coefficient of variation, defined as the ratio of the standard deviation to the mean.

[2] The ideal signal gain, noise gain and array gain are equal to $(N+1)^2/4$, $(3/8)(N+1)$ and $(2/3)(N+1)$ respectively, where N is the number of hydrophones in the subaperture.

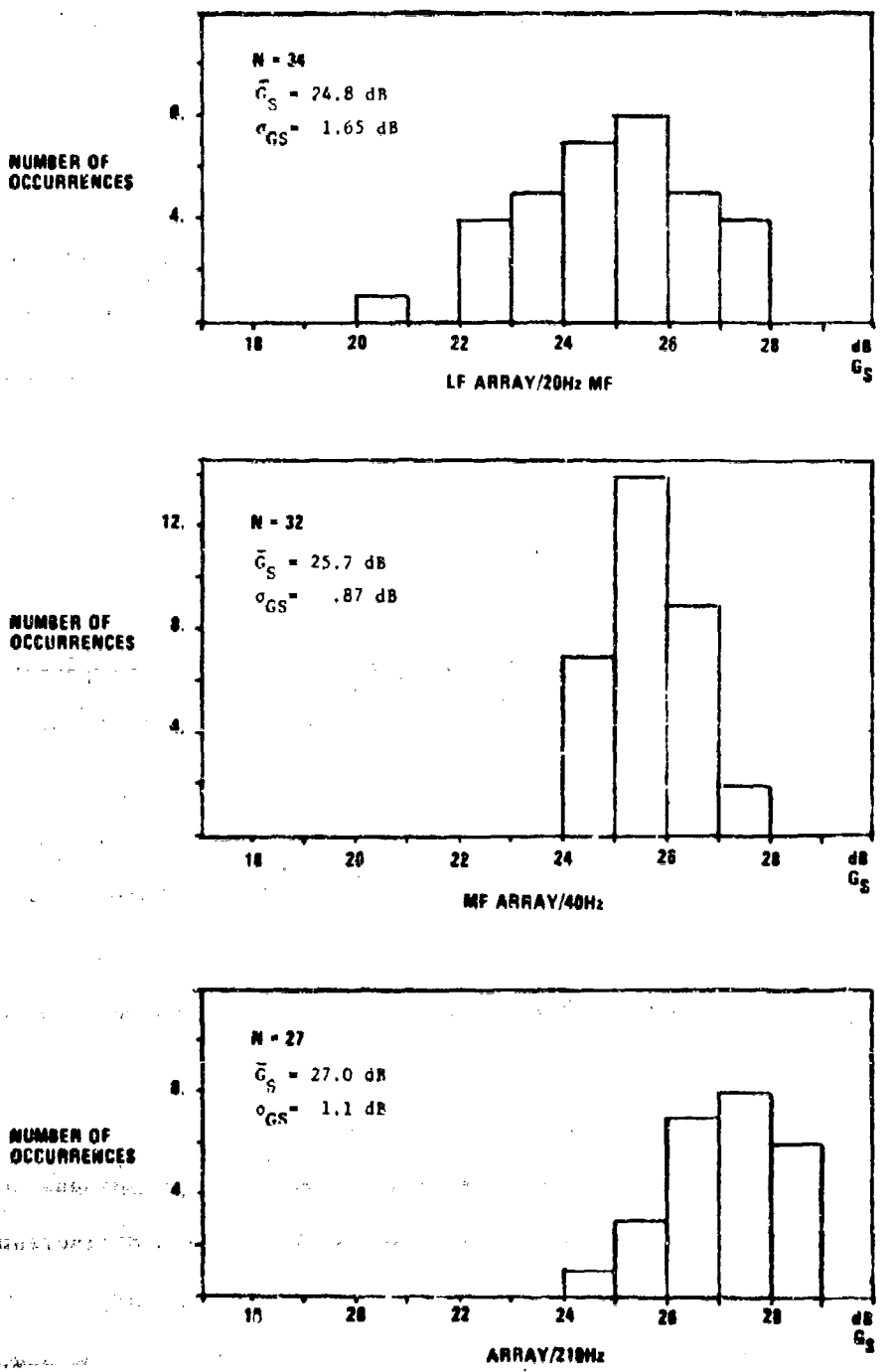

(C) Figure 2.1 Signal Gain Histograms (Full Aperture)

is 30dB. The degradation in the signal gain is the ideal value minus the observed mean value. It is seen that the greatest degradation occurs for the LF array with progressively smaller degradations for the MF and HF arrays. On the other hand, the spread in the histograms, as measured by the standard deviations, decreases in the order, LF array, HF array, MF array. Thus, an increase in the signal gain degradation, may be, but is not necessarily, accompanied by an increase in the spread of the histogram.

(C) The mean signal gains as a function of aperture length are illustrated in Figure 2.2. The ideal signal gain is represented by the discontinuous line segments. Its slope is 6dB/octave, where an octave represents a doubling of the length of the aperture. The continuous line segments connect the measured values. A comparison of these curves shows that the increase in the signal gain between the quarter and the half apertures is similar for all three arrays. Thus, the dipsparity in the signal gain for the three arrays occurswhen the aperture length is increased from half to full by the addition of the second half of the array. This phenomenon is believed to be heavily influenced by array deformations and will be discussed in Chapter 5.

(C) The signal gain standard deviations are plotted as a function of aperture in Figure 2.3a. For each array, the standard deviations increase linearly as the aperture is doubled, with the rate of increase for the LF array approximately double that for the MF and HF arrays. Furthermore, as is the case for the full aperture, the standard deviations for the half and quarter apertures, decrease in the order

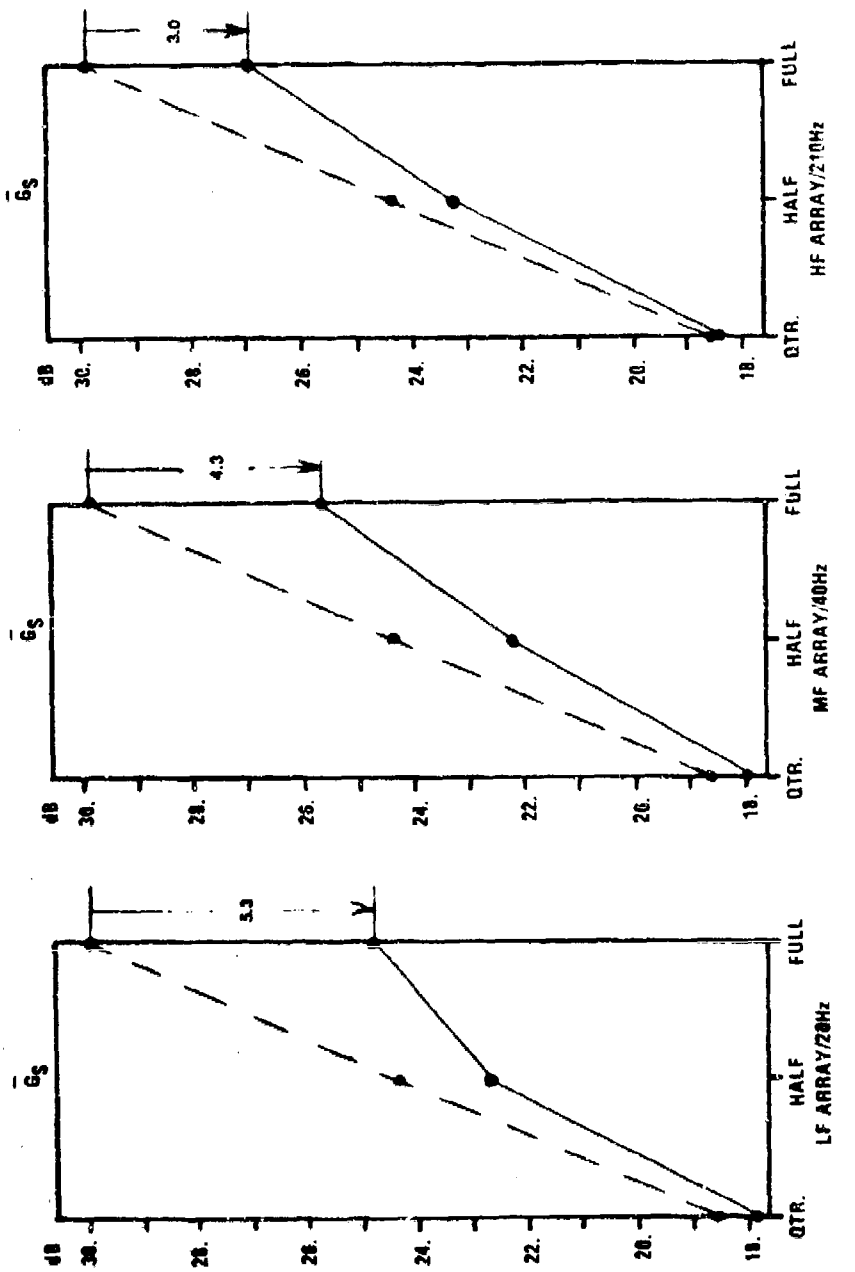

(C) Figure 2.2 Mean Signal Gain vs. Aperture

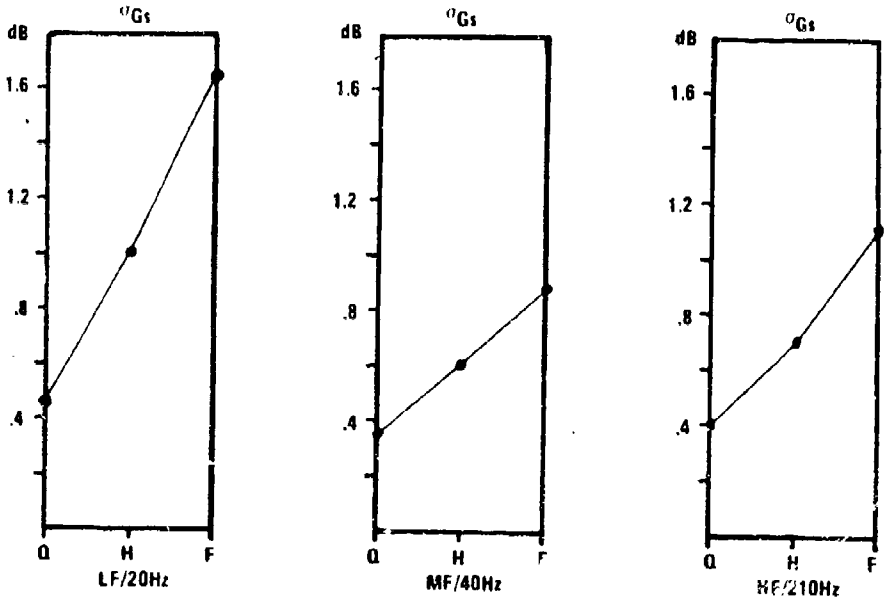

(C) Figure 2.3a Signal Gain Standard Deviation vs. Aperture

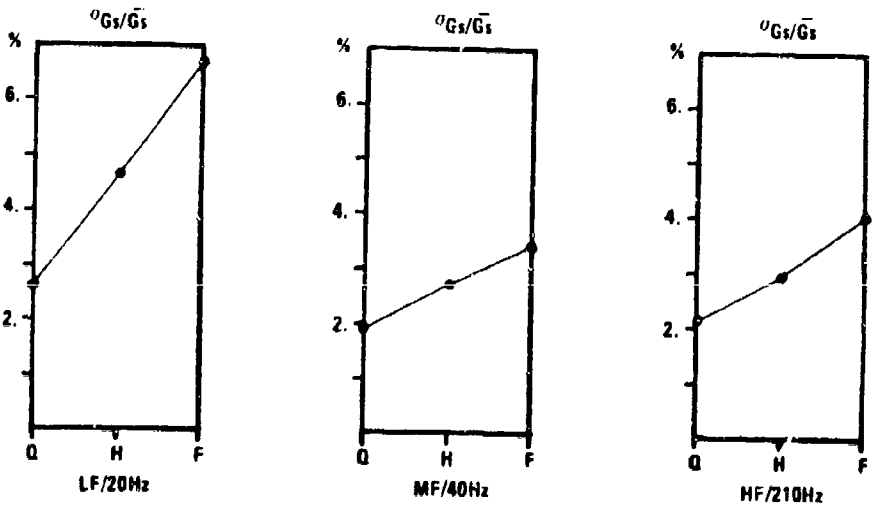

(C) Figure 2.3b Signal Gain Coefficients of Variation vs. Aperture

LF array, HF array, MF array.

(C) The relationship between the standard deviation and the mean is illustrated in terms of the coefficients of variation in Figure 2.3b. These plots show that, like the standard deviations, the coefficients of variatior increase linearly as the aperture length is doubled. Moreover, since the slopes are positive, the standard deviations are increasing with aperture at a greater rate than the means. Furthermore, the values of the coefficients of variation indicate that the standard deviation, as a percentage of the mean, is relatively small; less than 6.7% for the LF array and less than 4% for both the MF and HF arrays.

2.2 Noise Gain Statistics (U)

(C) The noise gain histograms for the full apertures are illustrated in Figure 2.4 with the means and standard deviations indicated at the side of each plot. The ideal noise gain[3] of 13.7dB is less than the mean noise gain for both the MF and the HF arrays and approximately equal to the noise gain for the LF array. The spread in the histograms for both the LF and MF arrays, as measured by the standard deviations, is almost twice that of the HF array histogram. As a result, all three arrays show a large percentage of noise gain occurrences in excess of the ideal value.

(C) The mean noise gains as a function of aperture are illustrated in Figure 2.5. The discontinuous line segments, which increase at a rate of 3 dB per octave, connect the ideal noise gains and the continuous

[3]The ideal noise gain is computed assuming a completely uncorrelated noise field.

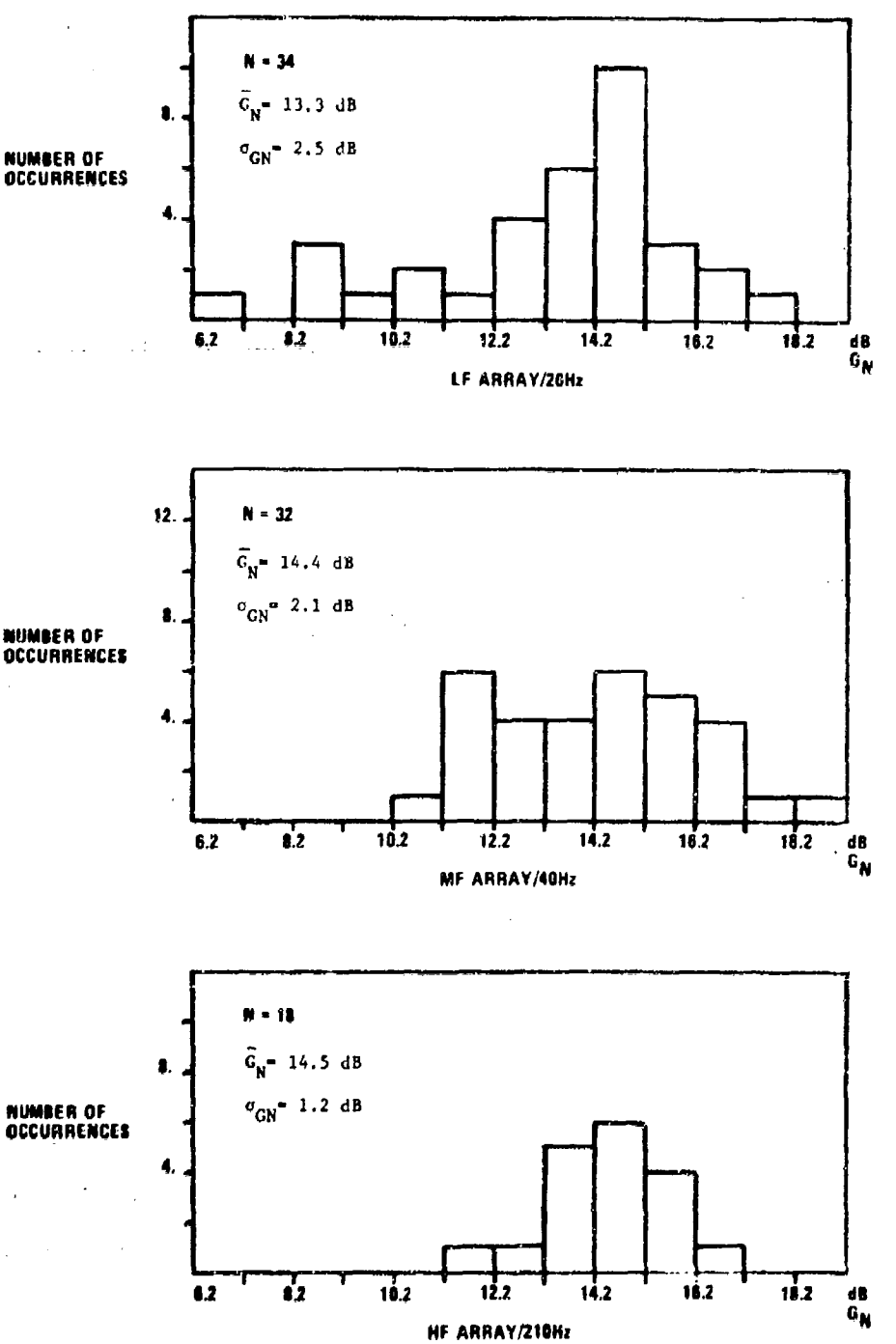

(C) Figure 2.4 Noise Gain Histograms (Full Aperture)

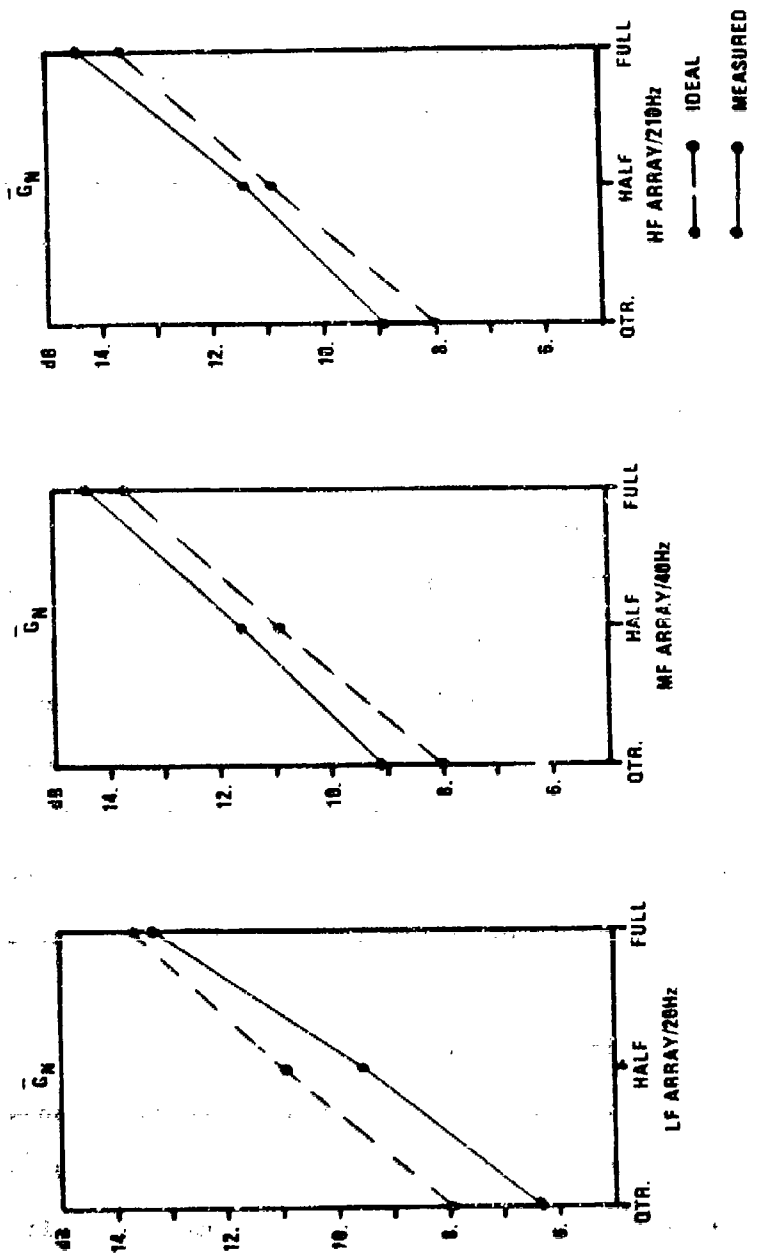

(C) Figure 2.5 Mean Noise Gain vs. Aperture

line segments connect the measured values. The plots show that the noise gains for all apertures on both the MF and HF arrays are larger than the ideal and increase at the rate of 3 dB/octave, indicating a concentration of noise power in the beam look direction. In contrast, the noise gain values for the LF array all lie below the ideal value, indicating a concentration of noise power in a direction other than the beam look direction. Furthermore, the increase in the slope between the half and the full apertures, provides further evidence of array distortion resulting from the addition of the last half of the array, since array distortion increases the effective noise beamwidth and, hence, the beam noise power.

(C) The noise gain standard deviations and the coefficients of variation are plotted in Figure 2.6. In Figure 2.6a, it is seen that for all apertures, the standard deviations decrease in the order, LF array, MF array, HF array. Furthermore, with the exception of the full aperture on the LF array, the standard deviations show little dependence on aperture. The plots in Figure 2.6b show that the standard deviation, as a percentage of the mean, is significantly higher than for the signal gain.

2.3 Array Gain Statistics (U)

(C) The array gain histograms for the full apertures are shown in Figure 2.7. The ideal array gain of 16.2 dB is the difference between the ideal signal gain and the ideal noise gain. In all cases, there are no occurrences of the array gain in excess of the ideal

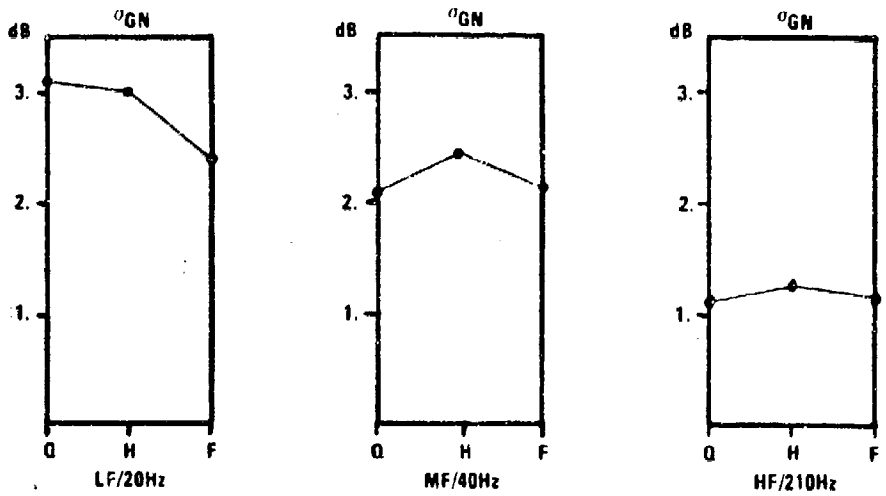

(C) Figure 2.6a Noise Gain Standard Deviations vs. Aperture

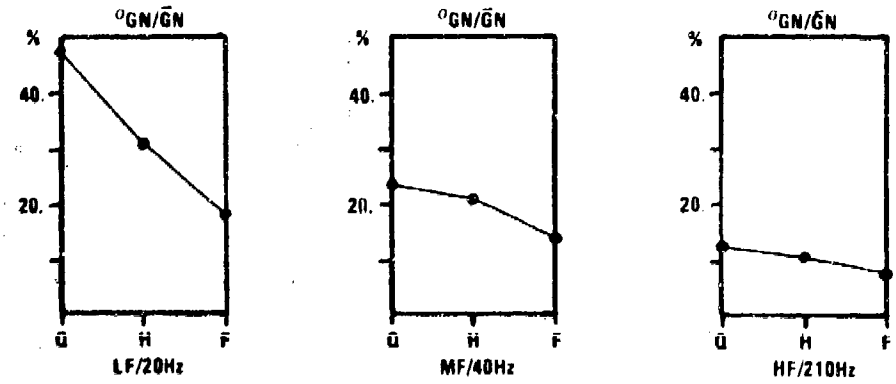

(C) Figure 2.6b Noise Gain Coefficients of Variation vs. Aperture

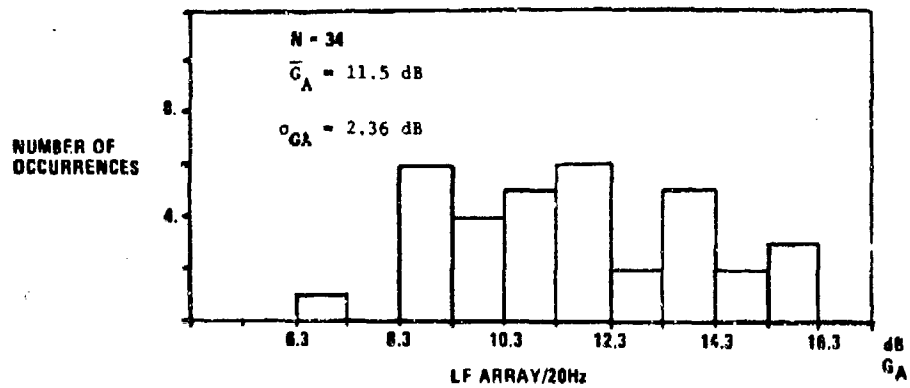

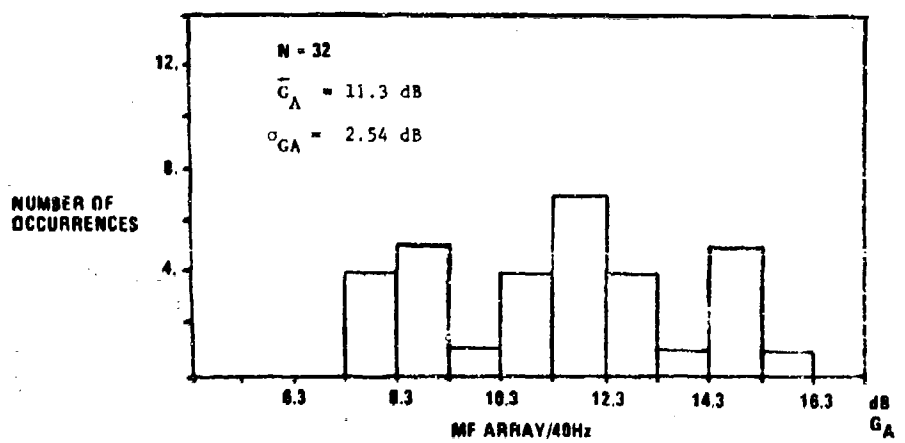

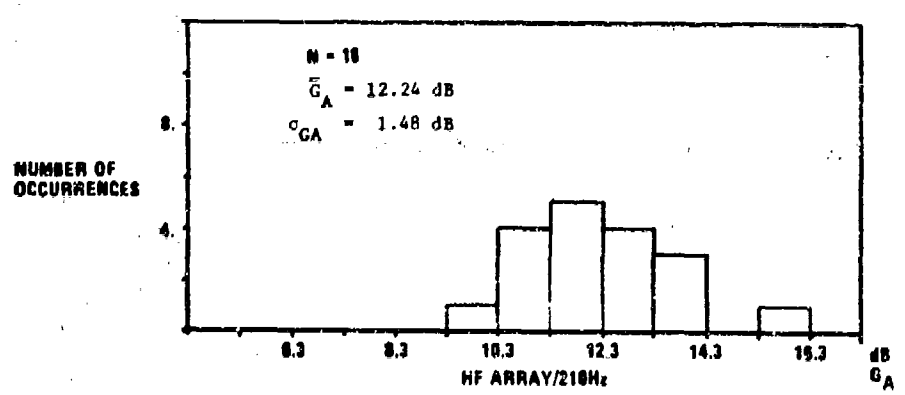

(C) Figure 2.7 Array Gain Histograms (Full Aperture)

values, indicating that high signal gains did not occur simultaneously with low noise gains. It is noted, however, from the signal gain and the noise gain histograms, (Figures 2.1 and 2.4), that these histograms in themselves, do not preclude occurrences of large values of array gain. For example, for the LF array, 15% of the noise gain values are less than -3.5 dB below the ideal, and 12% of the signal gain values are greater than -3 dB below the ideal.

(C) The mean array gains are plotted in Figure 2.8 with the ideal array gain indicated by the discontinuous line segments and the measured values indicated by the continuous line segments. It is noted that, except for the full aperture on the HF array, the array gains for both the MF and HF arrays are less than those for the LF array. This does not imply that the performance of these arrays is inferior to that of the LF array. The low values of the array gain on the MF and HF arrays are due to the high noise gains, which are determined by the angular distribution of the noise power in the beam look direction. Thus, to compare the performance of the different arrays soley on the basis of array gain, it is necessary to examine the change that results as the aperture length is increased. In Figure 2.8, it is seen that all three arrays show an increase in array gain as the aperture length is doubled from quarter to half and the MF and HF arrays continue to show an increase at the full aperture. For the LF array, however, the array gain at the full aperture is significantly less than that at the half aperture, being roughly equal to the value at the quarter aperture. Thus, as is

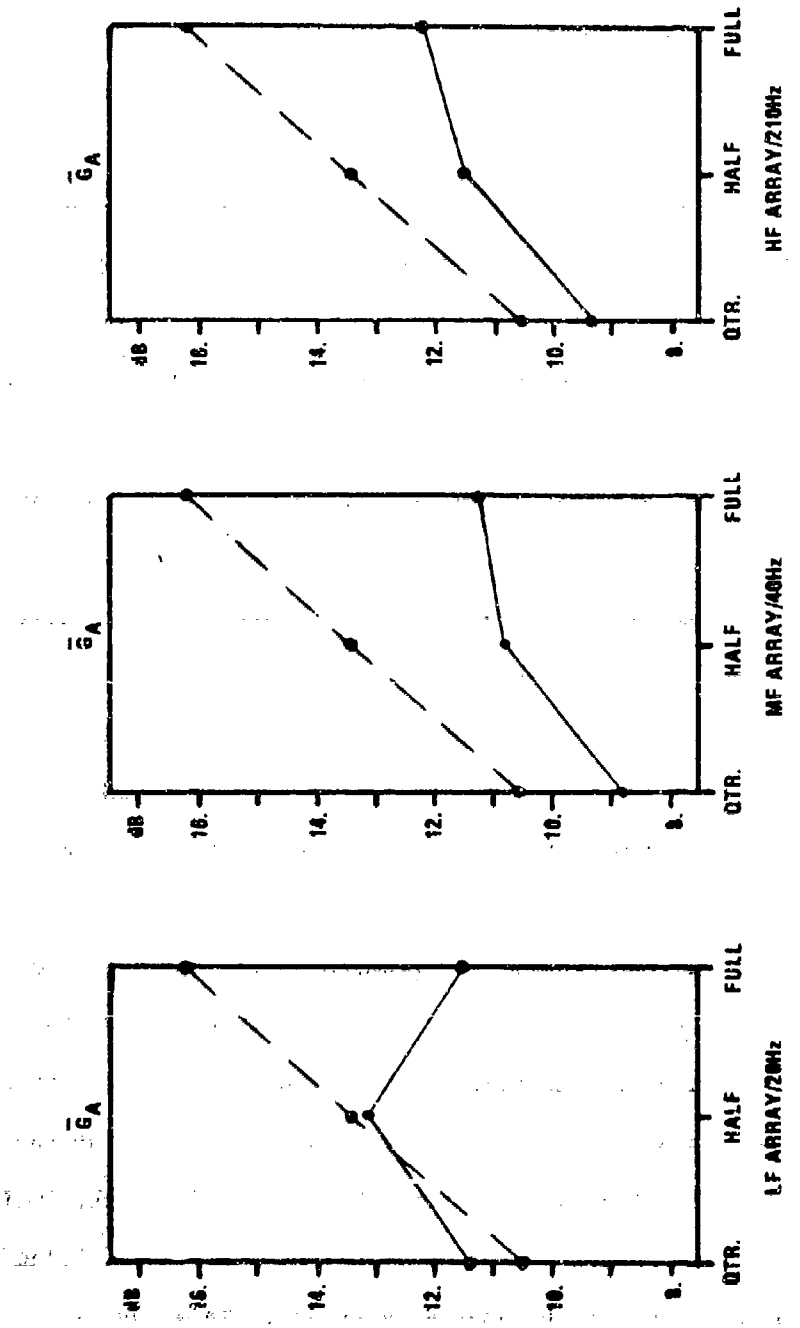

(C) Figure 2.8 Mean Array Gain vs. Aperture

expected from the results of Sections 2.2 and 2.3, there is a significant degradation in the array gain for the LF array due to the degradations in both the signal gain and the noise gain.

(C) The standard deviations and the coefficients of variation are plotted in Figure 2.9. A comparison of the noise gain and the array gain standard deviations, (Figures 2.6a and 2.9a) shows that the two sets of values are nearly identical. The difference in the noise gain and the array gain coefficients of variations, (Figures 2.6b and 2.9b), is due to the larger values of the array gain means.

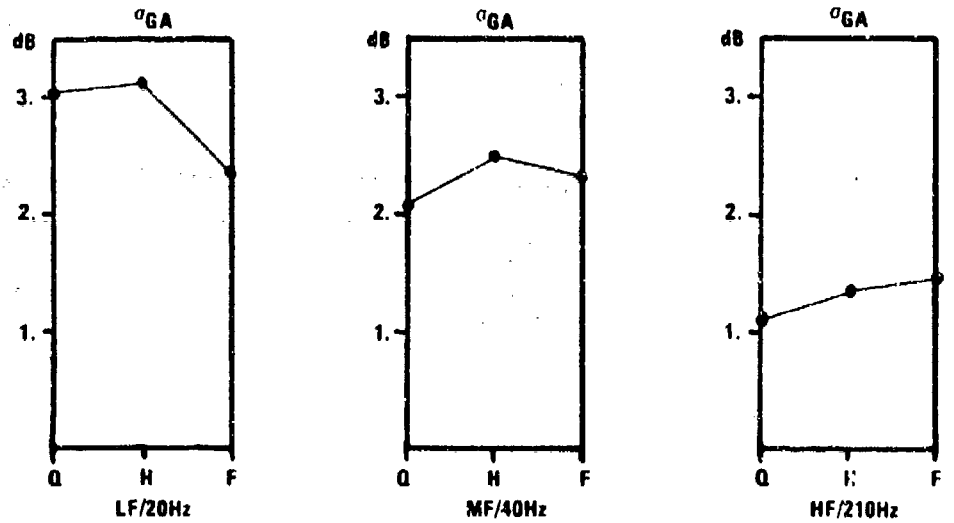

(C) Figure 2.9a Array Gain Standard Deviations vs. Aperture

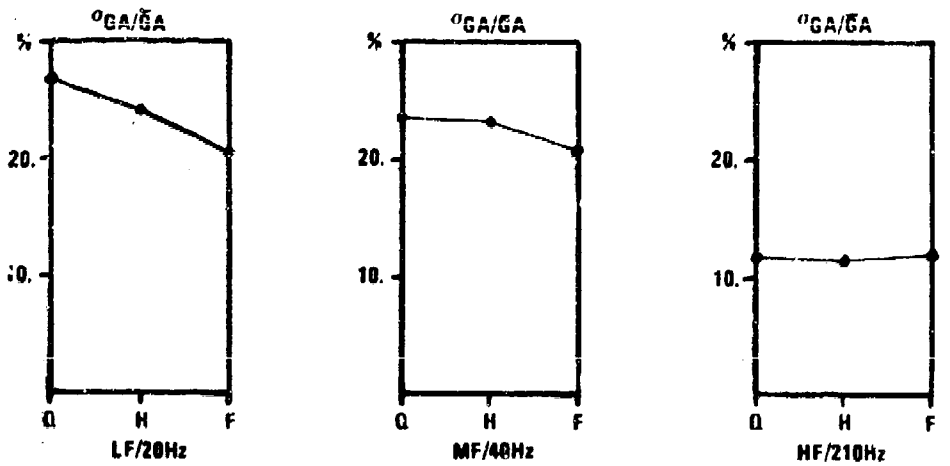

(C) Figure 2.9b Array Gain Coefficients of Variation vs. Aperture

III. STATISTICS OF SYSTEM GAIN CONSTITUENTS (U)

(U) The means and standard deviations of the beam signal and noise are of interest since detection decisions are based on these quantities The standard deviations for the omni and the cross-correlation coefficients between the omni and the beam are also of interest since these quantities are used to determine the standard deviations of the system gains. In particular, from the definition of the variance and equation 2.1a it follows that,

$$\sigma_{BS}^2 = \sigma_{BS}^2 + \sigma_{OS}^2 - 2\rho_{BS,OS}\sigma_{OS}\sigma_{BS} \tag{3.1}$$

where $\rho_{BS,OS}$ is the cross-correlation coefficient between the beam signal and the omni signal. In this chapter, the means and standard deviations of the constituents are summarized and the relationship of equation 3.1 is investigated. The means and standard deviations of the signal-to-noise ratios are plotted in Figures A.7& A.8 in the Appendix.

3.1 Beam Signal and Omni Signal (U)

(C) Plots of the standard deviations vs. the means for the omni signal are illustrated in Figure 3.1. The symbols, +, Δ and o are used to denote the full aperture, the half aperture and the quarter aperture respectively on all plots in this chapter. When the points are not easily distinguished, no aperture designation is used and and the value is represented by a point. The lack of dependence on aperture of both the means and the standard deviations for each array at each range is apparent, indicating that the 16 hydrophones for

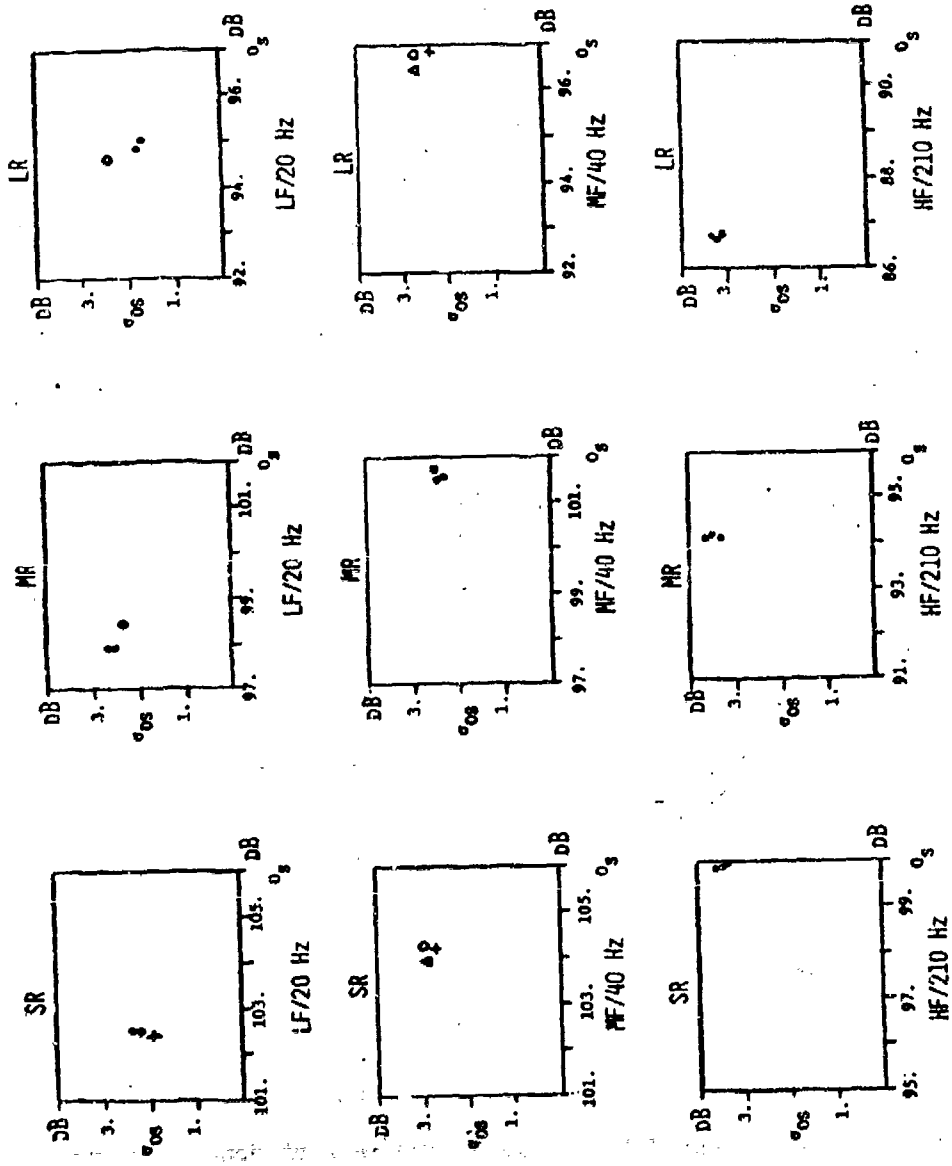

(C) Figure 3.1 Omni Signal Means and Standard Deviations

the quarter aperture are sufficient to generate an aperture-independent omni signal statistic. The lower values of the mean omni signal for the HF/210 Hz array at the medium range and long range data sets can be attributed to the 10 dB difference in the source level at the 210 Hz frequency (180 dB//μPa vs. 190 dB//μPa). The source logs also indicate the 10 dB difference at the short range, although the received omni signal levels do not reflect this difference.

(C) The corresponding plot for the beam signal is shown in Figure 3.2. In these plots the abscissa represents the mean of the relative beam signal defined as

$$B_{SR} = \overline{B_S} - \overline{G_{SI}} \tag{3.2}$$

where G_{SI} is the ideal signal gain. Thus, for an ideal planewave incident on a straight array, B_{SR} should be independent of aperture and equal to the corresponding omni signal value. Using the relative means, the degradation in beam signal for one aperture relative to another is read as the difference between the corresponding mean values. An inspection of the differences in the mean values in Figure 3.2, does not indicate a range dependence in the beam signal degradation. Furthermore, the standard deviations for each array are very nearly equal at each range showing no clear dependence on aperture.

(C) The relationship between the standard deviation of the array signal gain and the fluctuations in the beam and omni signals is investigated in the plots of Figure 3.3. Figure 3.3a shows the cross-correlation

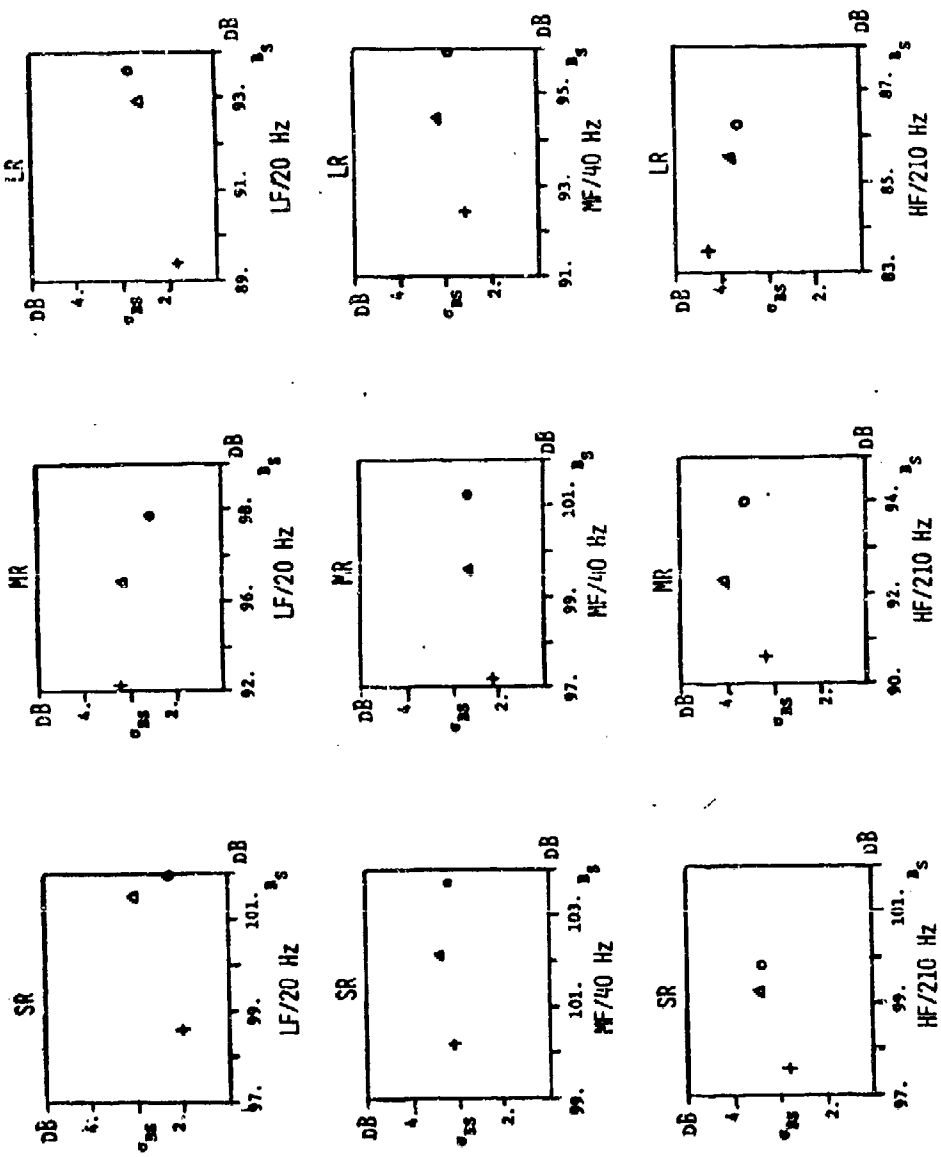

(C) Figure 3.2 Relative Beams Signal Means and Standard Deviations

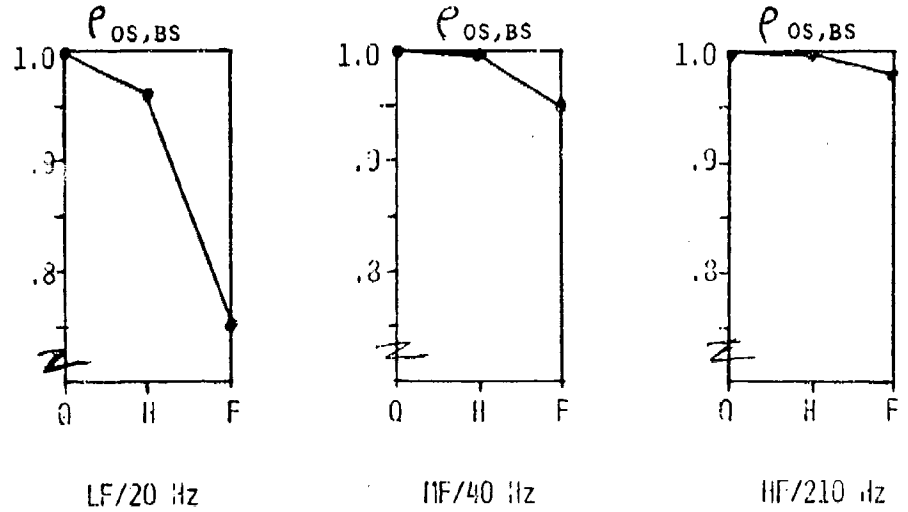

(C) Figure 3.3a Omni Signal and Beam Signal Cross-correlation Coefficients vs. Aperture

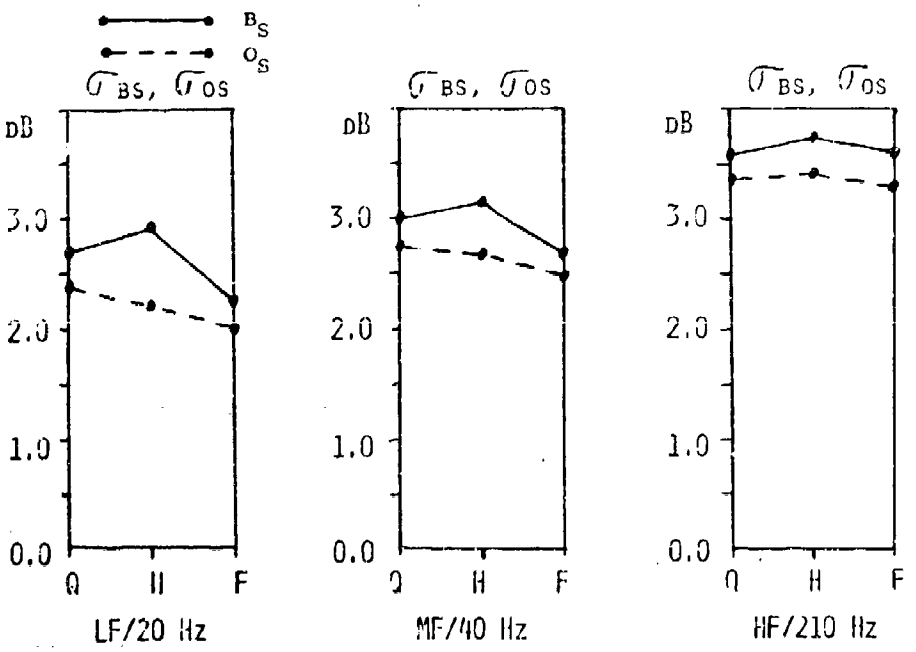

(C) Figure 3.3b Omni Signal and Beam Signal Standard Deviations vs. Aperture

coefficients between the beam signal and the omni signal averaged over range and plotted as a function of aperture. The standard deviations of the beam signal and the omni signal (also averaged over range) are plotted in Figure 3.3b. In Figure 3.3a, it is seen that for the small apertures the correlation coefficient is very nearly one so that the signal gain standard deviation is approximately given by, (see Equation 3.1 with $\rho_{OS,BS} = 1.$)

$$\sigma_{GS} = |\sigma_{BS} - \sigma_{OS}| \tag{3.3}$$

Thus, for the smaller apertures, the value of σ_{GS} is primarily determined by the difference in the standard deviations. At the larger apertures, the decrease in the correlation coefficient becomes the dominating factor which is most significant on the LF/20Hz array.

3.2 Beam Noise and Omni Noise (U)

(C) Plots of the standard deviations vs. the means for the omni noise are illustrated in Figure 3.4. As was the case for the omni-signal statistics, the means and standard deviations show almost no dependence on aperture for each array at each range. However a comparison of the clusters of points for the LF/20 Hz and the MF/40 Hz arrays show that the standard deviations increase when the mean values increase. This relationship does not appear to hold for the HF/210 Hz array. A dependence on the array/frequency combination is also evident in the standard deviations, with much smaller values occurring for the HF/210 Hz array.

(C) The plots of the beam noise standard deviations vs. the beam noise

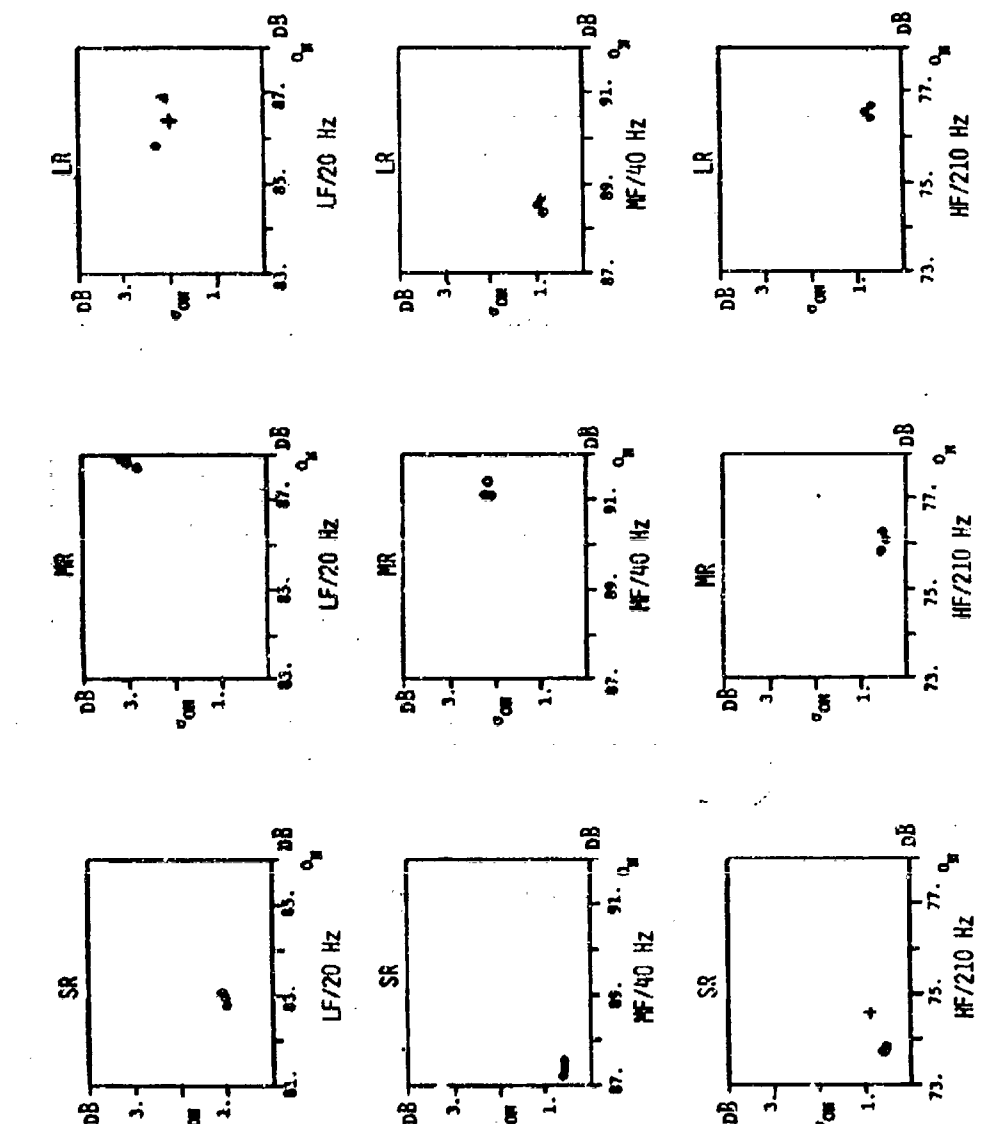

(C) Figure 3.4 Omni Noise Means and Standard Deviations

means, defined as the difference between the measured value and the theoretical value, are shown in Figure 3.5. Again, the standard deviations are approximately constant as a function of aperture with no clear dependence evident.

(U) The means and standard deviations of both the beam noise and the omni noise have also been computed for the total data set. These results are summarized in Table 3.1 and discussed in section 5.1.

	LF/20Hz	MF/40Hz	HF/210Hz
$\overline{O_N}$ (dB)	88.67	91.67	79.36
σ_{ON} (dB)	2.83	1.82	.71
$\overline{B_N}$ (dB)	87.52	92.55	80.06
σ_{BN} (dB)	2.28	2.54	1.19

TABLE 3.1 Means and Standard Deviations of Noise Gain Constituents Averaged Over Aperture.

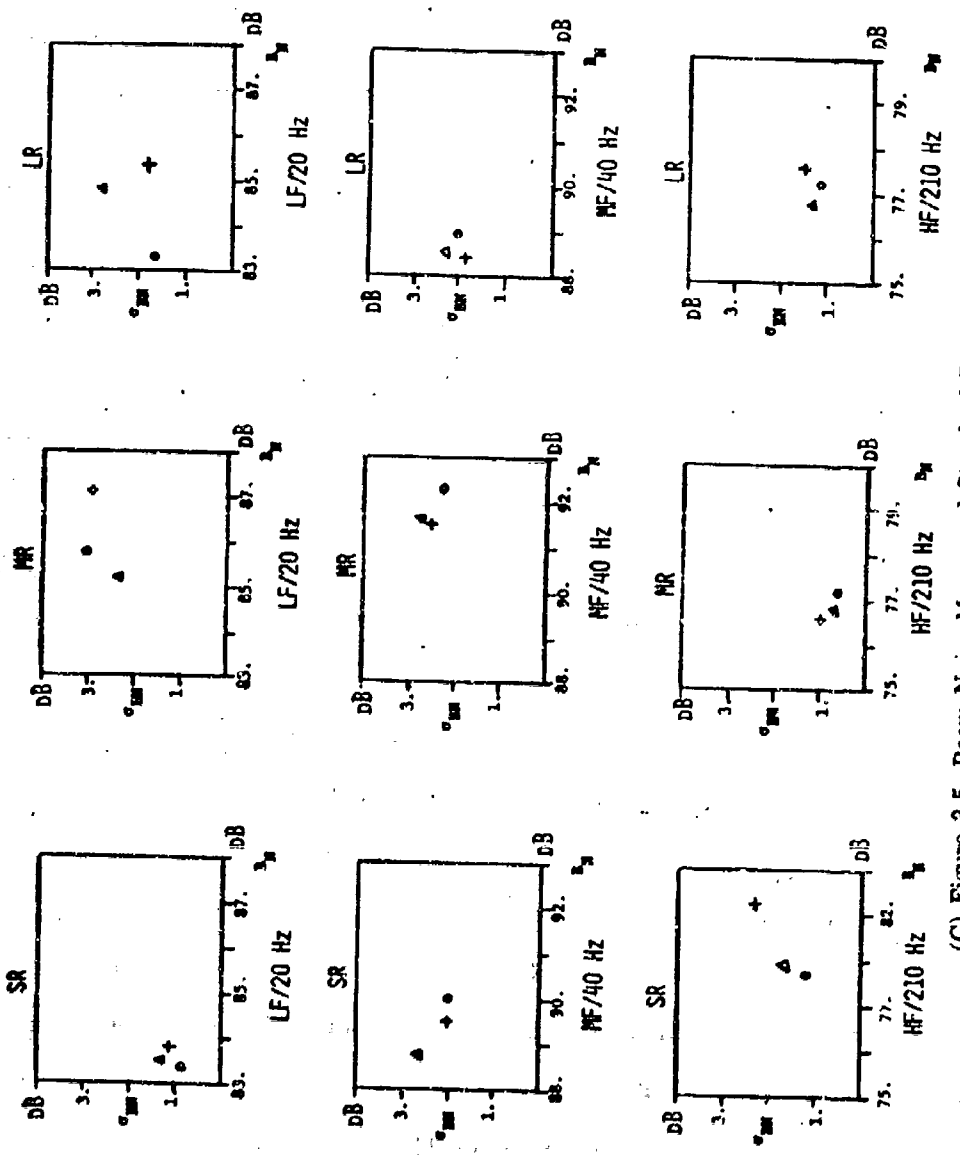

(C) Figure 3.5 Beam Noise Means and Standard Deviations

IV. STATISTICAL PROPERTIES OF THE INSTANANEOUS CONSTITUENTS (U)

(U) The fluctuations in the constituents of the system gains and hence in the gains themselves, depend on both the fluctuations in the instantaneous constituents and on the particular choice of the averager. In particular, since the system averager can be viewed as a linear time-invariant filter, the spectrum of the fluctuations at the output of any averager can be determined as the multiplication of the instantaneous fluctuations spectrum and the amplitude squared of the transfer function for the averager. (Similiarly, the auto-covariance function can be determined directly by a convolution relationship or indirectly as the inverse Fourier transform of the output fluctuation spectrum.) Thus, once the spectrum or the covariance function of the instantaneous time series is known, the selection of the averager can be made to achieve the desired system function.

(U) In this report, however, we restrict our attention to the 12-minute unweighted averager used in the computation of the system gain constituents. The fluctuations of the instantaneous constituents are described in terms of coefficients of variation, υ_i, (section 4.2). These, together with the correlation times (section 4.4) determine the coefficients of variation at the averager output, υ_a, (section 4.6) according to the relationship

$$(\upsilon_a/\upsilon_i)^2 = (\tau/T) \tag{4.1}$$

where T is the averaging time and τ is the equivalent rectangular correlation time as determined from the covariance function.

(U) A second application of the fluctuation spectrum occurs when the signal field at the hydrophone inputs is homogeneous and Gaussian. Under these conditions, the bandwidth of the fluctuation spectrum of the instantaneous beam signal is approximately equal to the bandwidth of the frequency-wavenumber spectrum describing the signal field.[4] This bandwidth in turn determines the extent to which narrowband processing can be used to reduce the signal-to-noise ratio; a reasonable criteria is to match the system analysis bandwidth to the bandwidth of the frequency-wavenumber spectrum.

(U) To complete the analysis, we investigate the hypothesis that the acoustic field for both signal and noise is time-stationary and Gaussian. A direct experimental verification of the Gaussian assumption requires testing the hypothesis that the quadrature components of the hydrophone outputs are zero mean, equal variance Gaussian random processes. An indirect method used in this report (section 4.2) is to compare the instantaneous beam output histograms against the exponential distribution since this is the expected distribution for time-stationary Gaussian fields.

In this chapter, the quantitative results are presented. The implications and interpretation of these results are discussed in Ch.V.

[4] See Section 5.4.

4.1 Histograms of the Instantaneous Beam and Omni Time Series (U)

(U) The histograms for the instantaneous beam signal and the beam noise computed on the long range data set are shown in Figures 4.1 and 4.2 respectively. Both sets of histograms exhibit the general characteristics of the exponential probability density with the possible exception of the LF array beam signal which has an apparent deficiency in probability mass at the low values. Nevertheless, all time series passed a χ^2 goodness-of-fit test against the exponential distribution at the 90% level.[5] The time series for the instantaneous beam signal and beam noise for the half and quarter apertures were not tested against the exponential distribution although a comparison of these histograms (see Figures A.9 and A.10 in the Appendix) strongly supports the hypothesis. (In fact, the noticable lack of probability mass for small beam signal values at the full aperture on the LF array is even less apparent at the quarter and half apertures.) Since the exponential density is the expected density for the unaveraged beamformer output when the acoustic field is Gaussian and wide sense stationary in time, these results support the hypothesis that both the signal and the noise fields at the hydrophone inputs are Gaussian and stationary over the time duration of the long range data set.

[5]The time-series were first decimated to obtain independent samples.

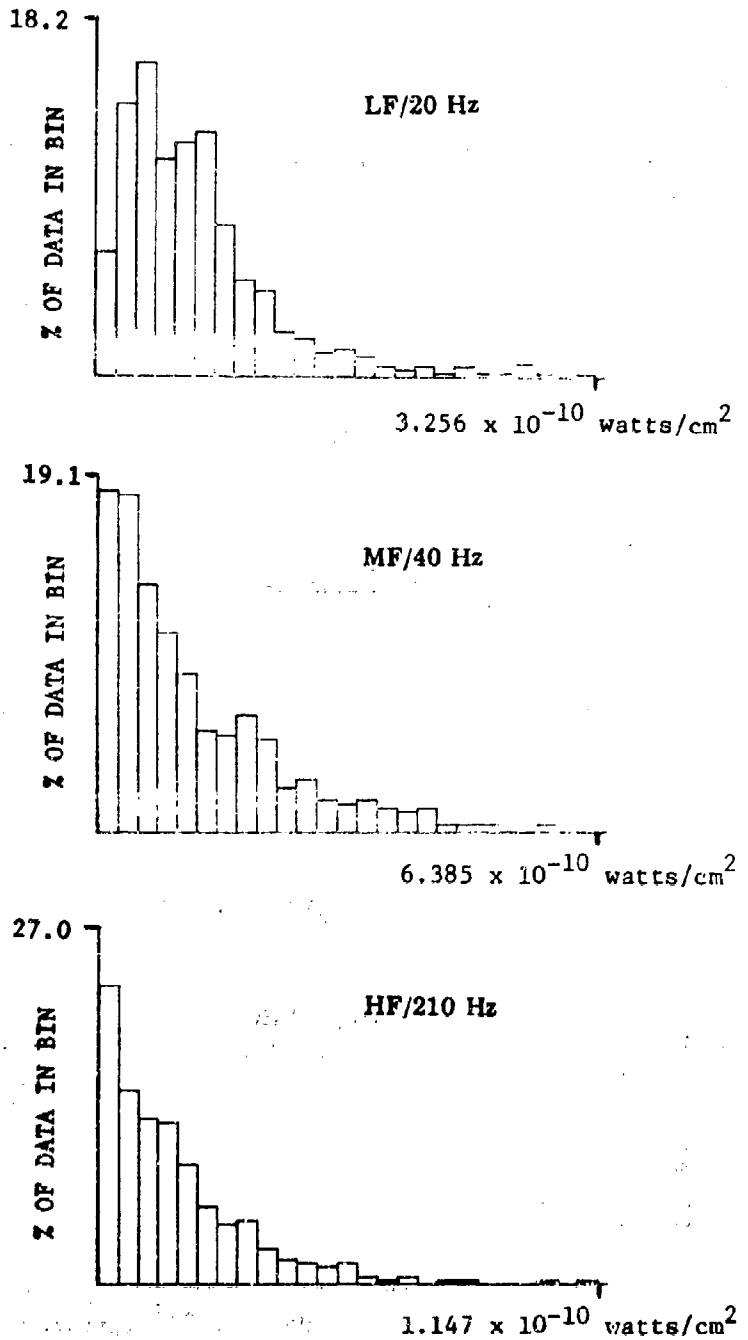

(C) Figure 4.1 Instantaneous Beam Signal Histograms (Full Aperture)

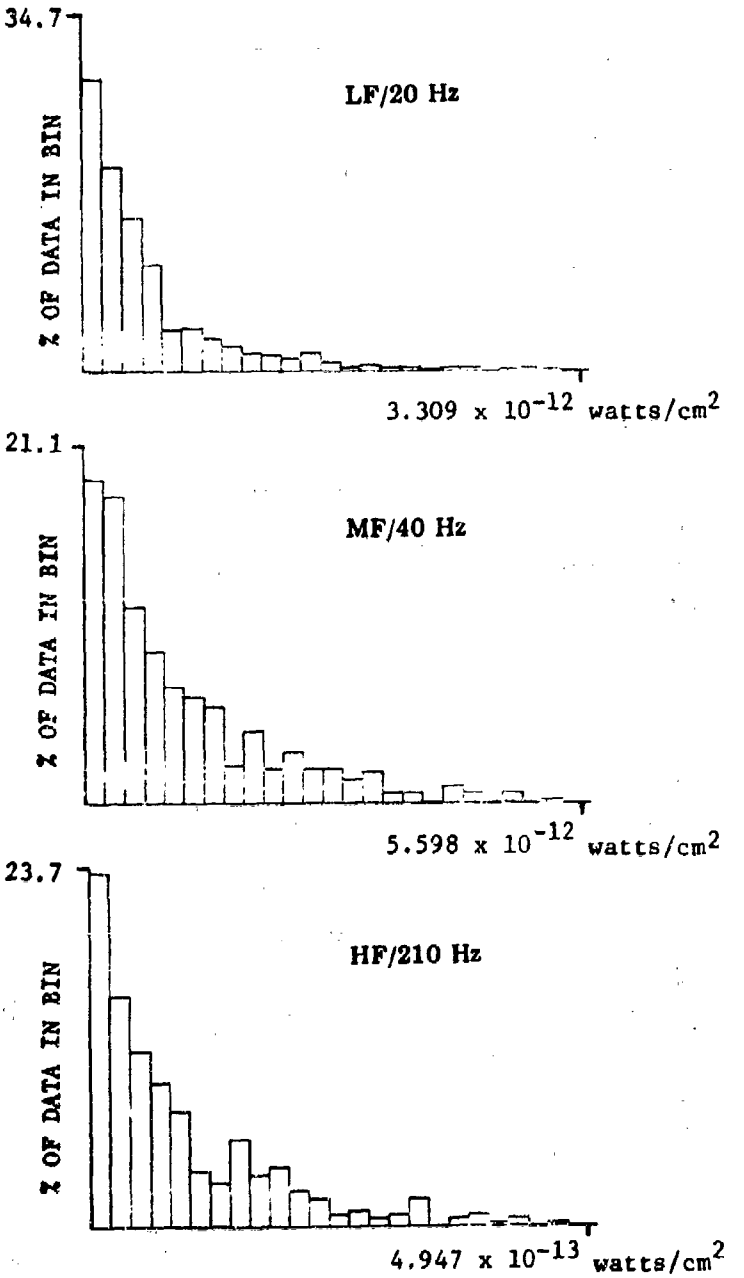

(C) Figure 4.2 Instantaneous Beam Noise Histograms (Full Aperture)

(U) The histograms for the signal and omni noise are illustrated in Figures 4.3 and 4.4 respectively. The noise histograms clearly do not exhibit the exponential charact', since there is no probability mass at the low values. This result is not inconsistent with the Gaussian field assumption, however, since the omni noise is derived as the average of the hydrophone intensities at the noise frequencies across the aperture. In fact, one would expect the probability densities for the omni noise to be approximately χ^2 with an equivalent number of degrees-of-freedom determined by the statistical dependence of the individual hydrophone intensities.[6] Extrapolating this reasoning to the omni-signal histograms in Figure 4.3, suggests that they too may be viewed as approximately χ^2, except with a smaller equivalent number of degrees-of-freedom since one would expect the hydrophone intensities for signal to be more dependent than the hydrophone intensities for noise.

(U) The histograms for the omni signals and omni noise at all apertures for the long range data set are collected for comparison and illustrated in Figures A.11 and A.12 in the Appendix. An examination of the form of these histograms indicates almost no dependence on aperture.

4.2 Coefficients of Variation for the Instantaneous Beam and Omni Signals (U)

(U) The coefficients of variation for the instantaneous beam signals and the omni signals, averaged over the three data-sets, are plotted in Figure 4.5. The measured values for the beam signal are connected by continuous line segments, while broken line segments connect the measured values for the omni signal. This convention will be followed throughout

[6] If the individual hydrophone intensities were statistically independent, the omni noise would be exactly χ^2.

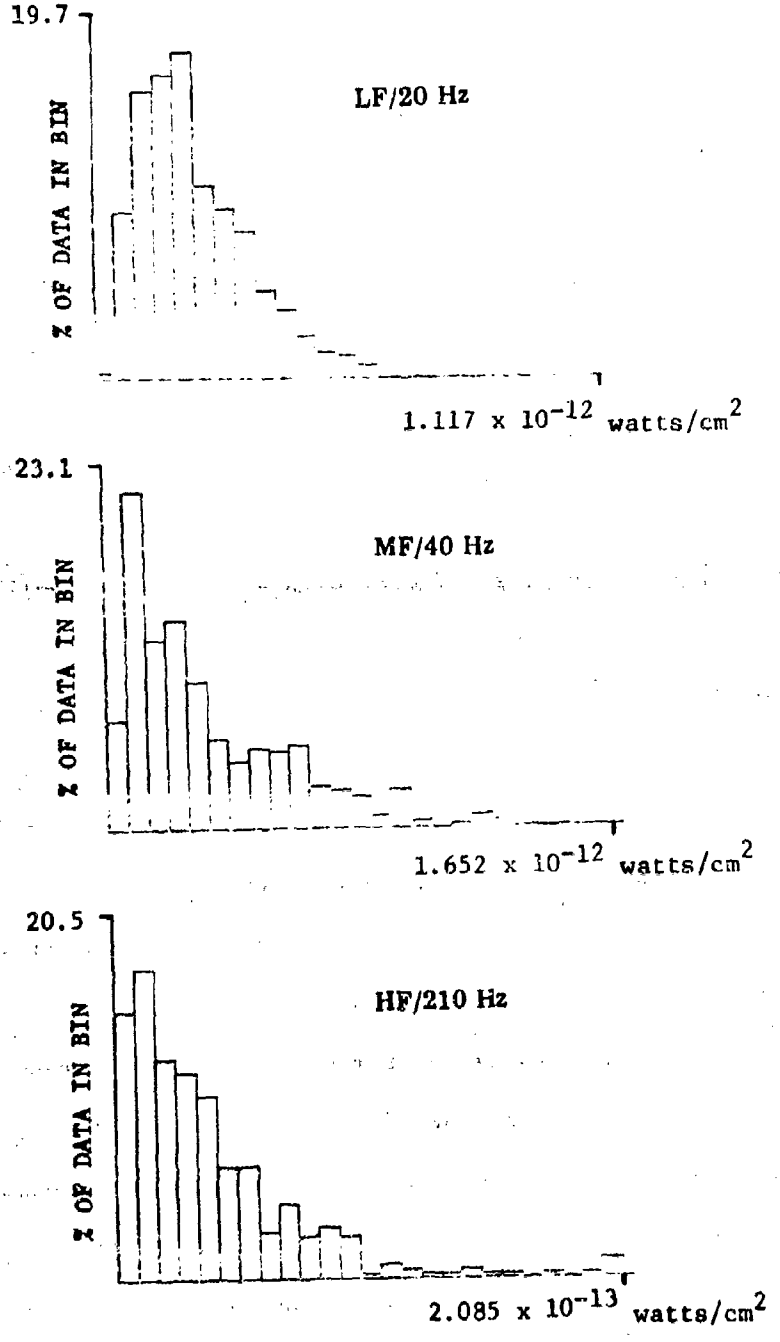

(C) Figure 4.8 Instantaneous Omni Signal Histograms (Full Aperture)

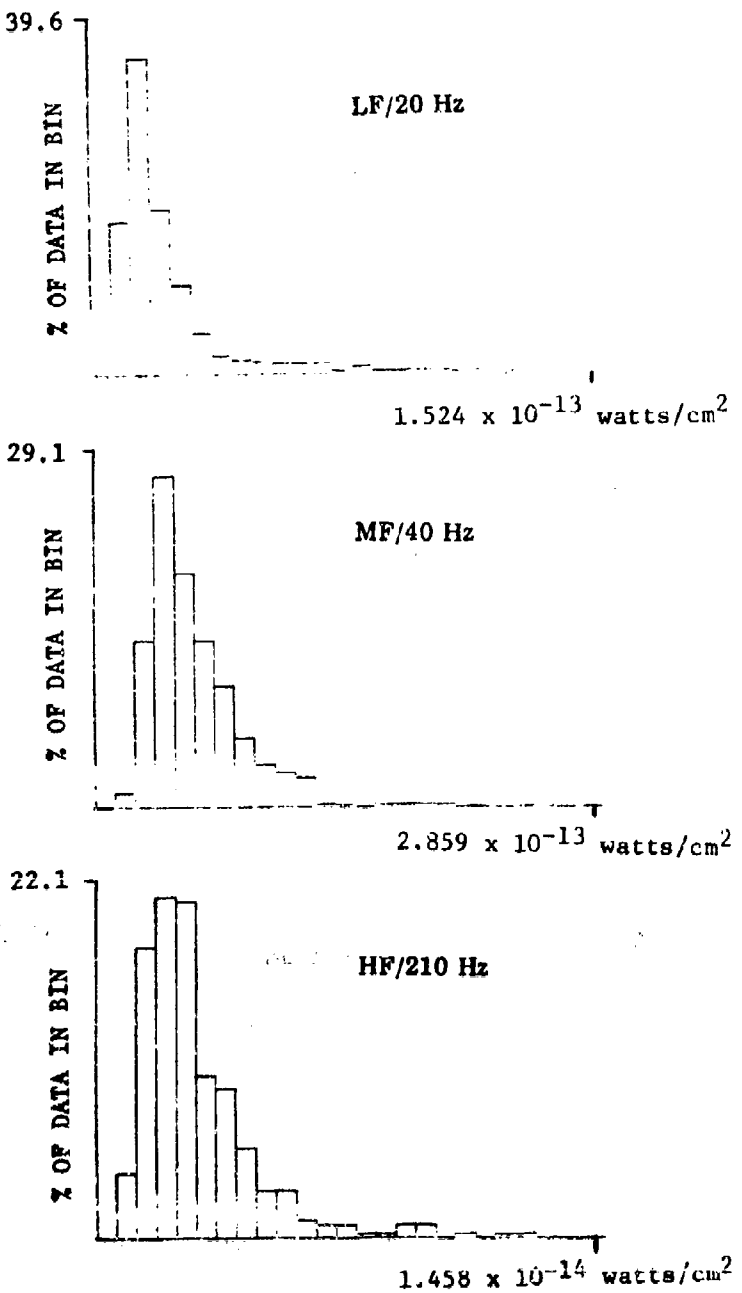

(C) Figure 4.4 Instantaneous Omni Noise Histograms (Full Aperture)

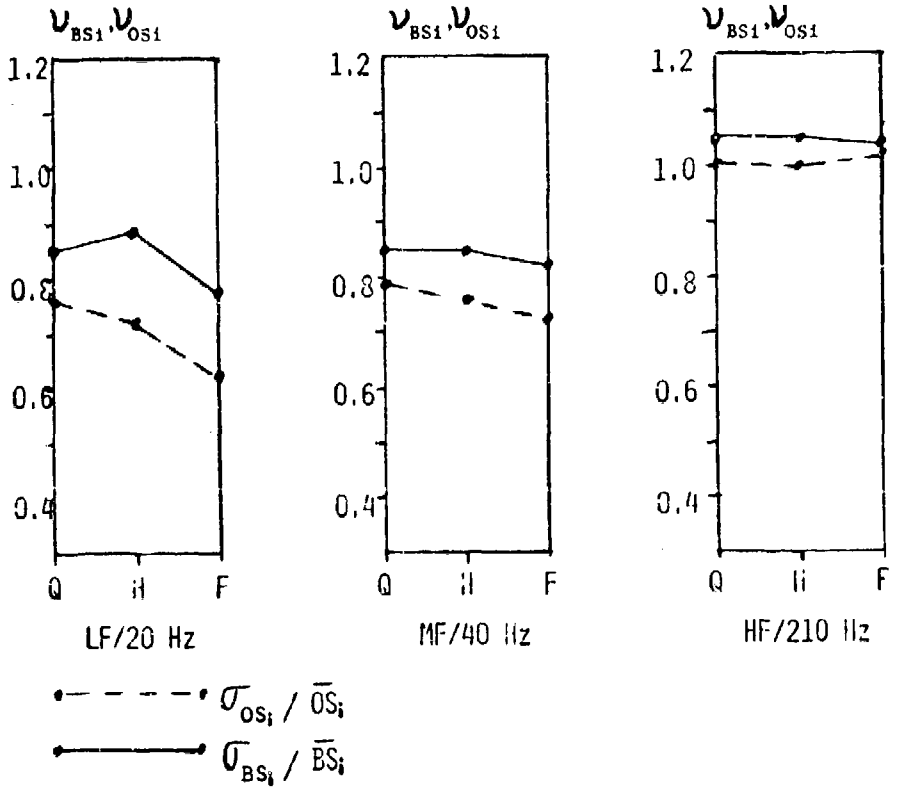

(C) Figure 4.5 Instantaneous Beam and Omni Signal Coefficients of Variation vs. Aperture

this chapter. Three phenomena are shown in this figure. First, the coefficients of variation are approximately constant with respect to aperture for a given array/frequency combination. Second, the coefficients of variation for the beam signals are higher than those for the omni signals, reflecting the difference in the coherent averaging used in the beamforming and the incoherent averaging used in the formation of the omni statistics. Third, there is a notable difference between the values for the HF/210 Hz array and those for the MF/40 Hz array and the LF/20 Hz array, indicating less fluctuations in the instantaneous signals at the lower frequencies.

4.3 The Instantaneous Beam Signal Fluctuations Spectra and Covariance Functions (U)

(U) In this section, the general character of the beam signal fluctuations spectra and covariance functions is described. The summary of the fluctuation bandwidths and correlation times is contained in the following section.

(U) The spectrum of a time series of instantaneous power has a specular component at zero frequency equal to the square of the mean power and a continuous portion representing the distribution in frequency of the fluctuations about the mean. In this report, the fluctuations spectrum is defined as the continuous portion of the total spectrum. It then follows, that the covariance function of the time series is the inverse Fourier transform of the fluctuations

spectrum, whereas the correlation function is the inverse transform of the total spectrum.

(U) The beam signal fluctuation spectrum for the full aperture, MF/40 Hz array,[7] is shown in Figure 4.a. The frequency axis for the fluctuations spectrum is expressed in cycles per hour (cph) on a linear scale with the maximum value equal to the folding frequency of 89.3 cph. The continuous curve, which describes the fluctuations spectrum itself, represents the fluctuations in 4.5 cph analysis bandwidths. For reference purposes, the specular component due to the mean in the time series is represented by the point at the zero frequency value. The value of the mean, expressed in decibel units, is indicated on the plot. As seen in Figure 4.6a, the fluctuations spectrum falls off rapidly with most of the power concentrated in the first 10 cph. The bandwidth of this spectrum, as computed using an equivalent rectangular definition,[8] is 5.0 cph.

(C) The covariance function for the MF array as illustrated in Figure 4.6b. The time axis is expressed in minutes and the ordinate values have been normalized by the value of the covariance function at zero delay. It is noted, that the covariance function falls off gradually,

---

[7] The fluctuations spectra are estimated as averages of spectra computed on 13.4 minute time intervals. The covariance functions are obtained as inverse transforms. All spectra and covariance functions illustrated in this section were computed on the long range data set.

[8] The equivalent rectangular bandwidth, BW, for a fluctuations spectrum, S(f), is defined as $BW = (\Sigma S(f))(\Delta f / \Sigma S(f))$. The equivalent rectangular correlation time is then given by $\tau = (2BW)^{-1}$.

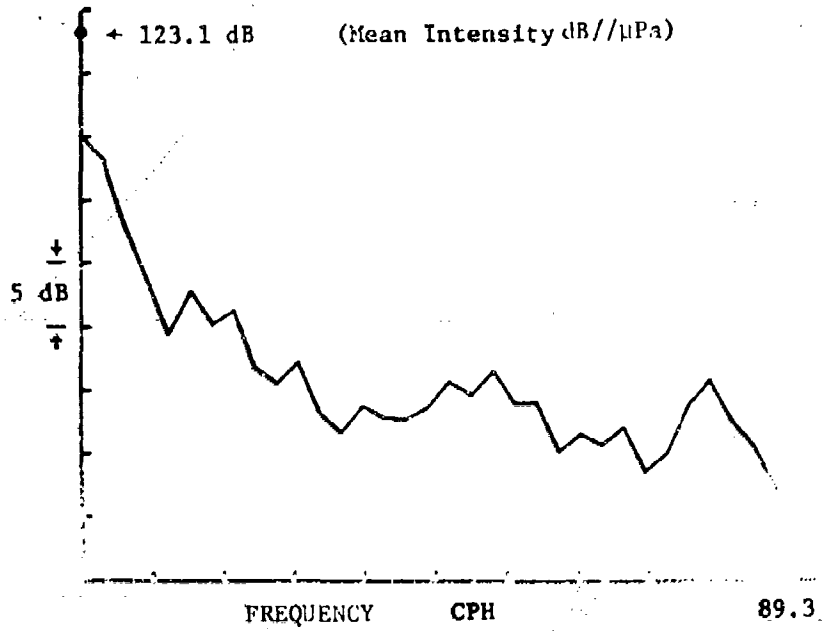

(a)

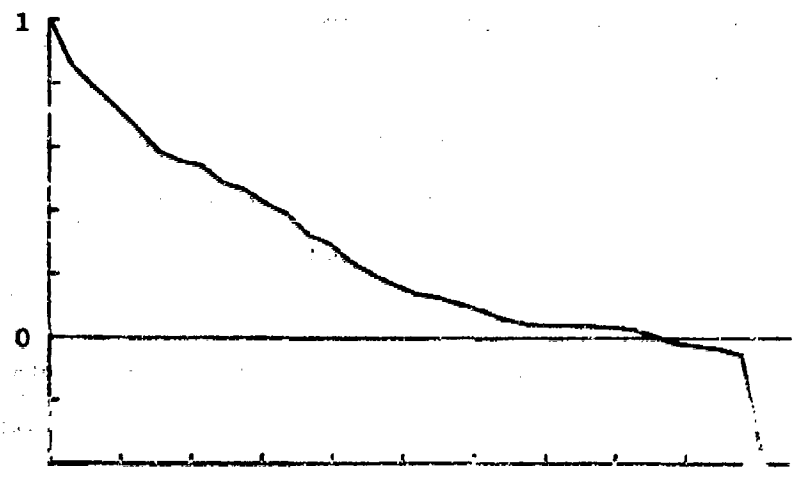

(b)

(C) Figure 4.6(a) Instantaneous Beam Signal Fluctuation Spectrum and (b) Normalized Covariance Function for MF/40 Hz Array (Full Aperture)

reaching zero after approximately 9 minutes. The correlation time, also computed using an equivalent rectangular definition, is 6.0 minutes.

(C) The fluctuations spectrum and the covariance function for the full aperture on the HF/210 Hz array are shown in Figure 4.7. In Figure 4.7a, it is seen that a greater percentage of the power in the fluctuations spectrum is contained near the zero frequency value and that there are two small broad specular components located at 16 cph and 38 cph. Nevertheless, even though the shape of this spectrum differs somewhat from that of the MF/40 Hz spectrum, the fluctuation bandwidth of 5.1 cph is only slightly larger. The covariance function for the HF/210 Hz array, illustrated in Figure 4.7b, shows more variation in the tails as a result of the greater specular content in the fluctuations spectrum. The correlation time of 5.8 minutes, however, is only slightly smaller than for the MF/40 Hz covariance function.

(C) The fluctuations spectrum and the covariance function for the full aperture, LF/20 Hz array are illustrated in Figure 4.8. These plots show that an even greater percentage of the power in this spectrum is resident near the zero frequency value, resulting in a smaller bandwidth of 4.4 cph. The larger values of the low frequency components of the spectrum appear as the plateau in the covariance function causing an increase in the correlation time to 6.8 minutes.

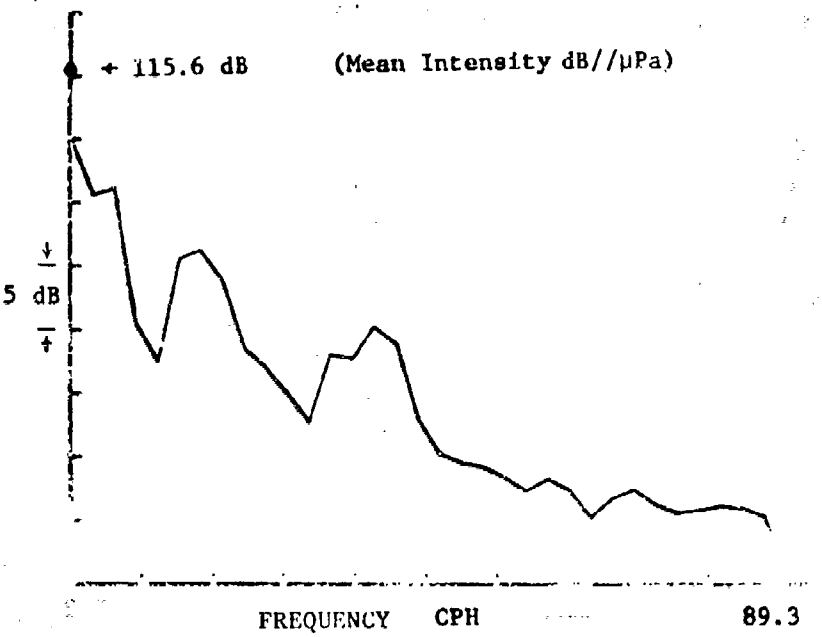

(a)

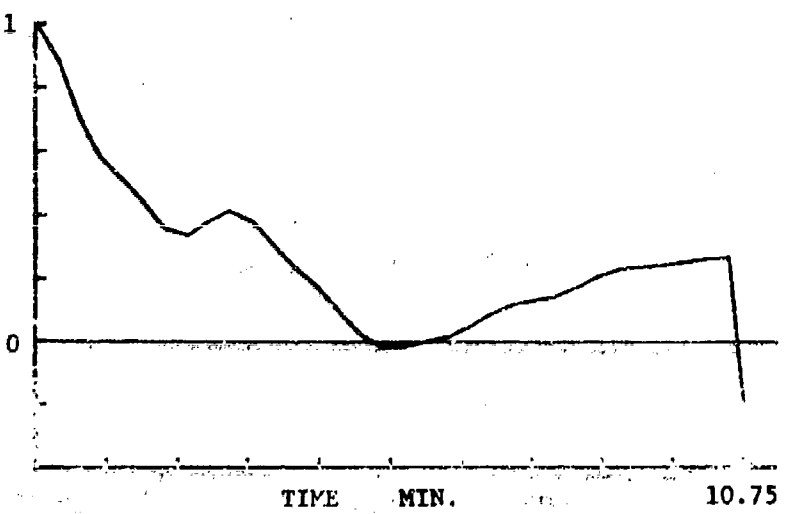

(b)

(C) Figure 4.7(a) Instantaneous Beam Signal Fluctuation Spectrum and (b) Normalized Covariance Function for HF/210 Array (Full Aperture)

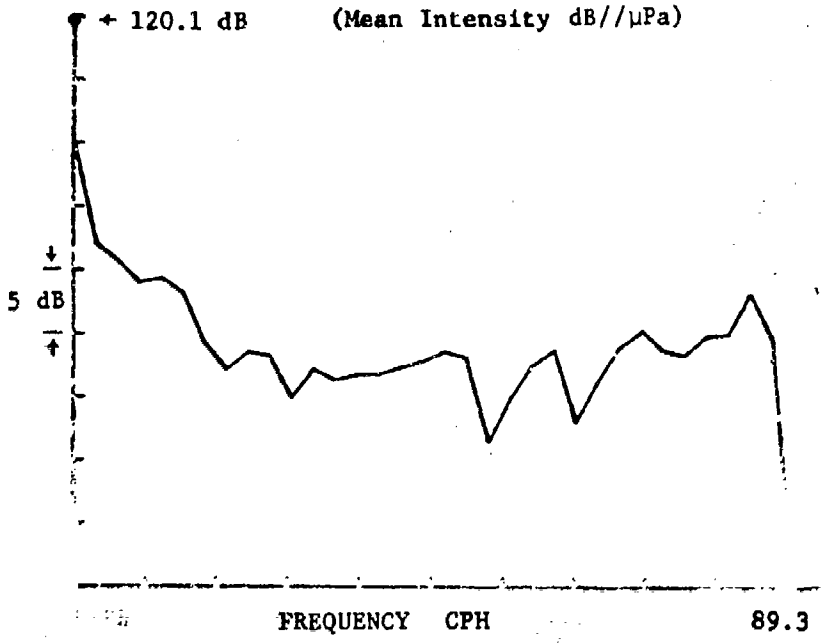

(a)

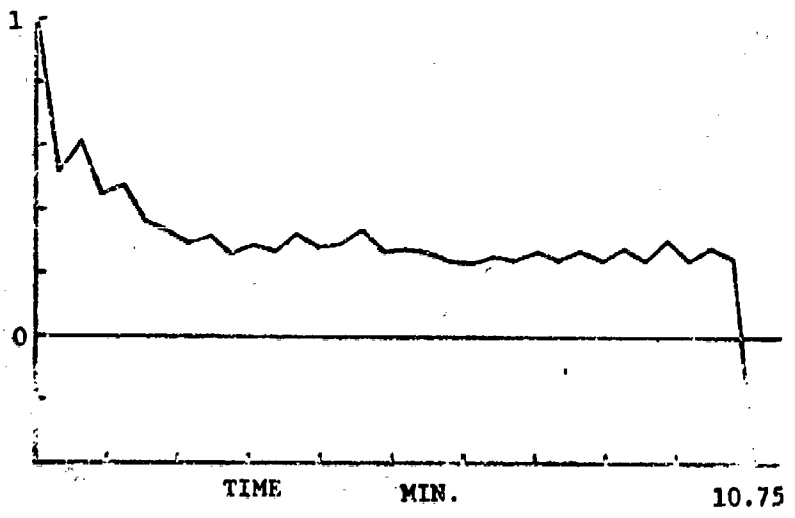

(b)

(C) Figure 4.8(a) Instantaneous Beam Signal Fluctuation Spectrum and (b) Normalized Covariance Function for LF/20 Hz Array (Full Aperture)

(C) The fluctuations spectra and covariance functions for all apertures on the long range data set are illustrated in Figures A.13 and A.14 in the Appendix. The similarity in the form of both the spectra and the covariance functions for the different apertures on each array is evident in these figures. The fluctuations power in the tails of the spectra is slightly larger for the shorter apertures due to the lower signal-to-noise ratio. In the low frequency region, however, which contains the significant signal power, there is essentially no difference for the MF/40Hz and HF/210Hz arrays and only a small reduction in the spread of the spectrum at the full aperture on the LF/20Hz array. These characteristics are also present in the spectra and covariance functions computed om the short range and medium range data sets.

4.4 The CorrelationTimes for the Instantaneous Signal Gain Constituents.

(C) The correlation times for the beam and omni signals have been averaged over the three data sets and are plotted in Figure 4.9. As expected from the form of the covariance functions, the beam signal correlation times (indicated by the continuous line segments) show no dependence on aperture for the MF/20Hz and HF/210Hz arrays and only a small increase with aperture for the LF/20Hz array. Furthermore, the beam signal correlation times do not show a dramatic decrease as the transmission frequency increases, as might be expected from physical considerations. A possible explanation for this lack of

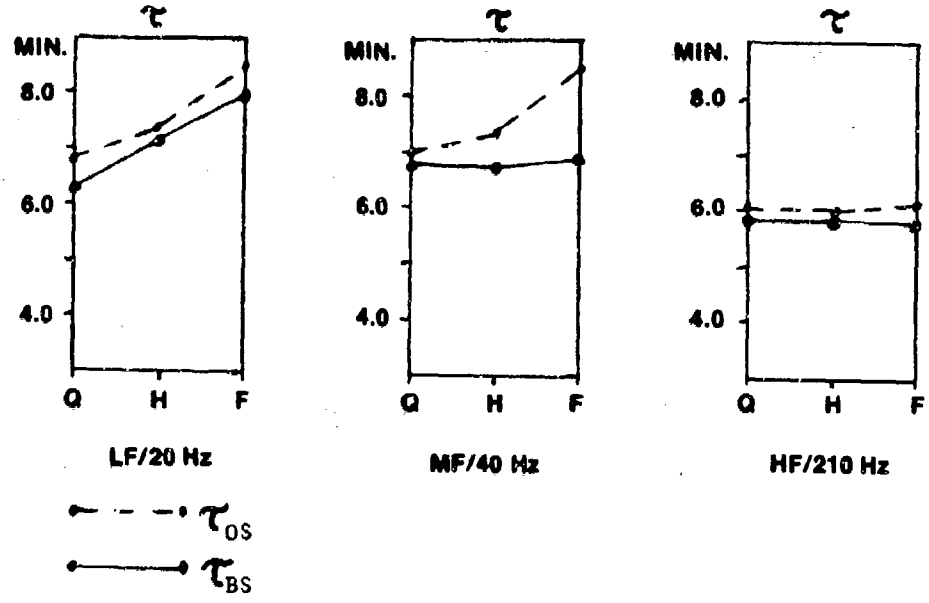

(C) Figure 4.9 Instantaneous Beam and Omni Signal Correlation Times vs. Aperture

dependence is that the temporal behavior of the received signal power may be strongly influenced by the dynamics of the array deformation process and these dynamics may differ on the three arrays.

(C) The correlation times for the omni signals are indicated by the discontinuous line segments in Figure 4.9. These correlation times show a small increase with aperture on both the LF/20Hz and the MF/40Hz arrays but are independent of aperture as the HF/210Hz arrays. Furthermore, the omni signal correlation times are slightly longer than the beam signal correlation times. Thus, the effect of the incoherent summation as compared to the coherent summation used in beamforming is to both reduce the total amount of fluctuations relative to the mean (see Figure 4.5) and to reduce the rate at which these fluctuations occur.

4.5 The Coefficients of Variation for the Averaged Signal Gain Constituents.

The coefficients of variation for the beam signal and the omni signal at the output of the 12 minute averager are illustrated in Figure 4.10. A comparison of these values with the values of the coefficients of variation for the instantaneous signal gain constituents (Figure 4.5), shows that the effect of the 12 minute averaging time has been to reduce the standard deviation by a factor of approximately $\sqrt{2}$. This result is consistent with equation 4.1 and the observed correlation times in Figure 4.9.

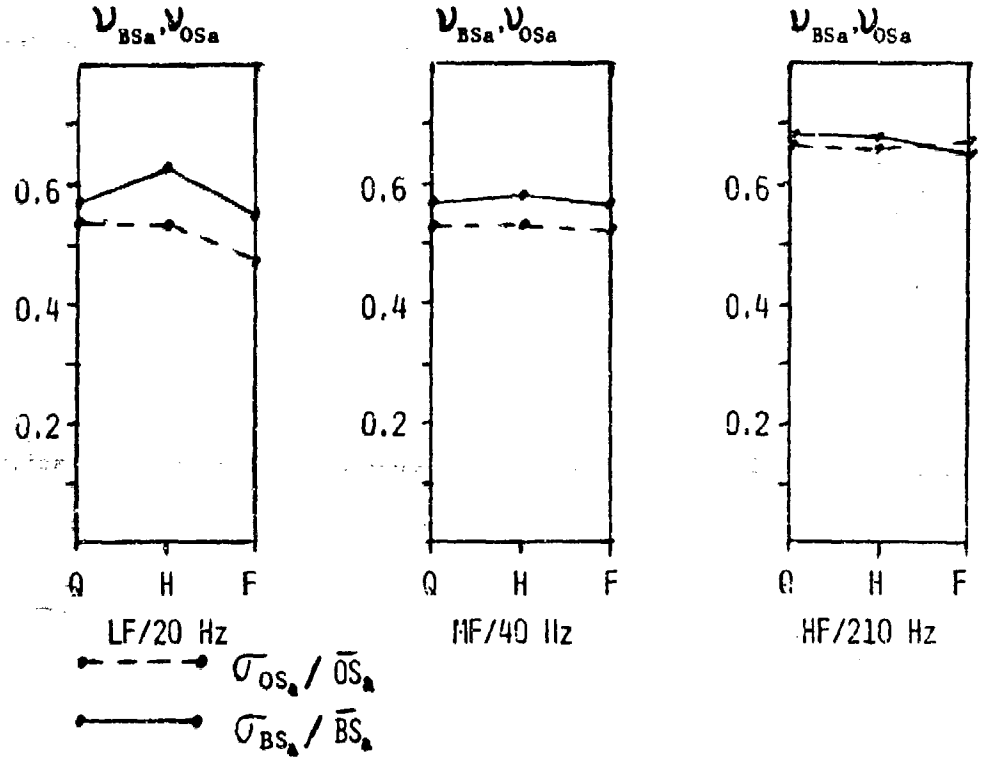

(C) Figure 4.10 Averaged Beam and Omni Signal Coefficients of Variation vs. Aperture

4.6 The Coefficients of Variation and the Correlation Times for the Noise Gain Constituents.

The coefficients of variation for both the instantaneous and the averaged beam and omni noise are illustrated in Figures 4.11 and 4.13. The correlation times are plotted in Figure 4.12. These results are discussed in section 5.2b.

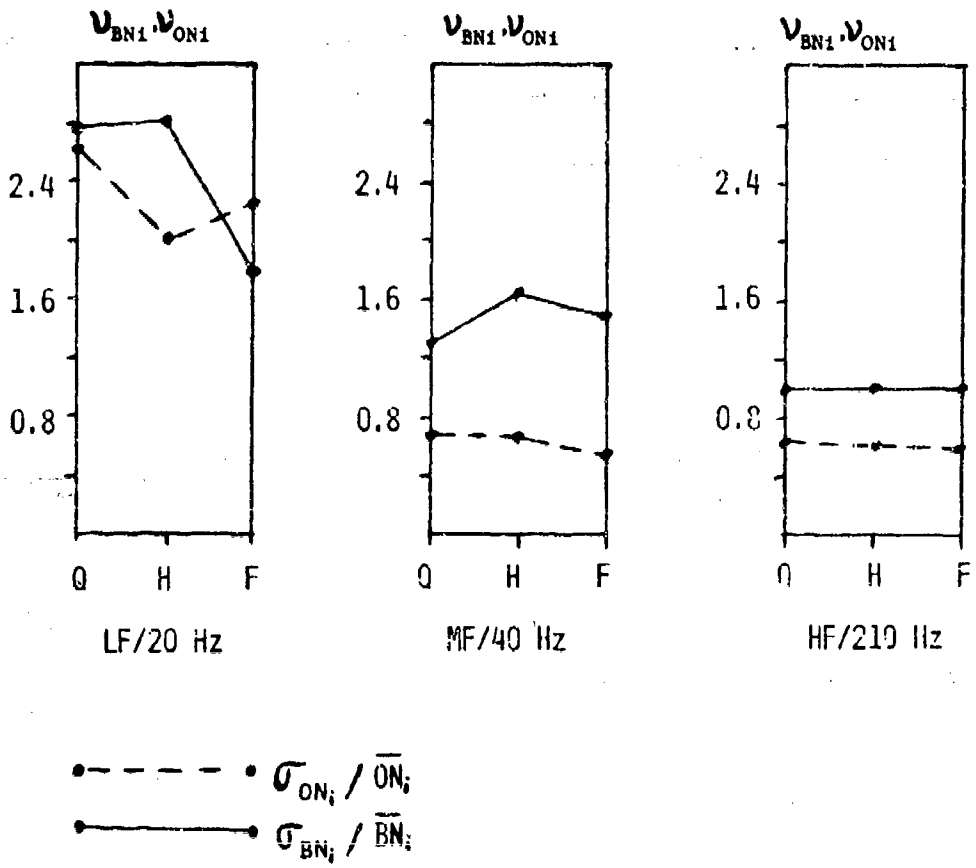

(C) Figure 4.11 Instantaneous Beam and Omni Noise Coefficients of Variation

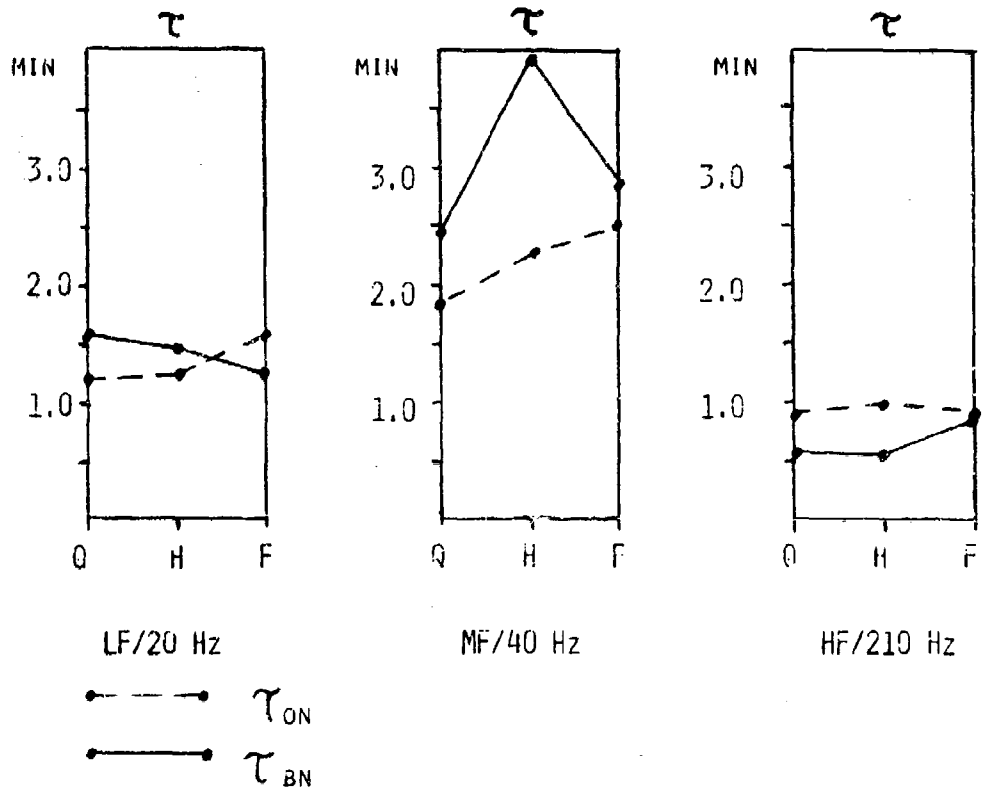

(C) Figure 4.12 Instantaneous Beam and Omni Noise Correlation Times vs. Aperture

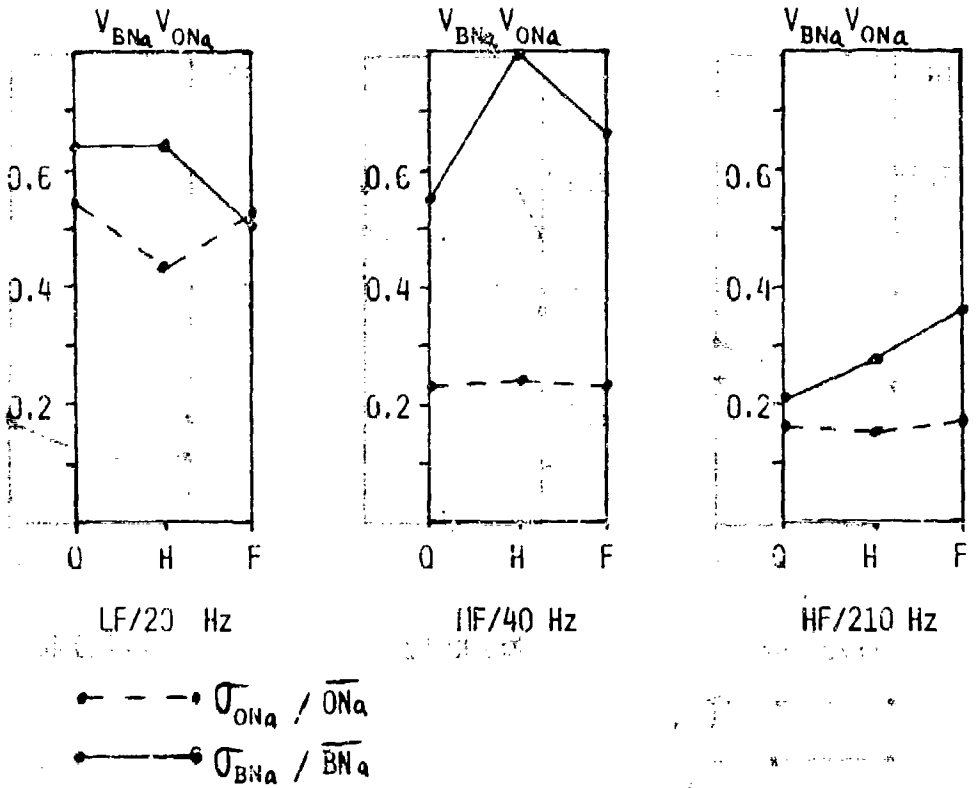

(C) Figure 4.13 Averaged Beam and Omni Noise Coefficients of Variation vs. Aperture

V. DISCUSSION OF THE RESULTS.

(U) The means and standard deviations of the three system gains and their beam and omni constituents are summarized in Section 5.1. The histograms and the temporal properties of the instantaneous beam and omni time series are summarized in Section 5.2. In Section 2.4, the implications of the beam signal temporal properties for narrowband processing are discussed. Finally, in Section 2.5, we characterize the relationship between the spatial and the temporal properties of the results for the three arrays. (U) The conclusions and the implications for the SEAGUARD/OMAT project are presented in Chapter VI.

5.1 The System Gains and Their Constituents

(C) The statistics of the system gains and their constituents have been measured using a fixed analysis bandwidth (.4Hz) and a fixed averaging time (12 min.). The dependence of the statistics on aperture is investigated at the quarter aperture (first 16 hydrophones), the half aperture (first 32 hydrophones) and the full aperture (first 62 hydrophones). In the following, references to slopes of functions of apertures are expressed as "per octave" changes where an octave is interpreted as a doubling of the number of hydrophones in the aperture.

(C) The Mean System Gains. The observed mean system gains are referred to ideal values obtained by assuming Hanning shading on a straight array with a planewave signal and uncorrelated noise. The quantitative results are as follows:

1. The full aperture signal gains for the HF, MF and LF arrays are 3.0dB, 4.3dB and 5.3dB below the ideal value of 30dB. The signal gain curves for the HF and MF arrays show a gradual increase in degradation with aperture whereas the LF curve shows a dramatic degradation between the half and the full apertures.

2. The noise gain curves for both the HF and MF arrays are linear with the ideal 3dB/octave slope and lie above the ideal curve by slightly less than 1dB. The noise gain curve for the LF array lies everywhere below the ideal curve and has a slope of 4 dB/octave between the half and full apertures.

3. The full aperture array gains for the HF, MF and LF arrays are 4dB, 5dB and 5dB below the ideal value of 16.2dB. The degradation occurs primarily between the half and full apertures with slopes of 1dB/octave, .5dB/octave and -2dB/octave for the HF, MF and LF arrays respectively.

(C) The quantitative results for the mean signal gains show the HF array to be working reasonably well with progressively larger degradations for the MF and LF arrays. Without measurements of the array dynamics and the signal coherence, it is not possible to quantify the contribution of either to the observed degradation. On the other hand, a qualitative explanation for the contribution of the array dynamics to the signal gain degradation can be found in a consideration of the configuration of three arrays, the on-line measurements of the vertical deformations of the LF array and the location of the subapertures within each array. As a result of the array configuration, the LF array acts as an 8000 foot drogue on the HF array tending to straighten it and minimize the degradation due to array deformation. On the other hand, the lack of the drogue on the LF array contributes to its instability and hence to the degradation in signal gain. This instability is evidenced by 4 depth sensor measurements which indicate

that the array tilts upward by approximately 350 feet over the front three-quarters and then drops by approximately 150 feet over the last quarter. Furthermore, since the subapertures are defined beginning at the front of each array, these measurements suggest that all apertures on all arrays can be viewed as segments which are approximately linear with the exception of the full aperture on the LF array which subtends the highly deformed last half. Thus, it is reasonable that the signal gain curve for the LF array should indicate a considerably larger degradation between the half and full apertures.

(C) The quantitative results for the noise gain emphasize the dependence of this measurement on the character of the noise field in the beam look direction. The large values of noise gain for the MF and HF arrays are due to a concentration of power in the beam look direction at 40 Hz and 210Hz whereas the smaller values for the LF array indicate that at 20Hz the noise power is concentrated elsewhere. Furthermore, the increase in the slope between the half and full apertures is additional evidence of array deformations on the LF array, since deformations of the type described above increase the effective noise beamwidth and hence increase the noise gain.

(C) The quantitative results for the array gain illustrate the shortcomings of using only full aperture measurements as an indicator of array performance. Had the analysis been based exclusively on the full aperture values of the array gain, the results would indicate that the performance of the LF and MF arrays is nearly identical and only slightly below that of the HF array. In reality, the low values of the array gain curves for

the HF and MF arrays are due to the high values of the noise gain curves and the array gain degradation is due almost entirely to signal gain degradation. On the other hand, the array gain curve for the LF array is actually enhanced, relative to the MF and HF curves, by the lower values of the noise gain and the degradation at the full aperture is due to both signal gain and noise gain degradation.

(U) The Signal Gain Constituents. The means, standard deviations and the cross-correlation coefficients for the beam signal and the omni signal have been computed on three range data sets. The time series for both the beam signal and the omni signal were obtained by expressing the averaged output in the decibel scale. The beam signal time series has been derived using a tracking algorithm based on 2 min. averages at the output of the beamformer (see section 1.2). The omni signal time series has been computed as the average of the hydrophone intensities over all of the phones in each aperture. The quantitative results are as follows:

1. For each array, the omni signal means are clustered within 1 dB of each other for each range data set with no apparent dependence on aperture. The standard deviations for each array lie within 1dB of each other for all range data sets. The averages of the standard deviations over both aperture and range are 3.4dB, 2.6dB and 2.3dB for the HF, MF and LF arrays respectively.

2. For each array, the beam signal standard deviations are clustered within 1.5dB of each other for all range data sets with no apparent dependence on aperture. The averages of the standard deviations over both aperture and range are 3.7dB, 2.9dB and 2.6dB for the HF, MF and LF arrays.

3. The cross-correlation coefficients between the beam signal and the omni signal are unity for the quarter aperture on all arrays. The curves of the cross-correlation coefficients have slopes that decrease with aperture yielding full aperture values of .98, .95 and .75 for the HF, MF and LF arrays.

(U) The omni signal results imply that the mean hydrophone intensity can be estimated with as few as 16 hydrophones distributed over one-quarter of the array. Furthermore, the fluctuations (standard deviations) do not depend on range even though the mean hydrophone intensity is range dependent.

(U) The fluctuations in the beam signal are also aperture independent and show only a slightly larger variation across the three range data sets. Furthermore, the beam signal standard deviations do not exceed the omni signal standard deviations by more than 1dB, indicating that a coherent spatial sum (beamforming) does not significantly increase the fluctuations over an incoherent spatial sum.

(U) The cross-correlation coefficients for the quarter apertures imply that the beam signal and the omni signal time series are essentially scaled versions of each other. As the aperture length is increased, however, the cross-correlation coefficient decreases and the two time series become less similar with the largest disparity occurring on the LF array. Since a coherent sum depends on the phase at the hydrophone inputs, whereas an incoherent sum does not, this result could be explained by the larger deformations experienced by the LF array. It is emphasized, however, that the relationship between the beam signal and the omni-signal time series is dependent on the particular beam tracking algorithm employed and other algorithms may yield a different relationship.

(C) The Noise Gain Constituents. The means and standard deviations of the beam noise and the omni noise have been computed on each of the three data sets and also on the combined data set. The beam noise is defined

at the same azimuth as the beam signal. Both the beam and omni noise have been computed as linear power averages over two frequencies, one on either side of the signal frequency. The omni noise for each aperture is computed as an average over the hydrophone intensities within that aperture. The quantitative results are as follows:

1. On each of the component data sets, the omni noise means are clustered within 1dB of each other and the standard deviations differ by less than .5dB with no dependence on aperture evident. The standard deviations for the HF array are essentially equal on all data sets whereas those for the MF and LF arrays differ by as much as 2dB.

2. For the combined data set, the averages over aperture of the omni noise means are 79.4dB, 91.6dB and 88.6dB for the HF, MF and LF arrays respectively; the standard deviations are .7dB, 1.8dB and 2.8dB in the same order.

3. On the component data sets, the means of the beam noise, referred to a single hydrophone, differ by as much as 2dB for the different apertures with no clear relationship on aperture size apparent. A similar disparity is evidenced by the standard deviations with a maximum difference of 1.5dB.

4. For the combined data set, the means of the relative beam noise differ by less than .75dB for the different apertures and the standrad deviations differ by less than .5dB. The averages over aperture of the mean beam noise are 80.1dB, 92.5dB and 87.5dB for the HF, MF and LF arrays respectively; averages of the standard deviations are 1.2dB, 2.6dB and 2.2dB in the same order.

(U) The omni noise results for the component data sets imply that the mean noise can be estimated with as few as 16 hydrophones as was the case for the omni signal. The fluctuations in the omni noise show a dependence on the mean for the MF and LF arrays which was not the case for the omni signal fluctuations.

(U) The beam noise statistics on the component data sets exhibit considerably more variation with aperture than on the combined data set,

emphasizing the necessity for using large data bases to estimate beam noise statistics. This requirement is a consequence of the fact that, unlike the beam signal, the beam noise time series is greatly influenced by the presence or absence of strong noise sources in the vicinity of the beam look direction. Furthermore, the variation with aperture of the statistics on the small component data sets can be attributed to the fact that the beam patterns themselves are aperture-dependent. Thus, a noise source can be at a null in the beam pattern for one aperture and at the peak of a sidelobe for another aperture causing significant differences in the two time series.

(U) The omni noise results for the combined data set show nearly a 10dB increase in the noise field at 20Hz and 40Hz (the LF and MF array frequencies) as compared to the 210Hz HF array frequency. Furthermore, the noise field is considerable less stable at the lower frequencies as evidenced by the larger standard deviations. It is important to note, however, that since the omni noise is computed from the hydrophone intensities, these statistics include the effect of the noise radiated from the array tow ship, and thus must be viewed as potentially biased estimates of the far field noise.

(U) Finally, the values of the beam noise means on the combined data set show that there is considerably more power in the beam look direction at the two lower frequencies (20Hz and 40Hz). Furthermore, the values of the standard deviations suggest a greater dependence on the presence or absence of strong noise sources in the vicinity of the beam look direction, and hence, a greater dependence on the dynamics of the shipping distribution at the

lower frequencies.

(C) System Gain Standard Deviations. The quantitative results are as follows:

1. The signal gain standard deviations for the HF, MF and LF arrays (full aperture) are 1.1dB, .9dB and 1.6dB respectively. The standard deviation curves are approximately linear with positive slopes and the common value of .4dB at the quarter aperture for all arrays.

2. The noise gain standard deviations for the HF, MF and LF arrays (full aperture) are 1.1dB, 2.1dB and 2.4dB respectively. The standard deviation curves for the HF and MF arrays do not show a significant dependence on aperture whereas the LF curve shows a .6dB drop at the full aperture.

3. The array gain standard deviations for the HF, MF and LF arrays (full aperture) are 1.4dB, 2.4dB and 2.4dB respectively. With the exception of the full aperture on the HF and MF arrays, these values are essentially equal to the noise gain values.

(U) The signal gain standard deviations are small relative to the mean signal gain (less than 7%) indicating that estimates of the mean with a small percentage error can be obtained with relatively small data bases. The results show, however, that the standard deviations increase with aperture at a faster rate than the mean so that the size of the data base required to achieve a desired quality estimate increases with aperture.

(U) The shape of the standard deviation curves can be interpreted in the light of the fluctuations of the signal gain constituents. At the quarter aperture on all arrays, both the beam signal and the omni signal are completely correlated so that the signal gain fluctuations are due to the difference in the fluctuations between the beam signal and the omni signal. At the larger apertures, however, the beam signal and the

omni signal become less correlated and the signal gain fluctuations increase even though the constituent fluctuations do not. Thus, the larger fluctuations in the signal gain for the LF array can be attributed to the smaller values of the cross-correlation coefficient.

(U) Both the noise gain and the array gain standard deviations are much larger, relative to the mean, indicating that larger data bases are required to achieve the same percentage error. This can be attributed to the larger data bases required to estimate the mean beam noise, as discussed in the preceeding section. It is noted, however, that in contrast to the signal gain results, the noise gain and the array gain fluctuations, as a percentage of the mean, decrease with aperture, indicating that the quality of the estimate increases with aperture size.

5.2 The Instantaneous Signal Gain Constituents.

(U) The results described in the preceeding section were obtained from the time series of the averaged system gain constituents expressed in a logrithmic (decibel) scale. In the remainder of this chapter, we interpret the results obtained from the instantaneous (unaveraged) constituents expressed in a linear scale.

(C) The Instantaneous Beam Signal.

(C) The salient features of the quantative results are discussed in the following paragraphs. The implications of the temporal results are discussed in sections 5.4 and 5.5.

1. The beam signal histograms exhibit the form of the exponential density for all apertures on all arrays. The full aperture histograms pass a χ^2 goodness-of-fit test against the exponential density at the 90% level.

2. The coefficients of variation for the instantaneous beam signal are independent of aperture on the HF and MF arrays and show a slight decrease at the full aperture on the LF array. The full aperture values are 1.0, 0.85 and 0.80 for the HF, MF and LF arrays respectively.

3. The beam signal covariance functions, normalized to unit variance, are independent of aperture on the HF and MF arrays and show a slight increase in time spread with increasing aperture on the LF array. The correlation times for all apertures on the HF and MF arrays are 5.8 min and 6.9 minutes respectively. The correlation times for the LF array increase from 6.4 minutes at the quarter aperture to 7.9 minutes at the full aperture.

4. The coefficients of variation of the averaged beam signal are essentially independent of aperture and equal to .63, .57 and .55 for the HF, MF and LF arrays respectively.

The exponential character of the histograms supports the hypothesis that the signal field at the hydrophone inputs is Gaussian and stationary. The Gaussian assumption is usually justified on physical grounds by viewing the propagation as a multipath phenomenon in which the receptions associated with each path are statistically independent. With this viewpoint in mind, it is not surprising that the histograms are aperture-independent since, if the inputs to some hydrophones in the array are Gaussian, then it is likely that the inputs to all hydrophones in the array are Gaussian. In this regard, however, it has been noted, (Section 4.1), that the histogram for the full aperture on the LF array bears the least resemblence to the exponential density. A possible explanation for this disparity is that the vertical deformations experienced by the LF array place some of the hydrophones in the last half of the array in a region with a different sound speed and hence a different acoustical character.

(U) The coefficients of variation for the instantaneous beam signal indicate that the fluctuations (the standard deviations) are approximately equal

to the mean and thus increase with aperture as the mean beam signal increases. Similarly, the coefficients of variation for the averaged beam signal imply that its fluctuations also increase with aperture as the mean increases. This result is consistent with the lack of dependence on aperture of the fluctuations in the logarithmic beam signal discussed in section 5.2b.

(U) A comparison of the coefficients of variation for the instantaneous with those of the averaged beam signal shows that the effect of the 12 min, averaging time has been to reduce the fluctuations by the factor $\sqrt{\tau/T}$ where τ is the correlation time and T is the averaging time. This result is a consequence of the definition of the correlation time as a measure of the equivalent rectangular spread of the covariance function. Thus, the factor $\sqrt{\tau/T}$ can be used to predict the effect of the averaging time, provided T is significantly larger than τ. In this regard, the correlation time can be viewed as the time separating independent values in the beam signal time series.

(U) To conclude the discussion, we point out that had the correlation times been aperture-dependent, then both the coefficients of variation at the averager output and the standard deviations for the logrithmic beam signal would be aperture-dependent. Thus, the lack of dependence on aperture of the logarithmic beam signal fluctuations can be explained as follows. Multipath propagation gives rise to a homogeneous Gaussian field at the hydrophone inputs. This implies an exponential density at the beamformer output at all apertures with a coefficient of varaition

equal to one. Furthermore, the signal field at the hydrophone inputs is such that its spatial and temporal properties are seperable (see section 5.4) with the result that the correlation times and hence the ratio $\sqrt{\tau}/T$ is aperture-independent. These results together insure that the coefficients of variation for the averaged beam signal are aperture-independent. Finally, the logarithmic transformation between linear power and decibel power converts the aperture independence of the coefficients of variation into an aperture independence of the standard deviations.

(C) The Instantaneous Omni Signal

The quantitative results are as follows:

1. The form of the omni signal histograms is independent of aperture on the HF and MF arrays and only slightly dependent on the LF array.

2. The coefficients of variation for the instantaneous omni signal are independent of aperture on the HF and MF arrays and show a slight decrease with aperture on the LF array. The full aperture values are 1.02, .72 and .62 for the HF, MF and LF arrays respectively.

3. The correlation times are equal to 6 minutes for all apertures on the HF array and increase from 7 minutes at the quarter aperture to 8.5 minutes at the full aperture on both the MF and HF arrays.

4. The coefficients of variation for the averaged omni signal are independent of aperture on the HF and MF arrays and show a slight decrease at the full aperture on the LF array. The full aperture values are .63, .52, and .48 for the HF, MF, and LF arrays respectively.

(U) The LF array histograms differ from the exponential density as a result of a deficiency in probability mass for the low values of the omni signal. This deficiency is less apparent on the MF array histograms and

the form of the HF array histograms is nearly identical to the exponential density. These results are consistent with the Gaussian signal field assumption since this assumption implies that the omni signal can be viewed as a sum of mutually dependent exponential random variables. Hence, the probability density should be approximately χ^2 with the number of degrees of freedom determined by the mutual dependence of the individual hydrophone intensities. Thus, the desparity between the observed histograms and the exponential density, that increases in the order HF array, MF array, LF array, can be interpreted as a decrease in the mutual dependence of the individual hydrophone intensities in the same order.

(U) The omni signal coefficients of variation express the fluctuations in the incoherent spatial average relative to the mean. For the LF and MF arrays, the coefficients of variation for the omni signal are lower than those for the beam signal, indicating that the coherent spatial averaging (beamforming) resulted in larger relative fluctuations than the incoherent spatial averaging. On the other hand, for the HF array, both the omni signal and the beam signal coefficients of variation are approximately equal, indicating that incoherent spatial averaging has not significantly decreased the relative fluctuations. A similar statement applies to the comparison of the beam signal and the omni signal correlation times. Specifically, the correlation times for the incoherent spatial average are longer than those for the coherent spatial average on the LF and MF arrays and approximately equal on the HF array.

(U) Finally it is noted that, as was the case for the beam signal, the omni signal coefficients of variation imply that the fluctuations in the omni signal increase with aperture at nearly the same rate as the means. In contrast to the beam signal, however, the omni signal fluctuations do not increase with aperture since the means do not increase with aperture. Thus, it is the lack of dependence on aperture of the coefficients of variation, rather than the fluctuations themselves, that results in aperture-independent fluctuations in the logarithmic time series discussed in section 5.1.

5.3 The Instantaneous Noise Gain Constituents.

(U) The instantaneous beam noise and omni noise were defined at a single frequency, 1.6Hz, below the signal frequency, in contrast to the logarithmic noise gain constituents which were defined as the average over two frequency bins. The intent of the single frequency definition has been to compare the temporal character of the beam noise with the beam signal to measure the extent to which averaging reduces the fluctuations in the noise relative to the signal.

(C) The Instantaneous Beam Noise.

The quantitative results are as follows:

1. The beam noise histograms for the long range date set exhibit the form of the exponential density for all apertures on all arrays. The full aperture histograms pass a χ^2 goodness-of-fit test against the exponential density at the 90% level.

2. The coefficients of variation for the beam noise are equal to unity for all apertures on the HF array, vary between 1.2 and 1.6 on the MF array and vary between 1.8 and 2.8 on the LF array. No clear relationship to aperture is evident for the MF and LF arrays.

3. The beam noise correlation times differ by less than 30 seconds at all apertures for the HF and LF arrays with average values of 0.7 minutes and 1.4 minutes respectively. The correlation times for the MF array lie between 2.4 minutes and 4.0 minutes with a full aperture value of 2.9 minutes.

4. The coefficients of variation for the averaged beam noise differ by less the 0.2 at the different apertures on each array. The averages over aperture are 0.27, 0.71 and 0.58 for the HF, MF and LF arrays respectively.

(U) The interpretation of the beam noise results is more complicated than for the beam signal since the beam noise depends not only on the acoustic propagation properties but on the dynamics of the shipping distribution in the beam look direction as well. In particular, although the hydrophone noise inputs may be Gaussian as a consequence of multipath propagation, the expected value of the noise power as seen on a particular beam may not be constant due to a time-varying mean shipping density in the beam look direction. If this is the case, the beam noise field can be viewed as Gaussian but not weakly stationary with the result that the probability density of the beam noise power is no longer exponential. On the other hand, if the mean shipping density in the beam look direction is time-independent, then the beam noise field should be both Gaussian and weakly stationary, resulting in an exponentially probability density for the beam noise power.

(U) The quantitative results for the instantaneous beam noise power support both points of view. The form of the histograms together with the χ^2 goodness-of-fit tests suggest that there are periods of

time when the mean shipping density can be considered constant, giving rise to the exponential probability density. On the other hand, the coefficients of variation for the LF and MF arrays, which were computed on the combined data set, indicate larger fluctuations than predicted by the exponential density. An examination of the time series of beam noise power vs. azimuth shows that the larger fluctuations result from strong noise sources which traverse the noise beam. Thus, the quantitative results suggest that at the lower frequencies, the beam noise field can be viewed as Gaussian and weakly-stationary only during those periods when no strong noise sources are present. In contrast, the coefficients of variation for the HF array are approximately equal to unity, the value corresponding to the exponential density, suggesting that at the 210 Hz frequency, the beam noise is effected less by occassional strong noise sources.

(U) The beam noise correlation times together with the beam signal correlation times determine the extent to which averaging can reduce the fluctuations of the noise relative to the signal. In particular, since averagers with $T \gg \tau$ reduce the fluctuations by $\sqrt{\tau / T}$, the ratio of the noise fluctuations to the signal fluctuations at the averager output can be written as

$$(5.1) \quad (\sigma_{BNa} / \sigma_{BSa}) = (\sigma_{BNi} / \sigma_{BSi}) \sqrt{\tau_N / \tau_S}$$

where the subscripts "a" and "i" denote averaged and instantaneous quantities respectively. If, in addition, the instantaneous beam fluctuations are equal to the mean values, as is predicted from the exponential

density, then equation (5.1) can be rewritten as

(5.2) $$(\sigma_{BN_i} / \sigma_{BS_i}) = \sqrt{\tau_N / \tau_S} / (S/N)_0$$

where $(S/N)_0$ is the signal-to-noise ratio at the beamformer output. In either case, the averager can reduce the fluctuations by no more than the factor $\sqrt{\tau_N / \tau_S}$. For the full aperture on the HF, MF and LF arrays these factors are .35, .66 and .42 respectively.

(C) The Instantaneous Omni Noise.

The quantitative results are:

1. The form of the omni noise histograms is independent of aperture on each array.

2. The coefficients of variation for the instantaneous onmi noise are independent of aperture and equal to 0.6 on both the HF and MF arrays and lie between 2.0 and 2.6 on the LF array.

3. The correlation times are approximately equal to 0.9 minutes for all apertures on the HF array, increase with aperture from 1.8 to 2.5 minutes on the MF array and from 1.2 to 1.6 minutes on the LF array.

4. The coefficients of variation for the averaged omni noise are independent of aperture on the HF and MF arrays with full aperture values of .17 and .22 respectively and vary between .43 and .53 on the LF array.

(U) The omni noise histograms show a greater deficiency in probability mass at the small values than do the omni signal histograms. In accordance with the discussion of the omni signal histograms, this difference can be interpreted as a larger equivalent degrees-of-freedom for the omni noise than for the omni signal, implying that the hydrophone noise intensities across the aperture exhibit less statistical dependence than the hydrophone signal intensities.

(U) The omni noise coefficients of variation and correlation times do not show a consistent relationship to their beam noise counterparts as do those for the omni signal and the beam signal. This is not unreasonable since the beam noise statistics are determined by only that portion of the total noise field in the beam look direction, whereas the beam signal statistics are determined by the total signal field.

5.4 Implications of the Beam Signal Temporal Results for System Analysis Bandwidths.

(U) The signal-to-noise ratio at the output of a beamformer is determined by both the array length and the system analysis bandwidth. The system averaging time determines the extent to which the fluctuations in the noise are reduced relative to those in the signal. If the array length is small relative to the coherence length of the signal field, then the signal field can be viewed as a time-varying planewave incident on the array. Thus, for short arrays, the effect of aperture length can be considered separately from the effect of the temporal system parameters: analysis bandwidth and averaging time. For longer arrays, however, the effects of array length and the two temporal parameters may be interrelated. For example, increasing the array length may alter the frequency spread of the signal field at the hydrophone inputs, hereafter referred to as the array signal bandwidth, and thus change the effect of the system analysis bandwidth on the signal-to-noise ratio. Furthermore, the change in the array signal bandwidth, relative to the system analysis bandwidth, can alter the correlation time of the beam signal and thus effect the extent to which the signal fluctuations are

reduced by averaging. Thus, in general, to predict the effect of the temporal system parameters on performance, it is necessary to determine the array signal bandwidth for those aperture lengths under consideration. In this section, the observed temporal properties are used to provide estimates of the array signal bandwidth at the different apertures. In the next section, the lack of dependence of the results on aperture is discussed in terms of the hydrophone input spectrum.

(U) To provide the theoretical background for the interpretation of the observed results, we first relate both the mean beam signal and its fluctuation spectrum to the signal field at the hydrophone inputs. To this end, let $B(pT; \alpha, f)$ be the beam signal time series in the frequency-azimuth resolution cell specified by (α, f) where $\alpha = (f/c) \sin\theta$ and T^{-1} is the sampling rate which is assumed to be large enough so that aliasing can be neglected. Next, let $P_I(\alpha, f)$ denote the spectrum of the hydrophone inputs, defined as the two-dimensional discrete fourier transform of the hydrophone correlation function. Let $P_K(\alpha)$ and $P_F(f)$ denote the array/processor "wavenumber" and "frequency" windows respectively, defined as the magnitude squared of the Fourier Transforms of the spatial and temporal weighting coefficients respectively. Thus, $P_K(\alpha)$ and $P_F(f)$ characterize the aperture length and the analysis bandwidth of the array/processor combination. In particular, if the array is not deformed, the response of the system to a planewave input at frequency f_o and wavenumber projection $\alpha_o = (f_o/c) \sin\theta_o$ is $P_K(\alpha - \alpha_o) P_F(f - f_o)$.

(U) With the notation at hand, the mean of the beam signal time series

can be expressed as iterated convolution integrals

$$\overline{B(pT;\alpha,f)} \approx \int_{-1/2\Delta}^{1/2\Delta} P_F(f-f')\,P_{OD}(\alpha,f')\,df' \tag{5.3a}$$

with

$$P_{OD}(\alpha,f) = \int_{-1/2d}^{1/2d} P_K(\alpha-\alpha')\,P_I(\alpha',f)\,d\alpha' \tag{5.3b}$$

where d is the hydrophone spacing and Δ^{-1} is the hydrophone sampling rate. The spectrum $P_{OD}(\alpha,f)$ describes the signal field at the hydrophone inputs as seen by the finite aperture array through the wavenumber window $P_K(\alpha)$. It is the relationship between the bandwidth of $P_{OD}(\alpha,f)$, the array signal bandwidth, and the bandwidth of $P_F(f)$, the analysis bandwidth, that determines the effect of the analysis bandwidth on the mean beam signal, and hence, the signal-to-noise ratio.

(U) Next, if it is assumed that the signal field is Gaussian, then it can be shown that the beam signal fluctuation spectrum, $S_B(\nu;\alpha,f)$, can be expressed as a correlation integral

$$S_B(\nu;\alpha,f) = \int_{-1/2T}^{1/2T} S_b(\nu+\nu';\alpha,f)\,S_b(\nu';\alpha,f)\,d\nu' \tag{5.4a}$$

where

$$S_b(\nu;\alpha,f) = P_F(\nu)\,P_{OD}(\alpha,\nu+f) \tag{5.4b}$$

and "ν" is the frequency variable associated with the beam signal time series. The spectrum $S_b(\nu;\alpha,f)$ can be interpreted as the spectrum of the "complex beam" in the frequency-azimuth resolution cell (α,f) which, according to equation (5.4b), can be viewed as the spectrum at the output

of a filter with power transfer function $P_F(f)$ and input spectrum $P_{OD}(\alpha, f)$. Equation (5.4a) then accounts for the "magnitude squaring" operation which is used to obtain the beam signal power from t.. complex beam signal.

(U) Equation 5.4 provides the basis for estimating the array signal bandwidth from the temporal characteristics of the beam signal. For the analysis bandwidth of 0.4Hz used in the computations, which is large relative to the array signal bandwidths, the effect of the frequency window in equation 5.4 can be neglected, so that the fluctuations spectrum is approximately given by

$$(5.5) \quad S_B(\nu; \alpha, f) \cong \int_{-1/2T}^{1/2T} P_{OD}(\alpha, \nu+\nu') P_{OD}(\alpha, \nu') \, d\nu'$$

Let B_F be the equivalent rectangular bandwidth of the fluctuations spectrum defined by

$$(5.6) \quad B_F = (1/2)\left(\int S_B(\nu; \alpha, f) d\nu\right) / S_B(0; \alpha, f)$$

For mathematical convenience define the "effective" array signal bandwidth of $P_{OD}(\alpha, f)$ by

$$(5.7) \quad B_{OD} = (1/2)\left[\int P_{OD}(\alpha, \nu) d\nu\right]^2 / \left[\int P_{OD}^2(\alpha, \nu) d\nu\right]$$

Then using equations (5.5), (5.6) and (5.7), it can be concluded that $B_F = B_{OD}$

(C) According to the above analysis, the effect of the analysis bandwidth on the mean beam signal depends on the array signal bandwidth through the correlation integral in equation (5.3a) and this bandwidth can be equated to the bandwidth of the fluctuations spectrum. Thus, to interpret the observed results in the context of this analysis, we first restate the observed temporal properties, (see Section 5.2), in terms of the fluctuations

spectrum:

> The form of the fluctuations specturm is independent of aperture for the HF and MF arrays and exhibits a slight decrease in spread at the full aperture on the LF array. The fluctuations bandwidths for all apertures on the HF and MF arrays are 1.4 mHz and 1.2 mHz respectively. The fluctuations bandwidths for the LF array decrease from 1.3 mHz at the quarter aperture tol.1mHz at the full aperture.

(C) There are two important features in the observed results, the numerical values of the fluctuations bandwidths themselves and the lack of dependence of the fluctuations specturm on aperture. In this section we discuss the implications of the values of the bandwidths, deferring the discussion of the aperture independence to the next section. From the convolution relationship of equation (5.3) it can be concluded that the mean beam signal increases in proportion to B_A^{-2} if $B_A >> B_{OD}$ where B_A is the system analysis bandwidth. Thus, for uncorrelated noise, the observed fluctuations bandwidths suggest that the signal-to-noise ratio could be improved by at least 20dB over that observed in the actual processing before the array signal bandwidth becomes a limiting factor. It is important to point out, however, that this inference is predicated on results obtained using a particular beam signal tracking algorithm and stable sources at near constant tow speeds and thus, should be viewed as upper bounds in predicting performance in tactical operating environments.

5.5 An Interpretation of the Aperture Dependence of the Temporal Results.

(U) The quantative results have indicated that the fluctuations spectra for both the HF and MF arrays depend on aperture only through a multiplicative constant, while the fluctuations spectra for the LF array show only a small

reduction in spread at the full aperture. For the large analysis bandwidth used in the data analysis, equation 5.4 applies, indicating that the fluctuations spectrum is determined by the frequency spread in the spectrum $P_{OD}(\alpha, f)$. Thus, to interpret the quantitative results, it is necessary to examine the conditions for which the convolution integral of equation 5.3b yields a spectrum whose frequency behavior is independent of the spread of the aperture window $P_K(\alpha)$. In this section, we consider three sets of conditions, each of which results in a fluctuations spectrum that is independent of aperture.

(U) The first two cases are obtained by restricting the length of the aperture relative to the coherence length of the input spectrum $P_I(\alpha, f)$.

Short Array: Assume that the length of the aperture is short relative to the coherence length associated with $P_I(\alpha, f)$. Then it can be shown that the mean beam signal is approximately given by,

$$\overline{B(\varphi T; \alpha, f)} \cong P_K(\alpha) \left(\int P_F(f - f') S_I(f') \, df' \right) \tag{5.8}$$

and the fluctuations spectrum is

$$S_B(\nu; \alpha, f) \doteq [P_K(\alpha)]^2 \left(\int S_b'(\nu + \nu'; \alpha, f) S_b'(\nu'; \alpha, f) \, d\nu' \right) \tag{5.9a}$$

where

$$S_b'(\nu; \alpha, f) = P_F(\nu) S_I(\nu + f) \tag{5.9b}$$

and $S_I(f)$ is the frequency spectrum of an individual hydrophone.

(U) The short array case is intuitively plausible since the short array

assumption implies that the combined effect of the signal field incident on the possibly deformed array can be viewed as a planewave incident on a straight array. Thus, the mean beam signal increases as the square of the aperture, as dictated by $P_K(\alpha)$, and the temporal characteristics of the beam signal are determined by the temporal characteristics of a single hydrophone.

(U) The next case represents the other extreme.

Long Array Assume that the length of the aperture is long relative to the coherence length associated with $P_I(\alpha, f)$. Then it can be shown that the mean beam signal and the fluctuation spectrum are given by equations that are identical to (5.8) and (5.9) with $S_I(f)$ replaced by $P_I(\alpha, f)$ and $P_K(\alpha)$ replaced by $R_K(0)$, where

$$R_K(0) = \int_{-1/2d}^{1/2d} P_K(\alpha)\, d\alpha \tag{5.10}$$

In the long array case, the mean beam signal increases in proportion to the aperture as dictated by $R_K(0)$. Thus from the point of view of beamforming, the signal field appears to be completely uncorrelated across the aperture, and thus the temporal properties are determined from the spectrum describing the aggregate of hydrophones.

(U) The final case is obtained by restricting the form of the input spectrum $P_I(\alpha, f)$.

Separable Input Spectrum Assume that the input spectrum can be factored into a product of the form

$$P_I(\alpha, f) = P_{ID}(\alpha)\, S_I(f) \tag{5.11}$$

Then it can be shown that the mean beam signal can be written as the product

(5.12a) $$\overline{B(\rho_T;\alpha,f)} = P_{0K}(\alpha)\left(\int P_F(f-f')\,S_I(f')\,df'\right)$$

where

(5.12b) $$P_{0K}(\alpha) = \int P_K(\alpha-\alpha')\,P_{ID}(\alpha')\,d\alpha'$$

and the fluctuation spectrum is given by equation (5.9) with $P_K(\alpha)$ replaced by $P_{0K}(\alpha)$.

(U) The separable input spectrum case differs from the previous cases in that it applies for all aperture sizes. Thus, an array with a separable input spectrum may also exhibit short array or long array properties depending on the relationship between the aperture size and the coherence length. From a physical point of view, the separable input spectrum assumption implies that the incident signal field need not be viewed as a planewave but that the temporal properties of the aggregate of hydrophones must be the same as those for the single hydrophone.

(U) The three special cases have a common property that simplifies the relationship between system performance and the selection of the three basic system parameters: array length, analysis bandwidth and averaging time. Specifically, in each case, both the mean and the fluctuations spectrum can be written as a product of two functions, one that depends only on aperture size and one that depends only on the analysis bandwidth. Thus, for these cases, the effect of the analysis bandwidth and the aperture size on the signal gain can be considered separately, and the

effect of the averaging time, although dependent on the analysis bandwidth, does not depend on the aperture size.

(U) To interpret the quantitative results, it is necessary to characterize the aperture dependence of both the mean beam signal and the fluctuations spectrum for each array. The aperture dependence of the mean beam signal can be investigated in terms of the mean signal gain since the observed mean omni signal is independent of aperture. The fluctuations spectrum was measured only at the quarter, half, and full apertures so that a direct comparison of the temporal properties of the beam signal and the single hydrophone is not possible.

(C) Of the three arrays, the HF array is the only array whose properties approximate those of the short array. The signal gain curve indicates that the mean beam signal increases with aperture at nearly the ideal rate and the beam signal fluctuations spectra are aperture-independent. Furthermore, the results of section 5.2 suggest that the incident signal hydrophone intensities are highly correlated across the full aperture which is consistent with the short array assumption. Additional evidence in support of the short array assumption is provided by the near equality of the beam signal and the omni signal fluctuations bandwidths and the almost perfect correlation between the beam signal and the omni signal logarithmic time series.

(C) The MF array results shows a greater departure from the short array properties since the signal gain curve indicates a larger degradation in the mean beam signal with aperture. On the other hand, the observed

fluctuation spectra show essentially no dependence on aperture, indicating that at least over the quarter, half and full apertures, the MF array properties are consistent with those of a seperable input spectrum array. As compared to the HF array results, however, there is less similarity between the beam signal and the omni signal temporal properties and the omni signal histograms are indicative of less correlation in the hydrophone intensities across the aperture.

(C) The LF array results show a small decrease in the fluctuations bandwidth as the aperture is increased and thus, strictly speaking, the LF array cannot be viewed as a separable input spectrum array over the full range of apertures. On the other hand, the signal gain curve indicates that the mean beam signal is approximately that of a short array between the quarter and half apertures, and similar to that of a long array between the half and the full apertures. Thus, the LF array results show that there is not a major inter-dependence between the spatial properties, as measured by the mean beam signal, and the temporal properties, as measured by the fluctuations spectrum, as the aperture size is varied from a short aperture to a long aperture. Thus, for the LF array, as well as the MF and HF arrays, the results show that the effects of analysis bandwidth and averaging time are essentially independent of aperture.

VI. CONCLUSIONS AND IMPLICATIONS FOR SEAGUARD

(C) The objective of this analysis has been to obtain quantitative statistical results from a large aperture system to provide an experimental basis for the design of the OMAT array/processing system and future experiments to be conducted under the SEAGUARD program. The details of the quantitative results have been summarized and discussed in the preceeding sections of this chapter. The major results of the analysis are as follows:

The spatial and temporal signal statistics for the HF array approximate those of an array that is short relative to the coherence length of the signal field at the hydrophone inputs. The signal gain shows only a modest degradation with increasing aperture while the temporal statistics are independent of aperture. The fluctuations bandwidths imply that the array signal bandwidth is 1.44 mHz, indicating that the temporal variations in the signal field and the array dynamics do not significnatly limit the ability to enhance the signal-to-noise ratio through narrowband processing. The beam signal histograms are exponential at all apertures in support of the Gaussian, time-stationary, signal field hypothesis and the coefficients of variation show that the fluctuations in the beam signal are approximately equal to the mean. The 5.8 minute correlation times indicates that the effect of the 12 minute averaging time used in the analysis is to reduce the coefficients, of variation and hence the fluctuations in the beam signal by approximately $\sqrt{2}$.

The signal results for the MF array are similiar to those of the HF array although the signal gain curve shows a slightly larger degradation with increasing aperture. The temporal statistics are aperture independent with essentially the same values for the fluctuations bandwidths and the correlation times.

The signal results for the LF array show a significant degradation in the signal gain with less than a 3dB increase between the half and full apertures. Depth sensor measurements along the array suggest that this degradation may be due to array deformations that occur in the last half of the

array. The temporal statistics, however show only a modest dependence on aperture with fluctuations bandwidth decreasing from 1.34 mHz at the quarter aperture to 1.07 mHz at the full aperture. Thus, even though the signal gain curve indicates a significant reduction in the signal coherence at the hydrophone inputs, the temporal statistics, and hence the effect on performance of the system analysis bandwidth and the averaging time, remain essentially independent of aperture.

The noise gain curves for both the HF and MF arrays increase with aperture at the rate of 3dB/octave and are both nearly 1dB higher than the theoretical curve for uncorrelated noise. As a consequence the array gain curves reflect only the degradation in the signal gain and are lower than the theoretical array gain curve.

The noise gain curve for the LF array increases by more than 3dB/octave between the half and full apertures. As a consequence, the array gain curve reflects both the signal gain degradation and the noise gain degradation and the combined effect is a reduction in the array gain at the full aperture over that at the half aperture.

(C) The implications of the results for the SEAGUARD program are as follows:

The ability of the OMAT system to generate the fluctuation time series of the three system gains simultaneously on the different subapertures is crucial to a meaningful measurement of array performance. This was seen to be the case in this analysis of the three arrays. For example, had only the full aperture values of the array gain been available, the results would have indicated that the performance of the LF and MF arrays was nearly identical and only slightly inferior to that of the HF array.

The ability of the OMAT system to measure the hydrophone positions is essential to determining the limitations on performance imposed by the array deformation process. These measurements were not available for this analysis.

The range of analysis bandwidths available in the OMAT system processor is adequate to determine the potential for signal-to-noise ratio improvement through narrowband processing as evidenced by the observed array signal bandwidths. The lack of dependence on aperture of these bandwidths implies that the same improvement will be realized on each of the subapertures in the OMAT system array.

The range of averaging times avilable in the OMAT system suffices to determine the extent to which averaging reduces the fluctuations in the noise relative to those in the signal. The observed correlation times imply that the OMAT fixed-time averager (5 minutes) would reduce the fluctuations in the noise with little effect on the fluctuations in the signal. Furthermore, the aperture-independence of the beam signal correlation time implies that the same effect will be experienced on each of the sub-apertures in the OMAT system array.

The sixteen hydrophones allocated for the measurement of both the omni signal and the omni noise in the OMAT system processor is adequate to obtain an aperture independent statistic as evidenced by the comparison of the observed means and standards at the different aperture lengths in the analysis.

The 24 hour data base should suffice for the measurement of the system gain statistics. The observed fluctuations (standard deviations) in the system gains indicate that the signal gain can be estimated with a relatively small data base, whereas a large data base is required for both the noise gain and the array gain. However, the observed increase in the signal gain fluctuations suggest that at the OMAT system aperture lengths, it too may require a large data base.

ACKNOWLEDGEMENTS

(U) This work was sponsored by the Defense advanced Research Projects Agency (ARPA) in support of the SEAGUARD PROJECT/Ocean Measurement and Array Technology (OMAT) program. Assistance in the problem definition by H. Cox (ARPA), B. Cole (NUSC), B. Adams and S. Marshall (NRL) is greatly appreciated. Critical reviews of the work at its different stages by the above along with V. Simmons, B. LaPlante and R. Lauer (NUSC) was very helpful. The Mediterranean experiment was gointly sponsored by the Long Range Acoustic Propagation Project (LRAPP) and ARPA and conducted as an inter-laboratory effort (NUC and NRL) with S. Marshall as scientist in charge. Compute software development by S. Boze and J. Padget is greatfully acknowledged.

REFERENCES

1. S.W. Marshall, "Acoustic Signal-to-Noise and Azimuthal Noise Directionality in the Mediterranean Sea Using LAMBDA II" (U), NRL Memorandum Report 3050, April 1975 (SECRET).

APPENDIX

(U) Figures referred to in the text are illustrated on the following pages.

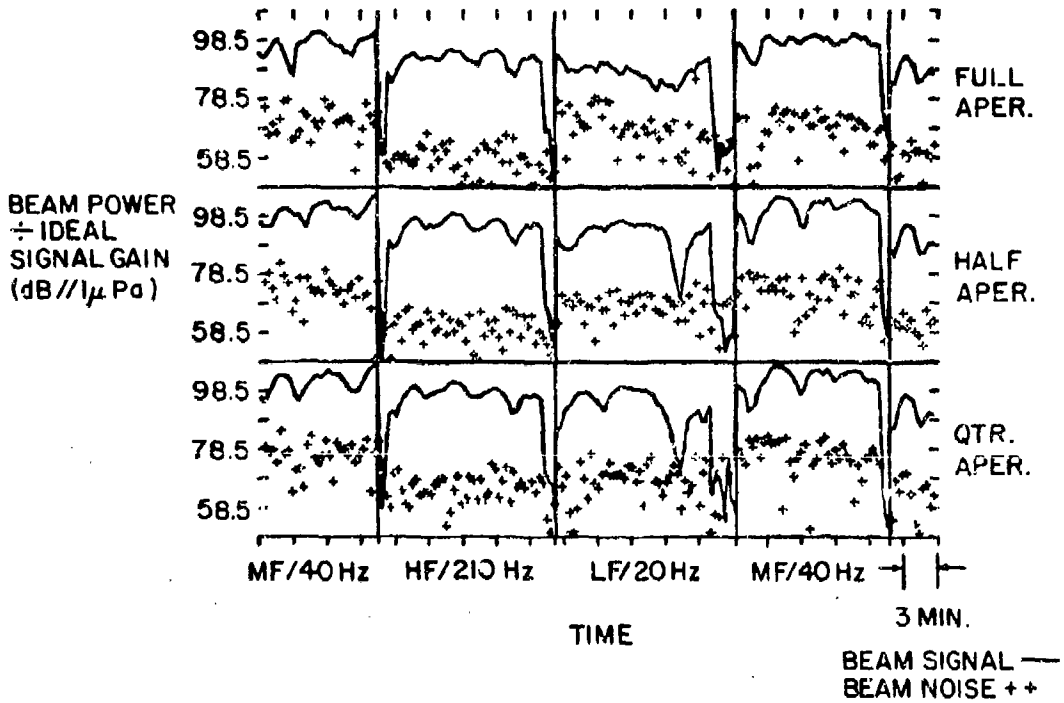

(C) Figure A.1 Instantaneous Beam Signal and Noise Medium Range

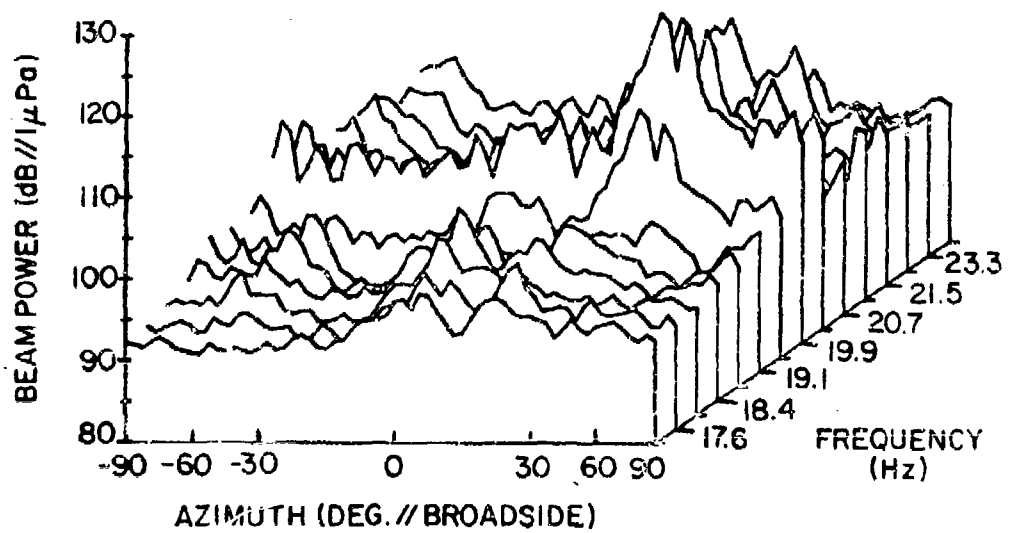

(C) Figure A.2 Frequency-Azimuth Power Distribution LF Array/20 Hz, Full Aperture 12 Minute Average Medium Range

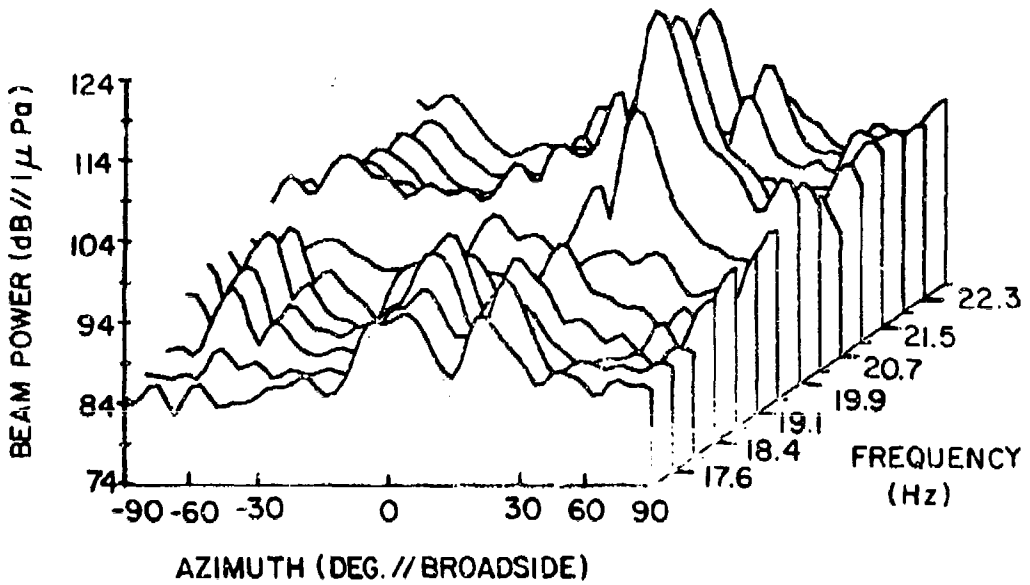

(C) Figure A.3 Frequency-Azimuth Power Distribution LF Array/20 Hz, Half Aperture 12 Minute Average Medium Range

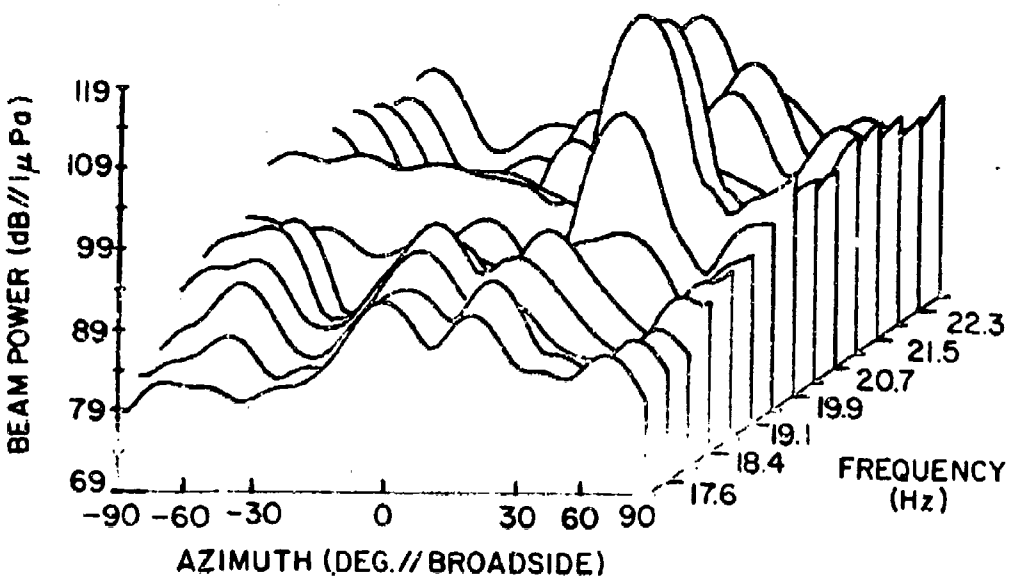

(C) Figure A.4 Frequency-Azimuth Power Distribution LF Array/20 Hz, Quarter Aperture 12 Minute Average Medium Range

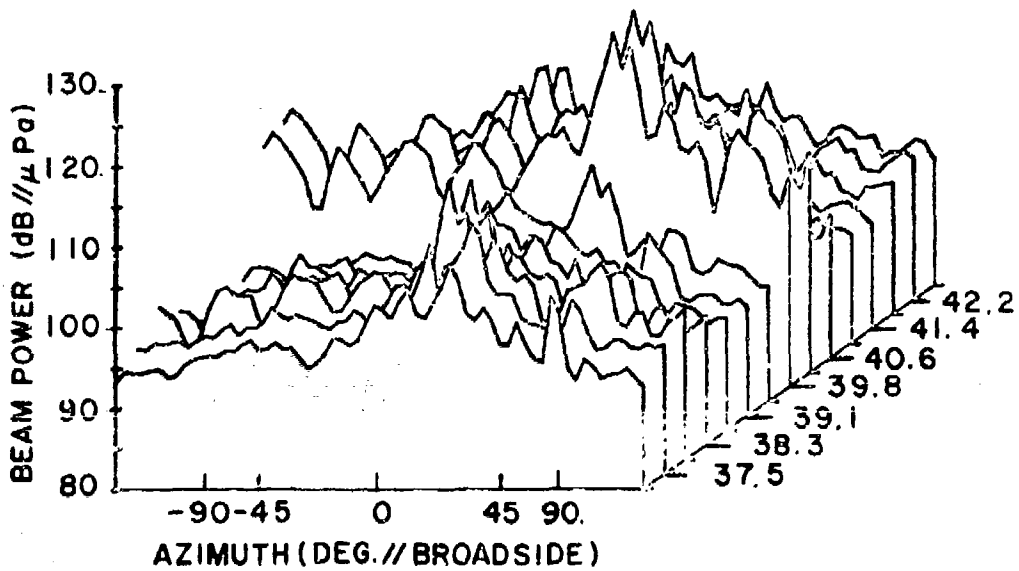

(C) Figure A.5 Frequency-Azimuth Power Distribution MF Array/40 Hz, Full Aperture 12 Minute Average Medium Range

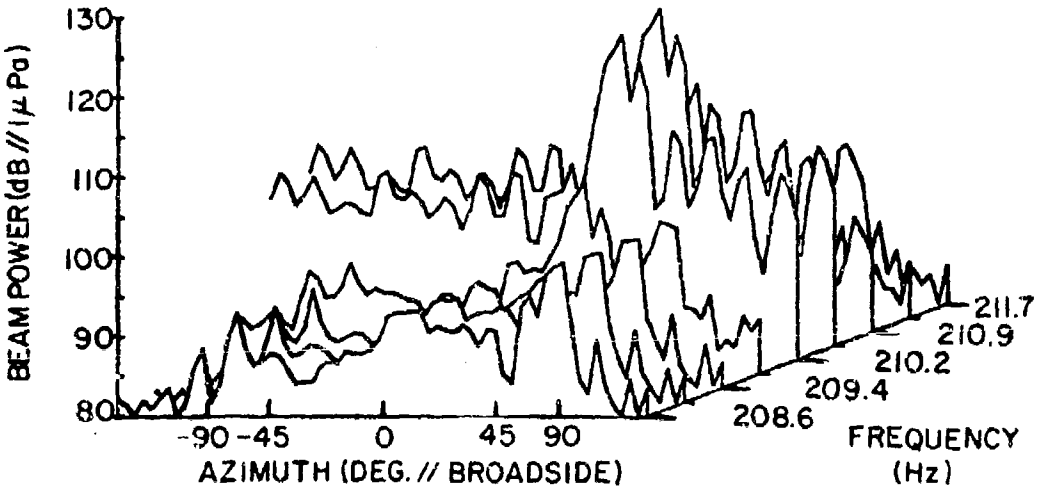

(C) Figure A.6 Frequency-Azimuth Power Distribution HF Array/210 Hz, Full Aperture 12 Minute Average Medium Range

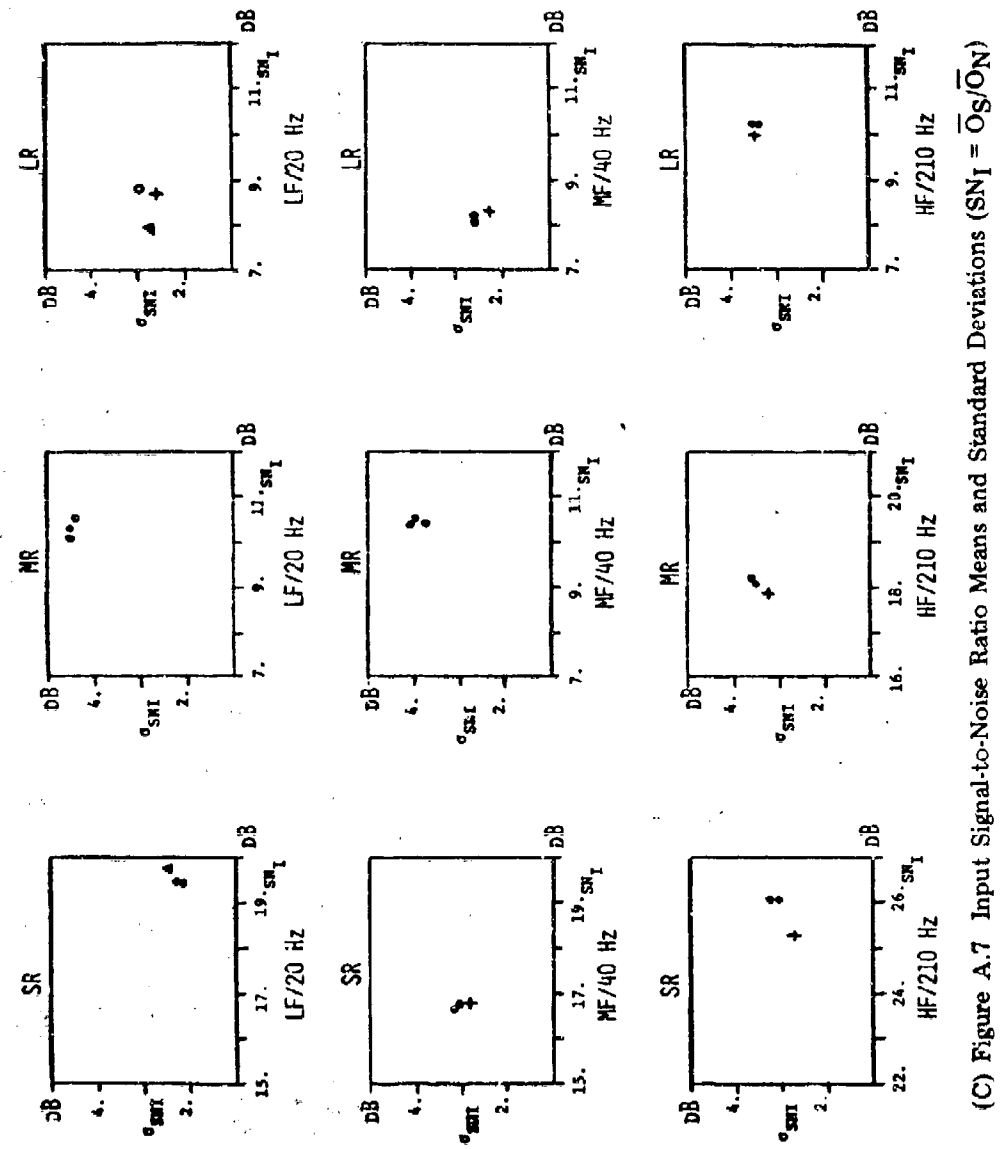

(C) Figure A.7 Input Signal-to-Noise Ratio Means and Standard Deviations ($SN_I = \bar{O}_S/\bar{O}_N$)

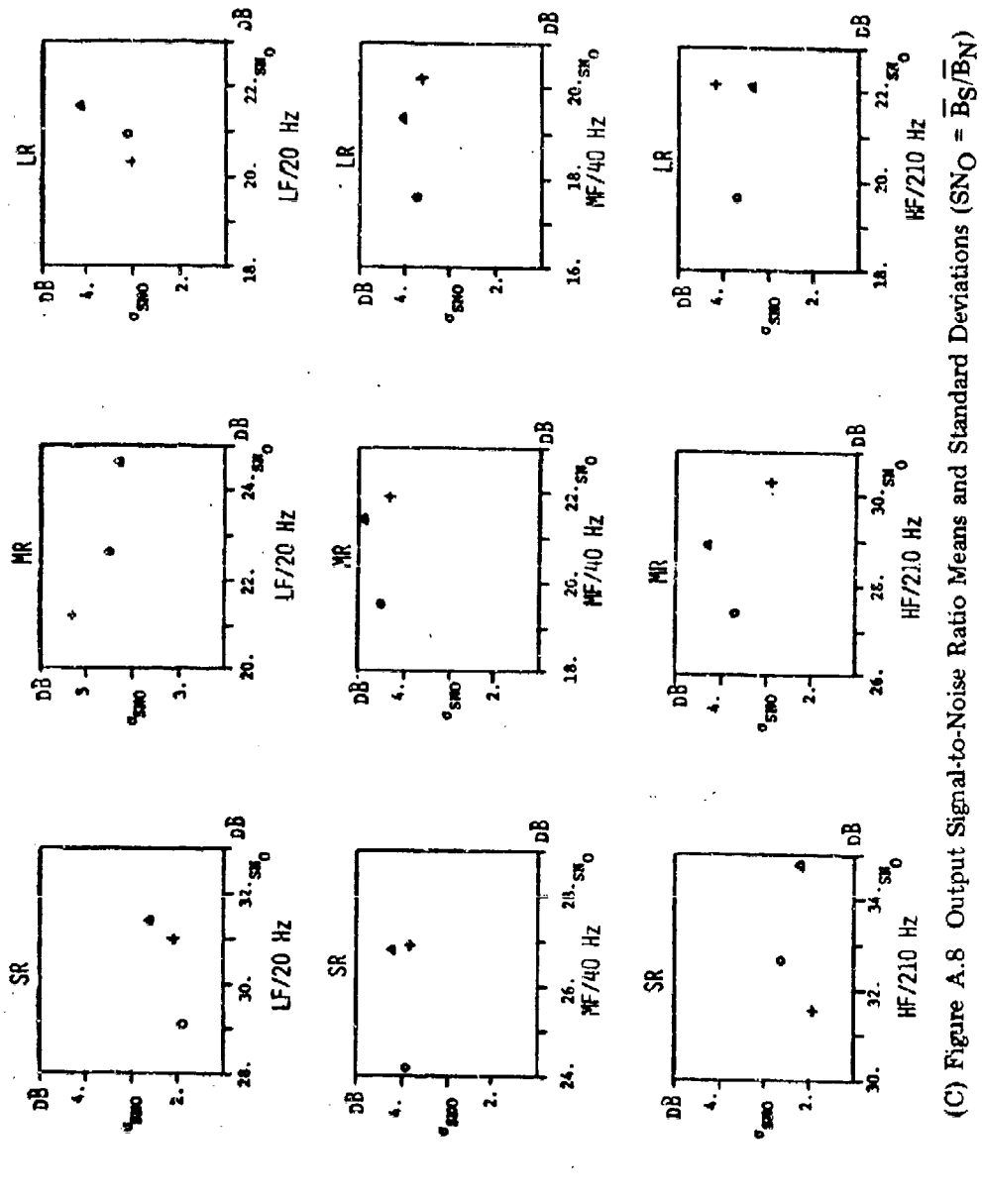

(C) Figure A.8 Output Signal-to-Noise Ratio Means and Standard Deviations ($SN_O = \overline{B_S}/\overline{B_N}$)

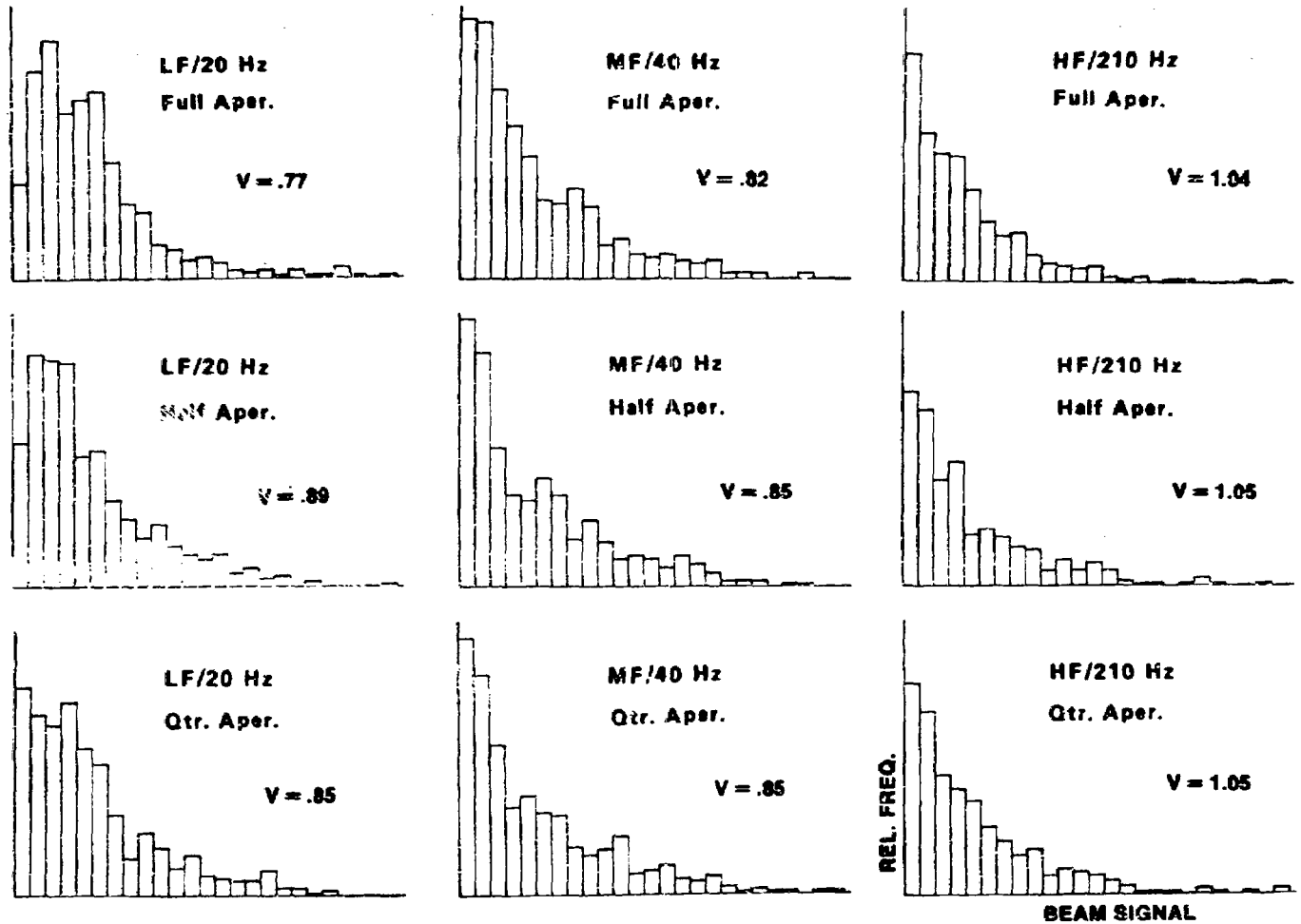

(C) Figure A.9 Beam Signal Histograms

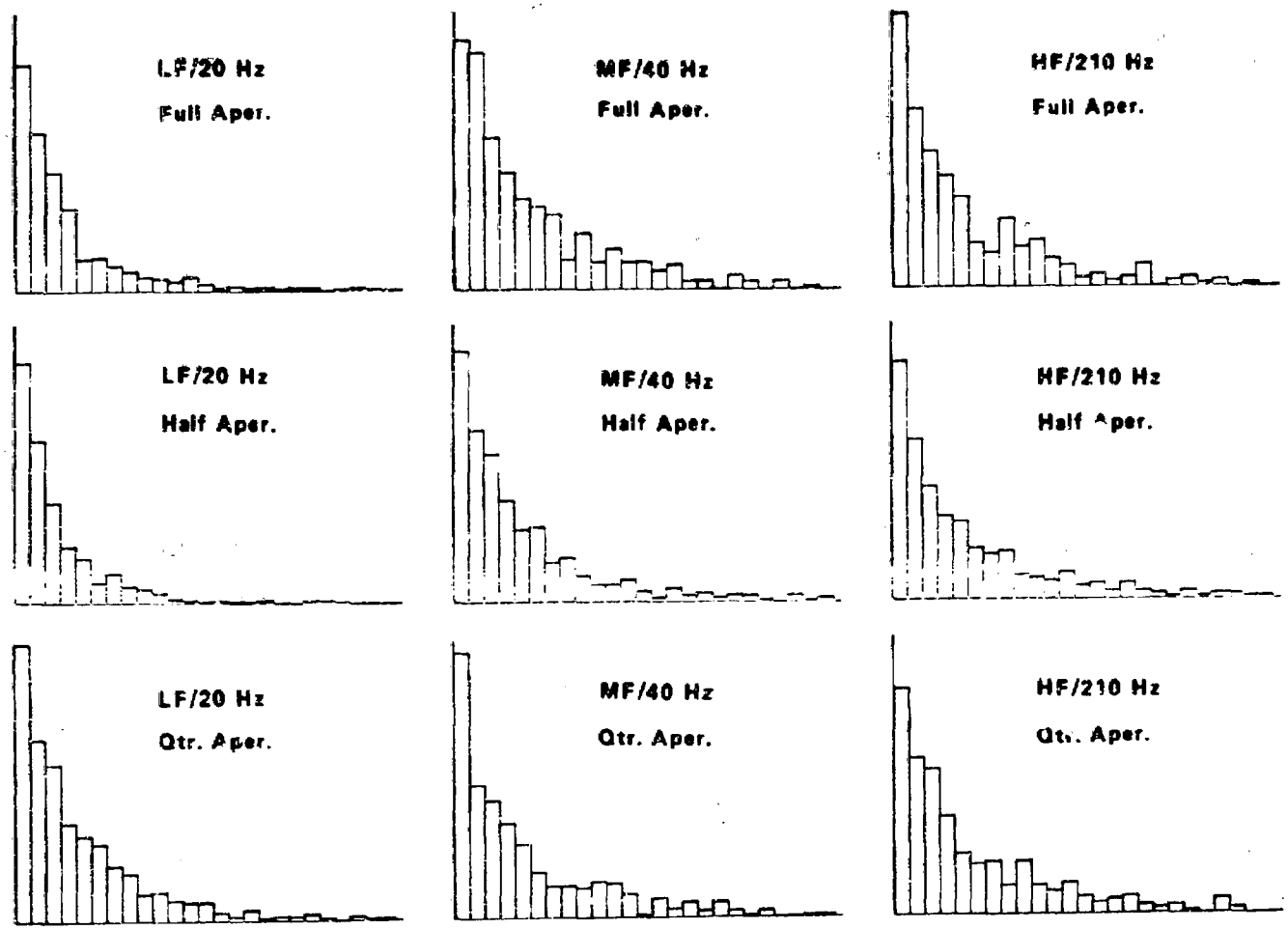

(C) Figure A.10 Beam Noise Histograms

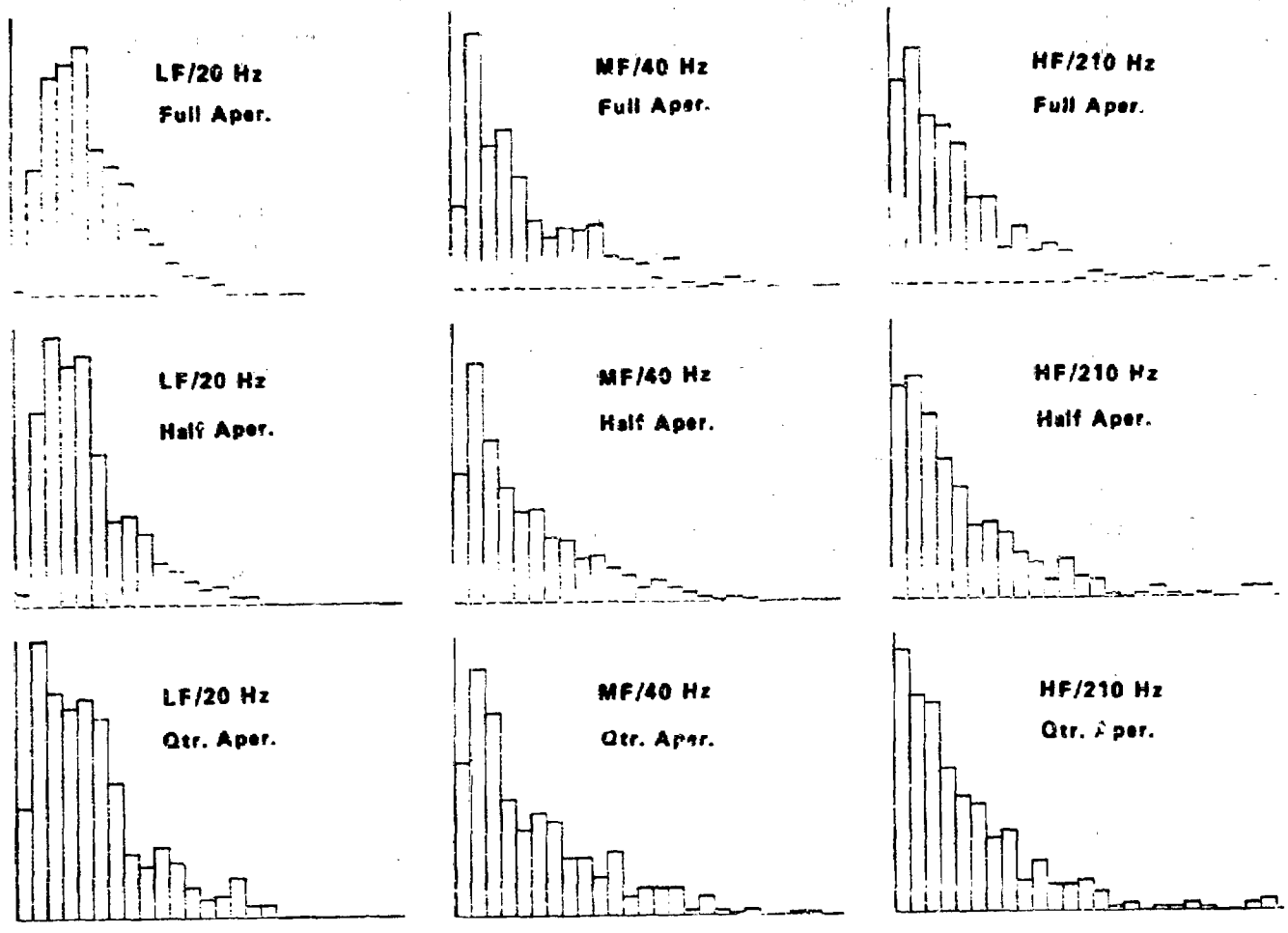

(C) Figure A.11 Omni Signal Histograms

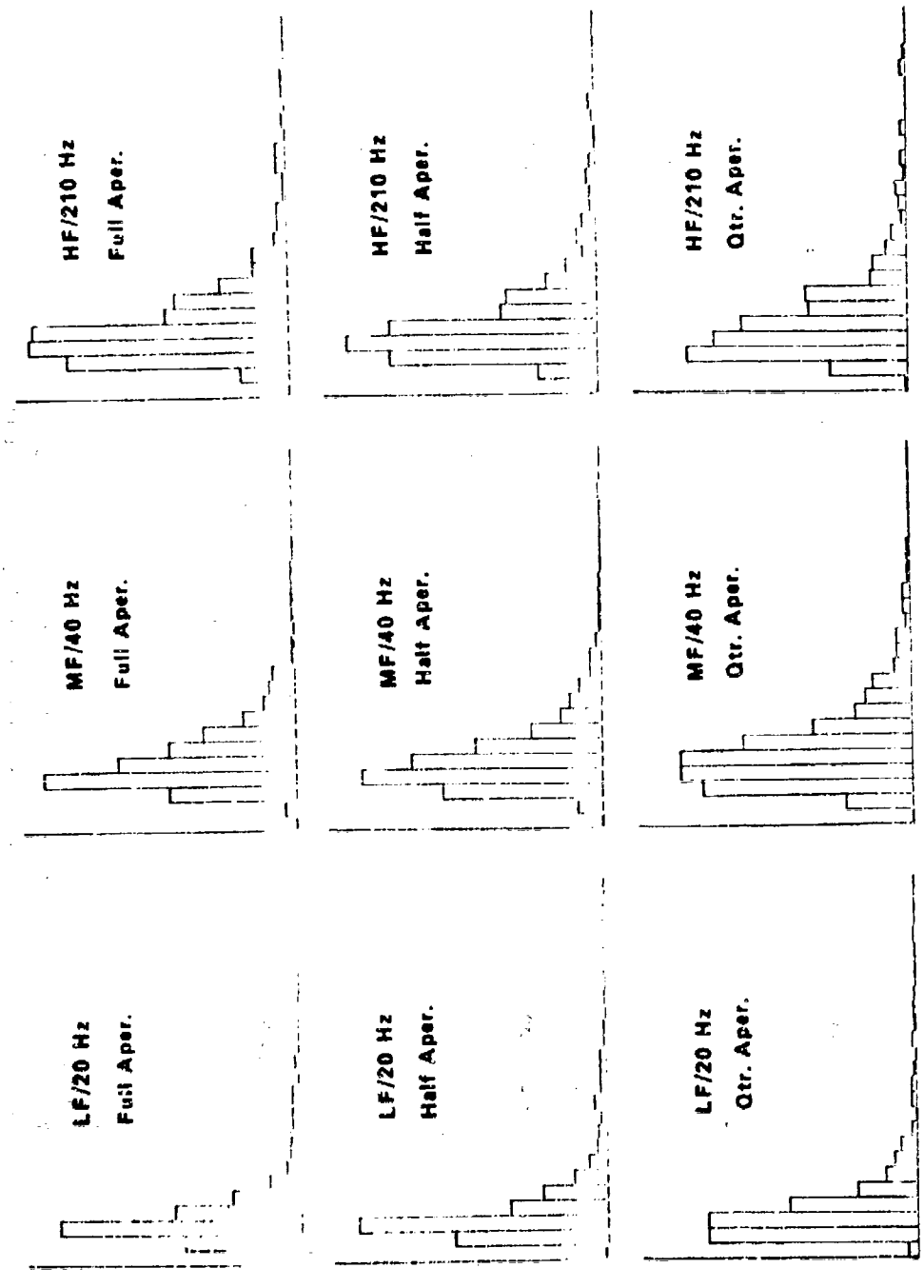

(C) Figure A.12 Omni Noise Histograms

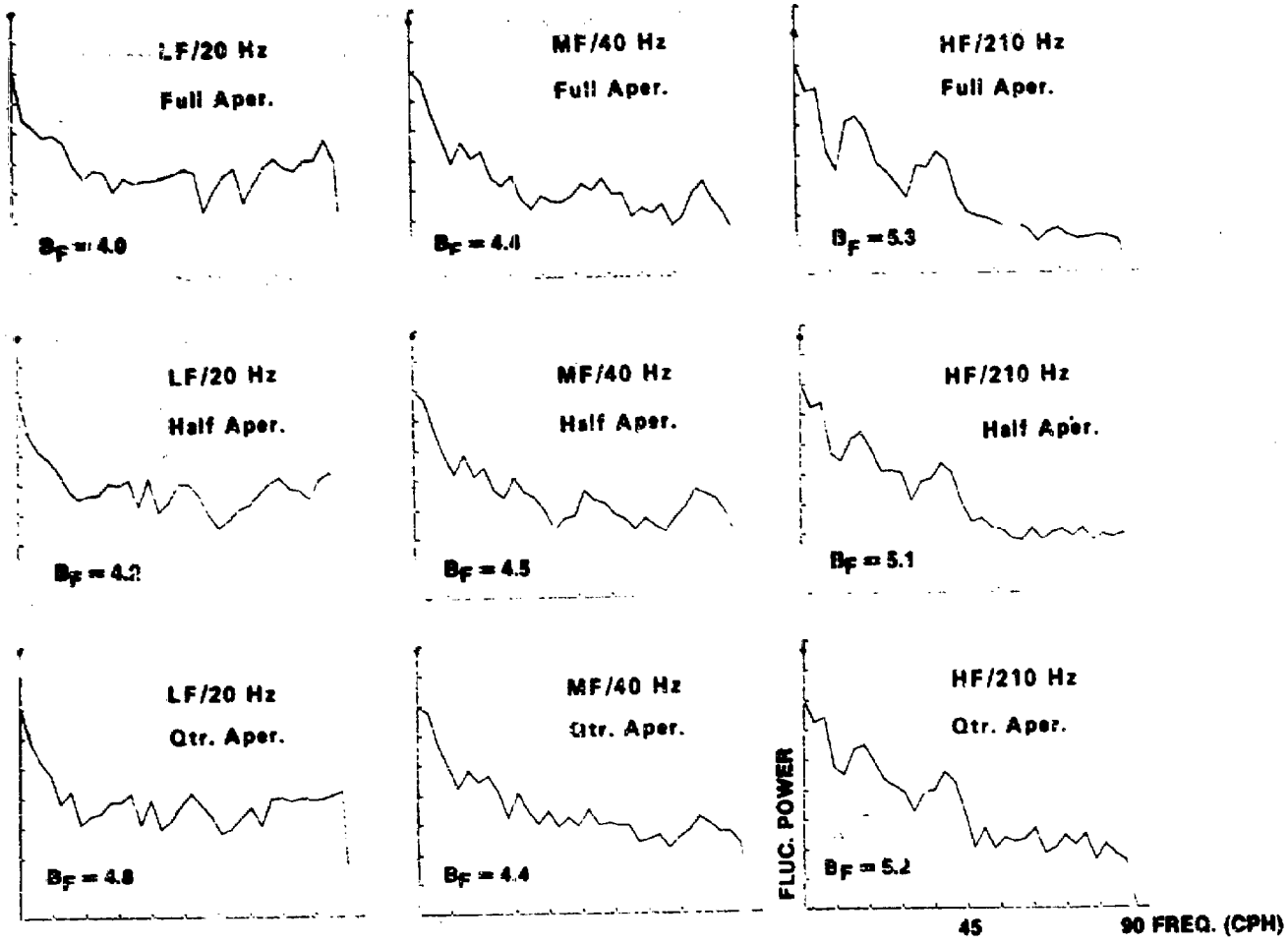

(C) Figure A.13 Beam Signal Spectra

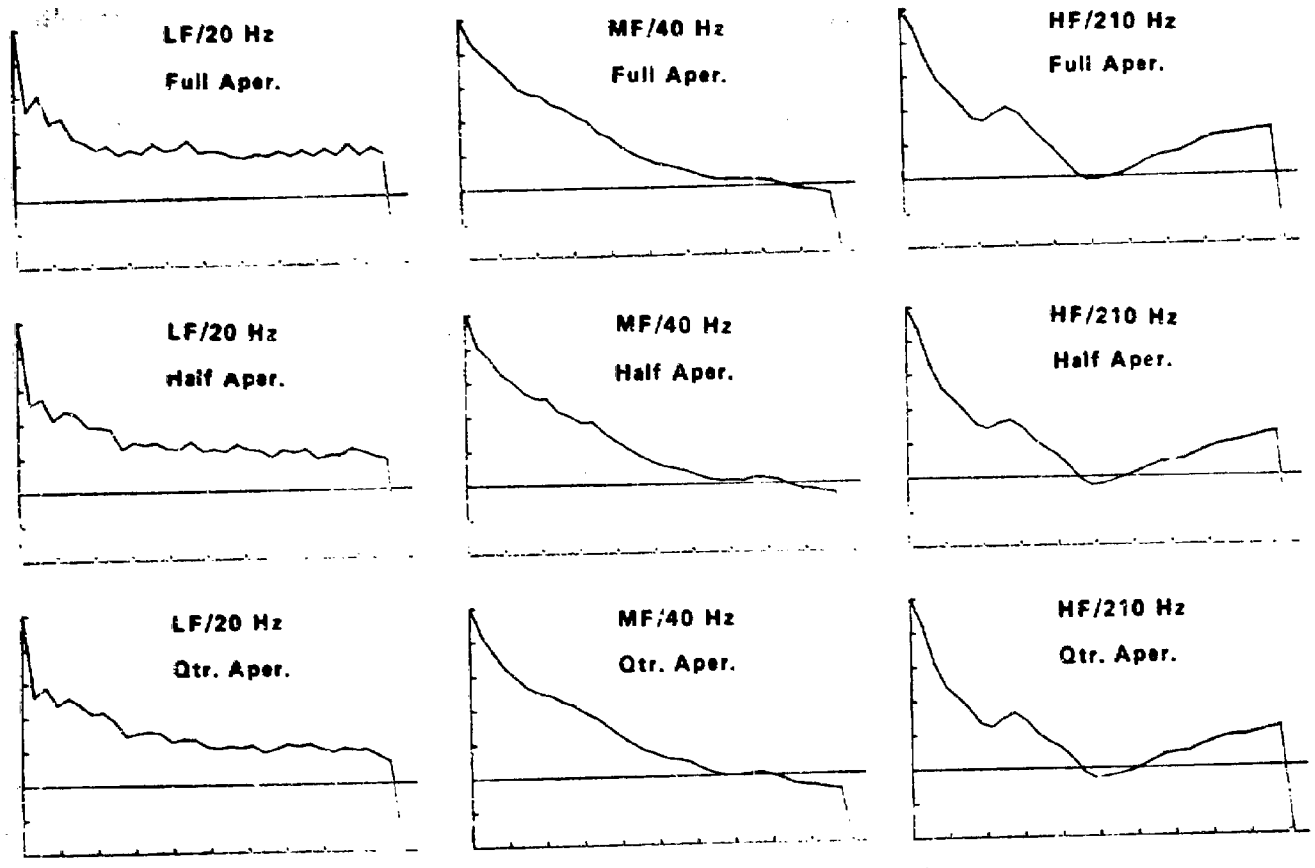

(C) Figure A.14 Beam Signal Covariance Functions

UNITED STATES GOVERNMENT

Memorandum

7100-033

DATE: 26 February 2004

REPLY TO ATTN OF: Burton G. Hurdle (Code 7103)

SUBJECT: REVIEW OF REF (A) FOR DECLASSIFICATION

TO: Code 1221.1

REF: (a) "A Statistical Analysis of the Performance of a Towed Array System" (U), Richard M. Heitmeyer, Stephen C. Wales and David T. Deihl, Acoustics Division, NRL Memo Report 3290, November 1976 (C)

1. Reference (a) describes the result of a Towed Array System based on an on-line analysis of data recorded during an experiment in November 1974, in the Ionian Basin of the Mediterranean. A three section towed array was employed. The analysis made of the array gain for three lengths of the array at three different frequencies (20, 40 and 210 Hz), Also a comparison of ambient noise was made. The differences based on aperture length, in array gain were very small

2. The technology and equipment of reference (a) have long been superseded. The current value of these papers is historical

3. Based on the above, it is recommended that reference (a) be declassified and released with no restrictions

Burton G. Hurdle

BURTON G. HURDLE
NRL Code 7103

CONCUR:

Edward R. Franchi 3/1/2004

E.R. Franchi Date
Superintendent, Acoustics Division

CONCUR:

Tina Smallwood 3/3/04

Tina Smallwood Date
NRL Code 1221.1